Coastal and Hydraulics Laboratory

US Army Corps of Engineers
Engineer Research and Development Center

Freeport Harbor Ship Simulator Hydrodynamic Study

Joseph V. Letter, Jr., William L. Boyt, Ben Brown, Chris T. Goodin, , and Darla M. McVan

February 2005

DRAFT

Approved for public release; distribution unlimited

The contents of this report are not to be used for advertising, publication, or promotional purposes. Citation of trade names does not constitute and official endorsement or approval of the use of such commercial products.

The findings of this report are not to be construed as an official Department of Army position, unless designated by other authorized documents.

D R A F T

ERDC/CHL TR-05-XX
February 2005

Freeport Harbor Ship Simulator Hydrodynamic Study

By Joseph V. Letter, Jr., William L. Boyt, Ben Brown,
Chris T. Goodin and Darla M. McVan

Coastal and Hydraulics Laboratory
U.S. Army Engineer Research and Development Center
3909 Halls Ferry Road
Vicksburg, MS 39180-6199

Final Report

Approved for public release; distribution is unlimited

Prepared for U. S. Army Corps of Engineers
Galveston, TX 77553-1229

Contents

Preface ……vii

Conversion Factors, Non-SI to SI Units of Measurement ……viii

1 – Introduction ……

1.1 Background ……
1.2 Project Description ……
1.3 Objective ……
1.4 Scope ……
1.5 Technical Approach ……

2 - Hydrodynamic Model Development ……

2.1 The TABS-MD Modeling System ……
2.2 Computational Environment ……
2.3 Mesh Development ……
2.4 Hydrodynamic Verification ……
2.5 Tidal Boundary Conditions ……
2.6 Hydrodynamic Model Coefficients ……

3 – Production Tests and Results ……

3.1 Design Alternatives ……
3.2 Procedures ……
3.3 Hydrodynamic Comparisons ……

4 - Summary and Conclusions ……

Appendix D: The TABS-MD System ……
Finite Element Modeling
The Hydrodynamic Model, RMA2
References

SF 298 ……

List of Figures

Figure 1-1. Freeport Harbor Location Map …….

Figure 1-2. Freeport Harbor Three Reaches of Different Depths ……..

Figure 1-3. Layout of Proposed LNG Terminal

Figure 2-1. Ocean Boundary and Computational Mesh

Figure 2-2. Base computational mesh bathymetry …….

Figure 2-3. Materials Categories in the Computational Mesh

Figure 2-4. Base Nodes at Tide Gage Locations for Water Surface Elevation Verification ……

Figure 2-5 Filtering of the boundary condition tide

Figure 2-6 Effects of tidal filtering on the current velocities in the GIWW west

Figure 2-7. Base Node 4254 and TG 363 East GIWW Water Surface Elevation – 1000 hrs

Figure 2-8. Base Node 7163 and TG 367 South Freeport Water Surface Elevation –1000 hrs

Figure 2-9. Base Node 3378 and TG 129 Entrance Channel Water Surface Elevation – 1000 hrs

Figure 2-10. Base Node 4254 and TG 363 South East GIWW Water Surface Elevation

Figure 2-11. Base Node 7163 and TG 367 South Freeport Water Surface Elevation

Figure 2-12. Base Node 3378 and TG 129 Entrance Channel Water Surface

Elevation

Figure 2-13. Location Map for the Field Velocity Ranges

Figure 2-14. Maximum Flood Velocity Line 1

Figure 2-15. Maximum Flood Velocity Line 2

Figure 2-16. Maximum Flood Velocity Line 3

Figure 2-17. Maximum Flood Velocity Line 4

Figure 2-18. Maximum Ebb Velocity Line 1

Figure 2-19. Maximum Ebb Velocity Line 2

Figure 2-20. Maximum Ebb Velocity Line 3

Figure 2-21. Maximum Ebb Velocity Line 4

Figure 3-1. Base channel condition

Figure 3-2. Plan 4 channel condition

Figure 3-3. Plan 5 channel condition

Figure 3-4. Freeport Harbor Plan 4

Figure 3-5. Plan 4 Computational Mesh Bathymetry

Figure 3-6. Freeport Harbor Plan 5

Figure 3-7. Plan 5 Computational Mesh Bathymetry

Figure 3-8. Station Locations for Water Surface Elevation Plots

Figure 3-9. Entrance Channel Water Surface Elevation Comparisons at Station A

Figure 3-10. GIWW East Water Surface Elevation Comparisons at Station B

Figure 3-11. GIWW West Water Surface Elevation Comparisons at Station C

Figure 3-12. Lower Turning Basin South Water Surface Elevation Comparisons at Station D

Figure 3-13. Lower Turning Basin North Water Surface Elevation Comparisons at Station E

Figure 3-14. Upper Turning Basin West Water Surface Elevation Comparisons at Station F

Figure 3-15. Upper Turning Basin East Water Surface Elevation Comparisons at Station G

Figure 3-16. Base Maximum Flood Velocity in the Entrance Channel

Figure 3-17. Plan 4 Minus Base Velocity Differences Maximum Flood in the Entrance Channel

Figure 3-18. Plan 5 Minus Base Velocity Differences Maximum Flood in the Entrance Channel

Figure 3-19. Base Maximum Ebb Velocity in the Entrance Channel

Figure 3-20. Plan 4 Minus Base Velocity Differences Maximum Ebb in the Entrance Channel

Figure 3-21. Plan 5 Minus Base Velocity Differences Maximum Ebb in the Entrance Channel

Figure 3-22. Base Maximum Flood Velocities in the Confluence

Figure 3-23. Plan 4 Maximum Flood Velocities in the Confluence

Figure 3-24. Plan 5 Maximum Flood Velocities in the Confluence

Figure 3-25. Plan 4 Minus Base Maximum Flood Velocity Differences in the Confluence

Figure 3-26. Plan 5 Minus Base Maximum Flood Velocity Differences in the Confluence

Figure 3-27. Base Maximum Ebb Velocities in the Confluence

Figure 3-28. Plan 4 Maximum Ebb Velocities in the Confluence

Figure 3-29. Plan 5 Maximum Ebb Velocities in the Confluence

Figure 3-30. Plan 4 Minus Base Maximum Ebb Velocity Differences in the Confluence

Figure 3-31. Plan 5 Minus Base Maximum Ebb Velocity Differences in the Confluence

Figure 3-32. Base Maximum Flood Velocities in the Turning Basins

Figure 3-33. Plan 4 Minus Base Velocity Differences Maximum Flood in the Turning Basins

Figure 3-34. Plan 5 Minus Base Velocity Differences Maximum Flood in the Turning Basins

Figure 3-35. Base Maximum Ebb Velocities in the Turning Basins

Figure 3-36. Plan 4 Minus Base Velocity Differences Maximum Ebb in the Turning Basins

Figure 3-37 Plan 5 Minus Base Velocity Differences Maximum Ebb in the Turning Basins

Preface

The ship simulator investigation and numerical modeling of hydrodynamic conditions for the Freeport Harbor, Freeport, Texas, as documented in this report were performed for the U.S. Army Engineer District, Galveston (CESWG)

Ms Laura L. Robinson Vera was the CESWG liaison during the study.

The hydrodynamic numerical model study was conducted in the U.S. Army Engineering Research and Development (ERDC), Coastal and Hydraulics Laboratory (CHL) August 2003 to February 2005, under the direct supervision of Messrs. Thomas W. Richardson, Director CHL, Bruce A. Ebersole, Chief, Flood and Storm Protection Division, and Robert T. McAdory, Chief, Estuarine Engineering Branch. The study was performed and the report written by Mrs. Darla McVan, and Messrs. Chris Goodin, Ben Brown, Joseph V. Letter, and William L. Boyt.

At the time of publication of this report, Dr. James R. Houston was Director of ERDC. COL James R. Rowan was Commander of ERDC.

The contents of this report are not to be used for advertising, publication, or promotional purposes. Citation of trade names does not constitute and official endorsement or approval of the use of such commercial products.

Conversion Factors Non-SI to SI Units of Measurement

Non-Si units of measurement used in this report can be converted to SI units as follows:

Multiply	By	To Obtain
Cubic feet	0.02831685	Cubic meters
Fahrenheit degrees	*	Celsius Degrees
feet	0.3048	meters
inches	2.540	centimeters
knots	0.5151	meters per second
microns	0.001	meters
miles (US statute)	1.609344	kilometers (km)
ounces	28.34952	grams
pounds	0.4535924	kilograms
square miles	2.5900	square km
tons (2000 pounds mass)	907.1847	kilograms
* To obtain Celsius © temperature readings from Fahrenheit (F) readings, use the following formula: C = (5/9)(F-32). To obtain Kelvin readings, use: K = (5/9)(F-32) + 273.15.		

1 Introduction

This report describes a numerical hydrodynamic model study of the Freeport harbor conducted to provide current velocity information for a navigation safety study. The navigation safety study was conducted in the ship simulator facility at ERDC to evaluate ship response for the existing and two channel designs proposed by the CESWG.

1.1 Background

Port Freeport is located on the Texas Gulf Coast, approximately 40 miles southwest of Galveston, Texas. The project area is shown in Figure 1. It is presently ranked as the 24th largest port in the United States in terms of total tonnage. Approximately 1,300 vessels call at Port Freeport annually. Most large ship traffic consists of crude or chemical tankers. Containerships call at Port Freeport. The port handles approximately 70,000 Total Equivalent Units (TEUs) annually.

The local Texan sponsor, the Brazos River Harbor Navigation District, is interested in examining the feasibility of improvements to the existing deep draft navigation channel to determine Federal interest in expanding the reach of the navigation channel to the Stauffer Channel and turning basin. The channel carries traffic that could be accommodated much more efficiently with a deeper (50-60 foot) channel. Many of the vessels that currently serve the chemical and oil industry in the area are light-loaded to enable them to operate in the existing channel, resulting in delays at the Stauffer Channel and turning basin.

Freeport Harbor (Figure 2) presently consists of three reaches of different depths. The portion of the entrance channel east of the jetties is 47 ft mean low tide (MLT). The

reach from the western end of the jetties through the Big Bend Channel is 45 ft MLT. The additional two ft depth of the Entrance Channel is to allow for the ship's vertical motion due to waves. The Brazos Harbor approach channel and Brazos Harbor turning basin are 40 ft MLT. The remainder of the channel to the Stauffer turning basin is 25 ft MLT. The tidal range for Freeport Harbor is typically 2 ft.

To accommodate larger, and possibly deeper drafted ships the SWG is presently evaluating several channel designs to widen and/or deepen portions of the harbor. These changes will allow larger tankers to use the harbor as far inland as the upper turning basin and containership traffic to continue into a portion of the channel to Stauffer turning basin

At the request of the SWG, the ERDC CHL proposed a two-dimensional numerical model study, including field data collection, of the Freeport Harbor area to access any effects resulting from the proposed changes to the system.

Freeport LNG has proposed to construct a new LNG terminal at Freeport Harbor. The new terminal would require enlarging and deepening an existing notch in the southwestern corner of the intersection of the deep water navigation channel and the Gulf Intracoastal Waterway (GIWW) and enlarging the turning basin at the intersection to the north of the proposed location. A separate ship maneuvering study was conducted by Waterways Simulation Technology, Inc. at the ERDC to test the safety of ship maneuvering and control in Freeport Harbor. The study concluded that ships could maneuver safely in and around the new LNG facility. The proposed improvement conditions for this study include the development of the LNG facility in conjunction with the channel modifications. Figure 3 shows a schematic of the proposed layout of the new LNG terminal.

1.2 Objective

The primary objective of this model study is to provide accurate and representative current velocity fields for use in the ship simulator for the navigation study. A secondary objective is the development of a tool that can be used to evaluate the general impacts of the design alternative improvements on circulation in the harbor.

1.3 Scope

This report addresses the hydrodynamic model development, verification, and production testing and results.

1.4 Technical Approach

The technical approach for this study was to develop a numerical hydrodynamic model using the TABS-MD modeling system with the Surface-water Modeling System (SMS) as the graphical user interface. The computational mesh was designed to capture all of the major details of the existing and proposed design alternatives.

The numerical model was verified to the field data collected by ERDC during the fall of 2003. The verification was performed by comparing the model to observed water surface elevation fluctuations and to current velocity variations. The current velocity observations were at four ADCP cross sections.

After the model was verified the computational mesh was revised to reflect the two design alternatives. The model was then run for the verification period with each of the two alternatives. The simulations were examined for extreme maximum flood and ebb currents and those conditions provided to the ship simulator for incorporation into the navigation study.

2 Hydrodynamic Model Development

2.1 The TABS-MD Modeling System

The technical approach utilized RMA-2, the TABS-MD depth-averaged numerical hydrodynamic model (US Army Engineer ERDC, 2002). RMA2 is a two-dimensional depth- averaged finite element hydrodynamic numerical model. It computes water surface elevations and horizontal velocity components for subcritical, free-surface two-dimensional flow fields.

RMA2 computes a finite element solution of the Reynolds form of the Navier-Stokes equations for turbulent flows. Friction is calculated with the Manning's or Chezy equation, and eddy viscosity coefficients are used to define turbulence dissipation. Both steady and unsteady (dynamic) problems can be analyzed.

The original RMA2 was developed by Norton, King and Orlob (1973), of Water Resources Engineers, for the Walla Walla District, Corps of Engineers, and delivered in 1973. Further development, particularly of the marsh porosity option, was carried out by King and Roig at the University of California, Davis. Subsequent enhancements have been made by King and Norton, of Resource Management Associates (RMA), and by the Engineer Research and Development Center (ERDC) at the Waterways Experiment Station (WES) Coastal and Hydraulics Laboratory, culminating in the current version of the code supported in TABS-MD.

The program has been applied to calculate water levels and flow distribution around islands, flow at bridges having one or more relief openings, in contracting and

expanding reaches, into and out of off-channel hydropower plants, at river junctions, and into and out of pumping plant channels, circulation and transport in water bodies with wetlands, and general water levels and flow patterns in rivers, reservoirs, and estuaries.

RMA2 is a general-purpose model designed for far-field problems in which vertical accelerations are negligible and velocity vectors generally point in the same direction over the entire depth of the water column at any instant of time. It expects a vertically homogeneous fluid with a free surface.

RMA2 operates under the hydrostatic assumption; meaning accelerations in the vertical direction are negligible. It is two-dimensional in the horizontal plane. It is not intended to be used for near field problems where vortices, vibrations, or vertical accelerations are of primary interest. Vertically stratified flow effects are beyond the capabilities of RMA2. RMA2 is a free-surface calculation model for subcritical flow problems.

Governing Equations

The generalized computer program RMA2 solves the depth-integrated equations of fluid mass and momentum conservation in two horizontal directions. The forms of the solved equations are

$$h\frac{\partial u}{\partial t} + hu\frac{\partial u}{\partial x} + hv\frac{\partial u}{\partial y} - \frac{h}{p}\left[\mathrm{E}_{xx}\frac{\partial^2 u}{\partial x^2} + \mathrm{E}_{xy}\frac{\partial^2 u}{\partial y^2}\right] + gh\left[\frac{\partial a}{\partial x} + \frac{\partial h}{\partial x}\right] + \frac{gun^2}{\left(1.486h^{1/6}\right)^2}\left(u^2 + v^2\right)^{1/2} - \zeta V_a^2\cos\psi - 2hv\omega\sin\Phi = 0 \qquad \textit{Equation 2-1}$$

$$h\frac{\partial v}{\partial t}+hu\frac{\partial v}{\partial x}+hv\frac{\partial v}{\partial y}-\frac{h}{p}\left[\mathrm{E}_{yx}\frac{\partial^2 v}{\partial x^2}+\mathrm{E}_{yy}\frac{\partial^2 v}{\partial y^2}\right]$$
$$+gh\left[\frac{\partial a}{\partial y}+\frac{\partial h}{\partial y}\right]+\frac{gvn^2}{\left(1.486h^{1/6}\right)^2}\left(u^2+v^2\right)^{1/2}$$
$$-\zeta V_a^2\sin\psi+2hu\omega\sin\Phi=0$$

Equation 2-2

$$\frac{\partial h}{\partial t}+h\left(\frac{\partial u}{\partial x}+\frac{\partial v}{\partial y}\right)+u\frac{\partial h}{\partial x}+v\frac{\partial h}{\partial y}=0$$

Equation 2-3

where

h	=	Water depth
u,v	=	Velocities in the Cartesian directions
x,y,t	=	Cartesian coordinates and time
ρ	=	Density of fluid
E	=	Eddy viscosity coefficient,
		for xx = normal direction on x axis surface
		for yy = normal direction on y axis surface
		for xy and yx = shear direction on each surface
g	=	Acceleration due to gravity
a	=	Elevation of bottom
n	=	Manning's roughness n-value
1.48	=	Conversion from SI (metric) to non-SI units
6		
ζ	=	Empirical wind shear coefficient
V_a	=	Wind speed
ψ	=	Wind direction
ω	=	Rate of earth's angular rotation
Φ	=	Local latitude

Equations 1, 2, and 3 are solved by the finite element method using the Galerkin Method of weighted residuals. The elements may be one-dimensional channel reaches, or two-

dimensional quadrilaterals or triangles, and may have curved (parabolic) sides. The shape (or basis) functions are quadratic for velocity and linear for depth. Integration in space is performed by Gaussian integration. Derivatives in time are replaced by a nonlinear finite difference approximation. Variables are assumed to vary over each time interval in the form

$$f(t) = f(t_0) + at + bt^c \qquad t_0 \le t < t_0 + \Delta t \qquad \textit{Equation 2-4}$$

which is differentiated with respect to time, and cast in finite difference form. Variables *a*, *b*, and *c* are constants for a given time step, but change with the solution.

$$f(t) = f(t_0) + \left.\frac{\partial f}{\partial t}\right|_{t_0} (t - t_0) + \frac{(t - t_0)}{c}\left\{\frac{\partial f}{\partial t} - \left.\frac{\partial f}{\partial t}\right|_{t_0}\right\} \qquad \textit{Equation 2-5}$$

The solution is fully implicit and the set of simultaneous equations is solved by Newton-Raphson nonlinear iteration.

The specification of the eddy viscosity in equations 2-1 and 2-2 has been developed based on a non-dimensional Peclet number, the ratio

$$P_e = \frac{\rho\ V\ L}{E_{xx}} \qquad \textit{Equation 2-6}$$

where V is the velocity magnitude and L is the characteristic horizontal dimension of each element. The value of the ratio is assumed to be fixed and the appropriate eddy viscosity computed from the ratio in equation 2-6. This results in a scale dependent eddy viscosity.

SMS, an interactive graphical user interface for TABS-MD, was used extensively for pre- and port- processing during this project.

2.2 Computational Environment

The Freeport channel hydrodynamic modeling for ship simulation was run on the ERDC High Performance Computing (HPC) SGI Origin 3000 (Ruby) parallel processing super computer during the spring and fall of 2004.

2.3 Mesh Development

A numerical computational mesh was developed for each bathymetric condition to which RMA2 was applied. Figure 2-1 presents the overall computational mesh with the Freeport harbor channel and inlet as well as the Brazos River inlet.

Figure 2-2 presents the detailed mesh resolution and the bathymetry color contours in the study area. Figure 4 presents the computational mesh spatial resolution in the study area.

The base geometry for the primary Freeport study area (Figure 2-2) was derived from the fall of 2003 survey conducted by the CHL under the guidance of the SWG. All coordinates were converted with the North American Datum Conversion (NADCON). The National Ocean Service/National Oceanic and Atmospheric Administration (NOAA) nautical chart number 11322 was used extensively for defining bathymetry in areas away from the navigation channels.

The bathymetry data is referenced to mean low tide (MLT). The bathymetry of the model ranges from –94 ft in the Gulf to 0.04 ft in the shallows. All parts of the computational domain remain submerged during the periods of simulation. The lowest water surface elevation in the boundary condition file was approximately +0.5 ft MLT. The existing condition mesh has 2371 elements and 7381 nodes. Approximately 450 elements define the primary study area.

2.5 Hydrodynamic Coefficients

User specified coefficients for the hydrodynamic model, RMA2, include Manning-n values and eddy viscosity. Both were controlled by the element material type (IMAT) descriptor. By grouping elements into 10 different IMAT categories (Figure 2-3), the roughness and viscosity values were easily assigned.

The Peclet number assigned on the PE card can be used as an indicator of numerical stability. A value of 20 or less is typically recommended for numerical stability. A Peclet number of 10 was used for the entire computational domain, and for all hydrodynamic runs; base, plan 4, and plan 5.

Mannings' N values were assigned using the automatic assignment of roughness by depth card, RD.

2.4 Tidal Boundary Conditions

The tide data collected during the field data collection effort during the October of 2003 was used for the development of tidal boundary condition. The locations of the field tide gages are presented in Figure 2-4. The initial model simulations were made with the raw tidal signal from TG 129 as the gulf tidal forcing signal. These simulations proved to yield reasonable water level variations and the currents from those simulations were used in the ship simulator. However, upon more careful analysis of the current velocities it was discovered that the noise in the raw tidal signal, assumed to be associated with local meteorological effects, resulted in erratic current velocities.

The tidal signal was then filtered to remove the short-term fluctuations. The results of the filtering on the tidal boundary signal are shown in Figure 2-5. The filter applied was a band pass filter, which passed periods between 4 and 200 hours. The impact that the filtering of the tidal forcing had on the current velocities is illustrated in Figure 2-6, at a location in the GIWW west of Freeport. The currents generated by use of

the raw tidal signal are very erratic and flip-flop between ebb and flood at period of several hours, especially between model simulation hours 600 to 650. Model hour zero was defined as midnight on 1 October 2003.

The currents generated by use of the filtered tidal signal are much less erratic, but the peak current velocities are somewhat lower than with the unfiltered results. At the times when the currents were supplied to the ship simulator, these differences were not significant. However, when comparing the current velocities from the model to the field observations the use of the filtered results was required.

The cause of the erratic current velocity response is believed to be the result of the creation of an artificial head difference oscillation between the two inlets in the model. With noisy fluctuations in the tidal signal as driven at the gulf boundary of the model (see e.g. hours 610 to 630 in Figure 2-5) and a differential time of tidal propagation to each of the inlets an alternating water level differential was generated in the model. That differential was spurious and in order to obtain reasonable current velocity comparisons the filtered tidal results are used.

2.6 Hydrodynamic Verification

The comparison of the numerical model and the field observations at the three tide gages monitored are shown in Figures 2-7, 2-8 and 2-9 for the full duration of the 1000 hour simulation. The tides at TG 363 in the east GIWW are shown in Figure 2-7. Tide gage 367 at South Freeport is presented in Figure 2-8 and the tides in the entrance channel TG 129 are shown in Figure 2-9. The tidal response is very accurate with the exception of several short periods when there are strong meteorological effects in the tidal signal. The numerical model was not run with wind applied.

The response of the water levels at the same three locations for the period near the collection of the ADCP current velocity profiles are presented in Figures 2-10, 2-11 and 2-12. These also show god agreement between modeled and observed tidal fluctuations.

The locations of the ADCP transects are presented in Figure 2-13. There are transects across the northwest end of the entrance channel (line 2), a composite range across the east GIWW and the DOW channel (line 1), in the western GIWW (line 2) and in the extended channel west to Freeport (line 4). Representative current velocity profiles across each of the transects for a flood and ebb are presented in Figures 2-14 through 2-21. The flood profiles are presented in Figures 2-14 through 2-17. The ebb profiles are presented in Figures 2-18 through 2-21. These show that the only field profile with a clear consistent coherent lateral distribution is line 2, in the entrance channel. The remaining profiles show considerable scatter. The model agrees reasonably well in the entrance channel and lies within the scatter for the remaining profiles.

3 Production Testing and Results

3.1 Design Alternatives

For this study there were three meshes; existing condition (base), Plan 4, and Plan 5. Each of these has the same computational domain, but differ only in the design definition of the Freeport channel width, depth, and turning basin. The bathymetry for the base condition is presented in Figure 3-1, showing the full length of the navigation channel to deep water. The details of the base bathymetry in the study area were presented in Figure 2-2. The full channel bathymetry for the Plan 4 and Plan 5 alternatives are presented in Figures 3-2 and 3-3.

. The proposed Plan 4 channel design is presented in Figure 3-4. The details of the Plan 4 mesh resolution and bathymetry are presented in Figure 3-5. The proposed Plan 5 channel design is presented in Figure 3-6. The details of the Plan 4 mesh resolution and bathymetry are presented in Figure 3-7. The only difference between the two alternatives was in the size of the turning basin; 1350 ft for Plan 4 and 1100 ft for Plan 5. Both of the plan alternative meshes had 2528 elements and 7778 nodes.

3.2 Procedures

The plan channel design simulations followed the same procedures as outlined for the hydrodynamic model verification**.** Results from the existing condition geometry using the October 2003 bathymetry survey data were compared with the two proposed plan design conditions for evaluation of impacts.

Water surface elevation time history plots for base, plan 4, and plan 5 simulations are presented for the following seven selected stations (see Figure 3-8); the entrance

channel, the GIWW east, the GIWW west, the lower turning basin north, the lower turning basin south, the upper turning basin east, and the upper turning basin west. Figure 3-8 shows these seven base node locations.

3.3 Tidal Elevation Comparisons

Base, Plan 4, and Plan 5 water surface elevation time history comparison plots are shown in Figures 3-9 through 3-15 for these seven locations. The effects of the channel deepening were to have the tidal signal arrive slightly sooner (about 30 minutes) for the alternatives over the base. The tide range was increased very slightly, by only about 0.3 percent, based on a comparison of an RMS for the entire simulation period. That increase was consistent throughout the study area. There is no discernable differences between the two plans for the tidal response.

3.4 Current velocity comparisons

Current velocity patterns are compared between the base and plans for three detailed plot windows: entrance channel, the confluence of the GIWW and the Freeport channel, and the upper turning basin and channel area. Comparisons are made for a peak flood and a peak ebb corresponding to the times when currents were provided to the ship simulator.

The currents in the entrance channel area for the base condition for the strength of flood are presented in Figure 3-16. Because the vector patterns for the plans are very similar to the base and difficult to compare to the base, the differences in the velocity magnitude between the plans and the base are presented in Figures 3-17 and 3-18 for Plans 4 and 5, respectively. These show that the deepening of the channel results in a reduction in currents of as much as 0.2 fps in the western side of the channel, with a small localized increase of 0.1 fps on the eastern flank of the channel.

The currents in the entrance channel area for the base condition for the strength of ebb are presented in Figure 3-19. Similarly, the plan differences from the base for the strength of ebb are presented in Figures 3-20 and 3-21. These show a greater reduction in ebb current magnitudes than seen on flood. There is no discernable difference, however, between the two design alternatives.

The base flood current patterns for the confluence area are presented in Figure 3-22. The current patterns for the two alternatives on flood are presented in Figures 3-23 and 3-24 for Plans 4 and 5, respectively. These patterns are presented because of the LNG facility changes in the shoreline. It can be seen that the circulation pattern qualitative differences are localized to the LNG expansion. The contours of current velocity magnitude differences are presented in Figures 3-25 and 3-26. These show that the currents are reduced most dramatically at the gulfward limit of the LNG expansion. The current velocities are increased slightly in the GIWW east.

The same series of data presentations are made for the ebb currents in Figures 3-27 through 3-31. These also show reductions in the currents at the eastern end of the LNG expansion. And increases in the eastern GIWW. The eddy that forms just off the edge of the confluence of the GIWW on the east side of the GIWW and the north side of the entrance channel is more pronounced in the plans than the base. This appears to be associated with the ebbing currents from the GIWW east having room for a broader turn into the entrance channel

The peak flood base currents for the upper turning basins are presented in Figure 3-32. The differences in the velocity magnitude between the plans and the base for peak flood are presented in Figures 3-33 and 3-34 for Plans 4 and 5. The same sequence of data plots are presented for peak ebb currents in Figures 3-35 through 3-37. These show that the currents in the upper portion of the system are already relatively low so that the changes are generally very low. The exception is in the end of the GIWW west that appears to be influenced by the larger turning basin in the Plan 4 results.

4 Summary and Conclusions

The results of the numerical modeling presented here result in the following conclusions:

1. The numerical model is reasonably verified against field observations to make it a valuable tool in the evaluation of circulation effects associated with design alternatives as considered in this study
2. The impact of the deepening of the navigation channel to 60 feet will have a slight effect on the phasing f the tides and only a minor increase in the tide range.
3. The effects of the deepening on circulation is generally to reduce the current velocities in the navigation channel.
4. Changes in the phasing of the tide and the efficiency of evacuating the tidal prism can lead to changes in current velocities in the GIWW adjacent to the deepened channel.

References

US Army Engineer Research and Development Center, 2003, " Users Guide to RMA2-WES Version 4.5," Coastal and Hydraulics Laboratory, Vicksburg, MS.

Norton, W. R., King, I. P. , "Operating Instructions for the Computer Program RMA-2V", February 1997, Resource Management Associates, Lafayette, CA

Norton, W. R., I. P. King, and G. T. Orlob, "A Finite Element Model for Lower Granite Reservoir," prepared for the Walla Walla District, U.S. Army Corps of Engineers, Walla Walla, WA, 1973.

Figures 1-53

Figure 1-1. Freeport Harbor Location Map.

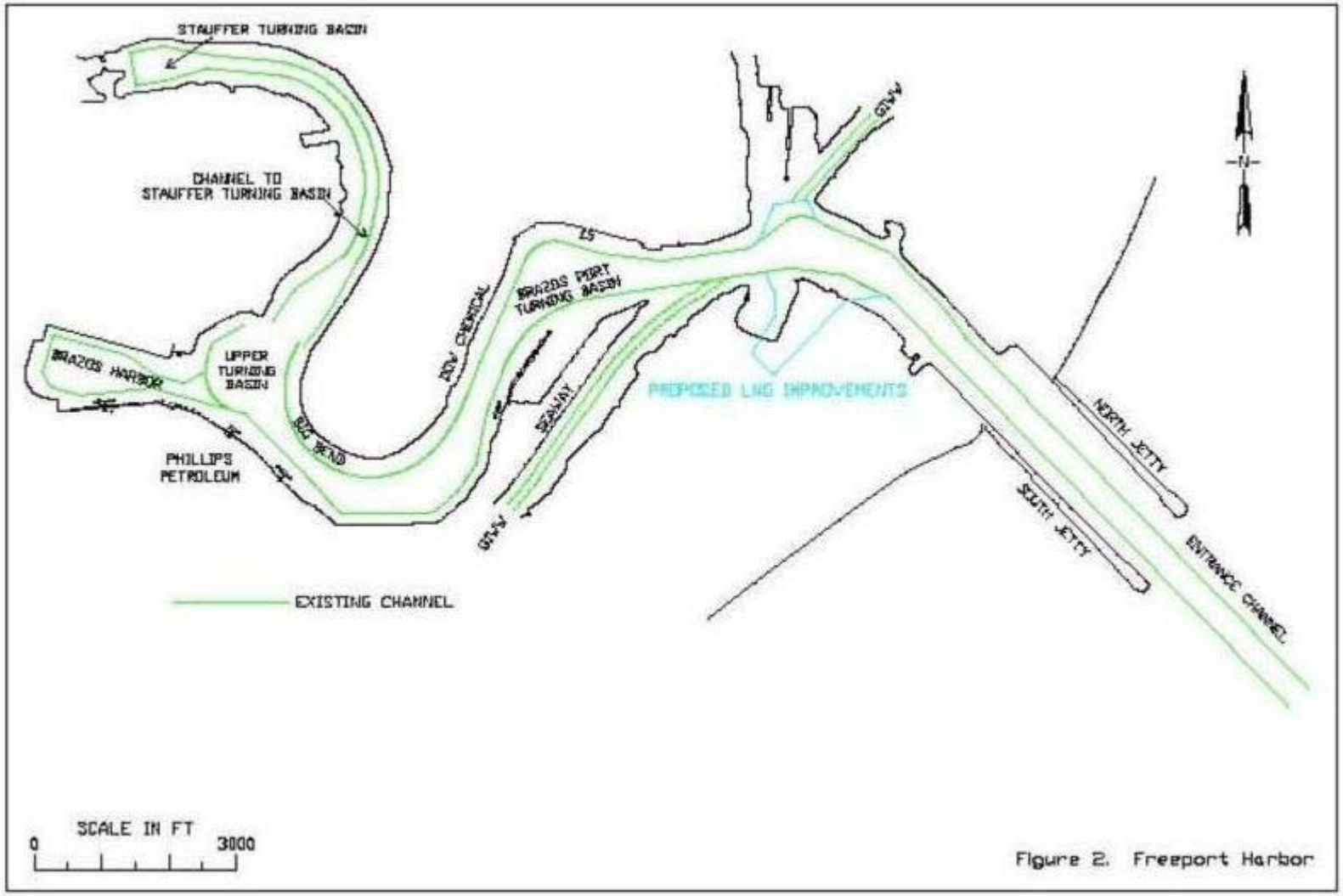

Figure 1-2. Freeport Harbor Three Reaches of Different Depths

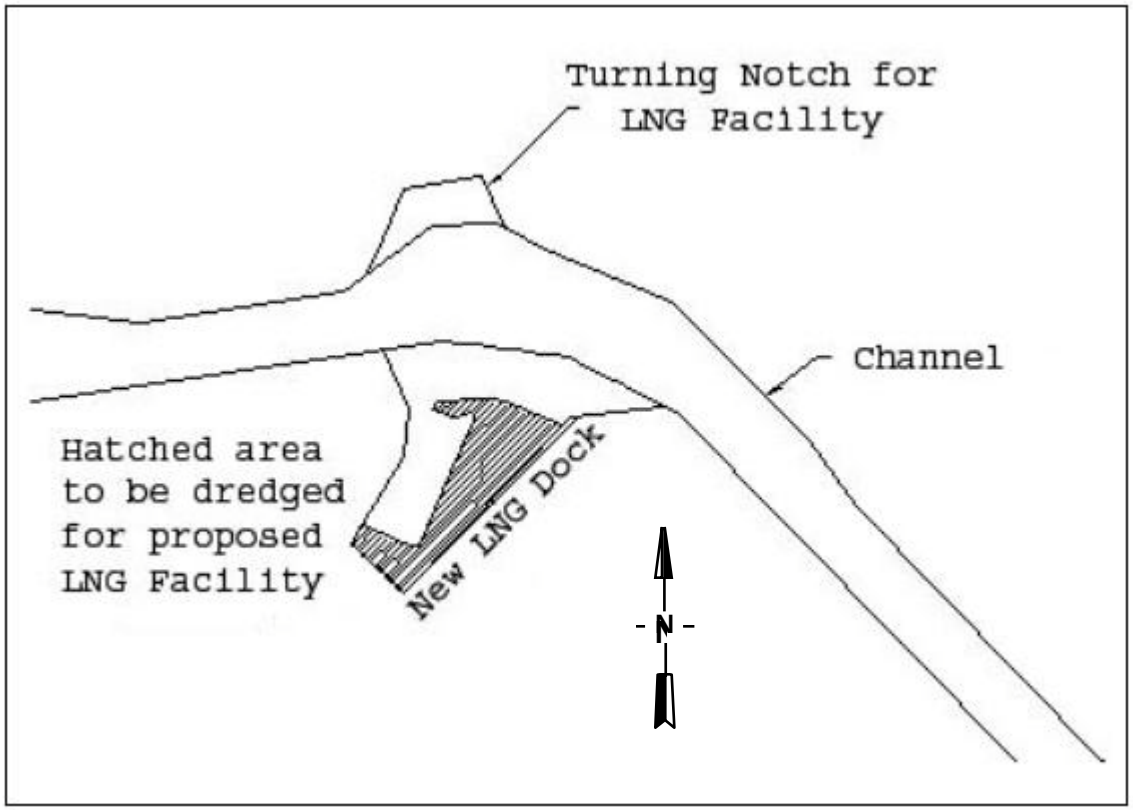

Figure 1-3. Layout of Proposed LNG Terminal

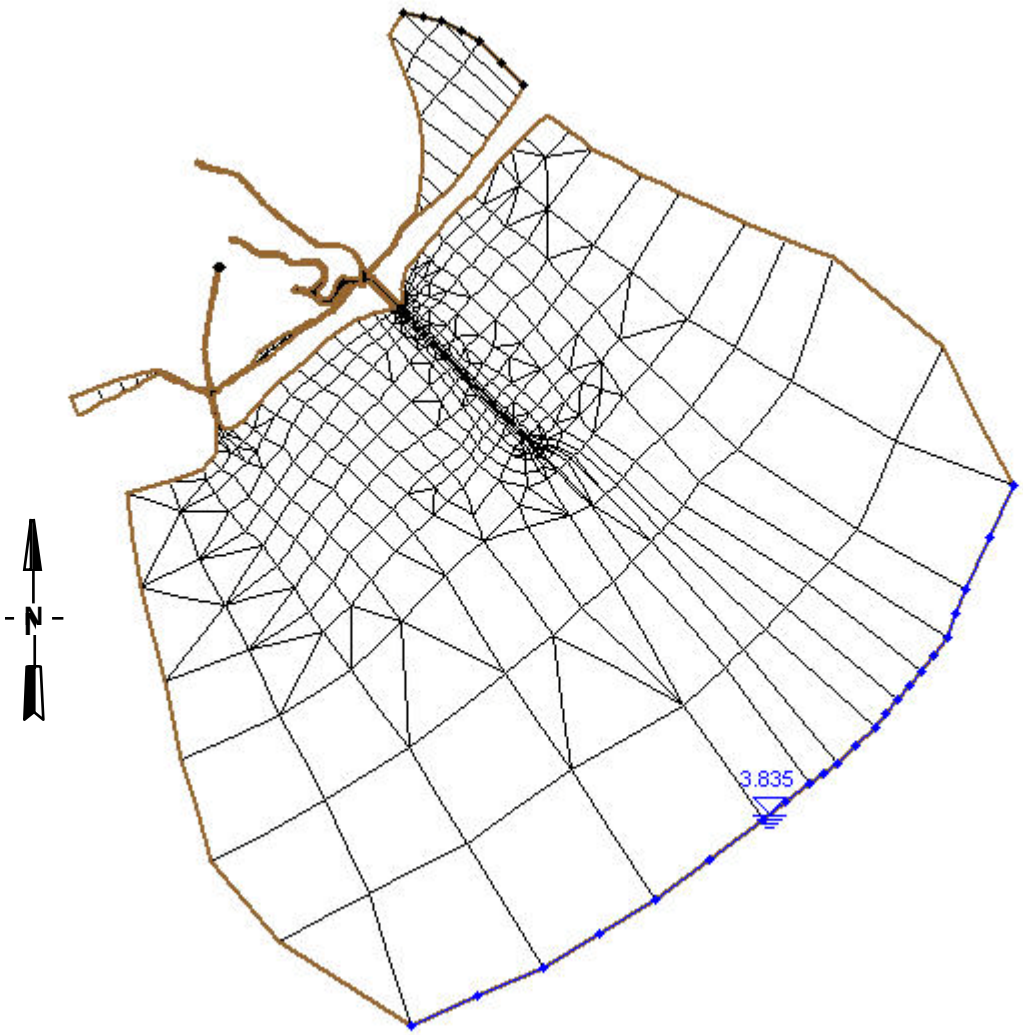

Figure 2-1. Ocean Boundary and Computational Mesh

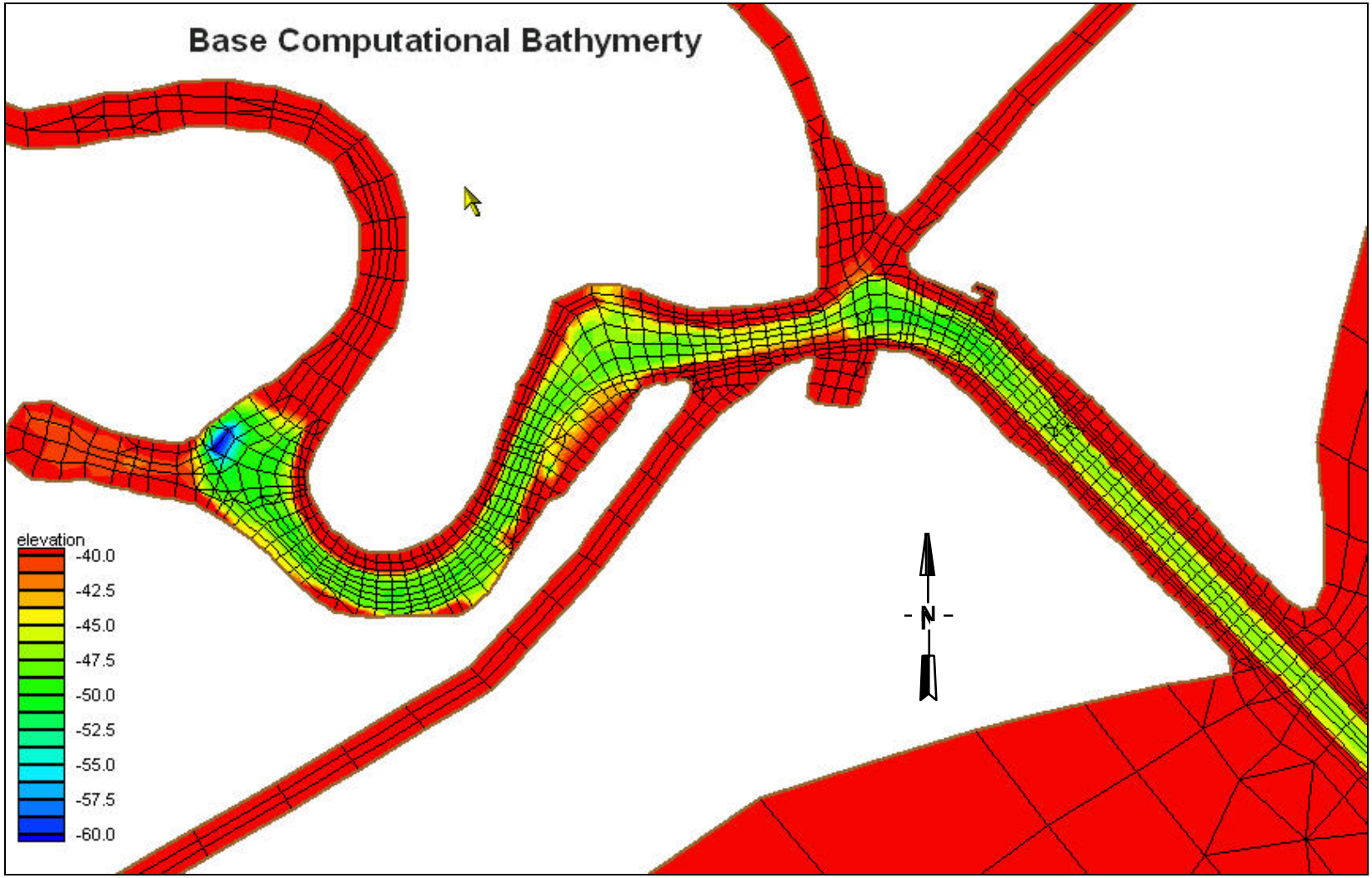

Figure 2-2. Base computational mesh and bathymetry in study area

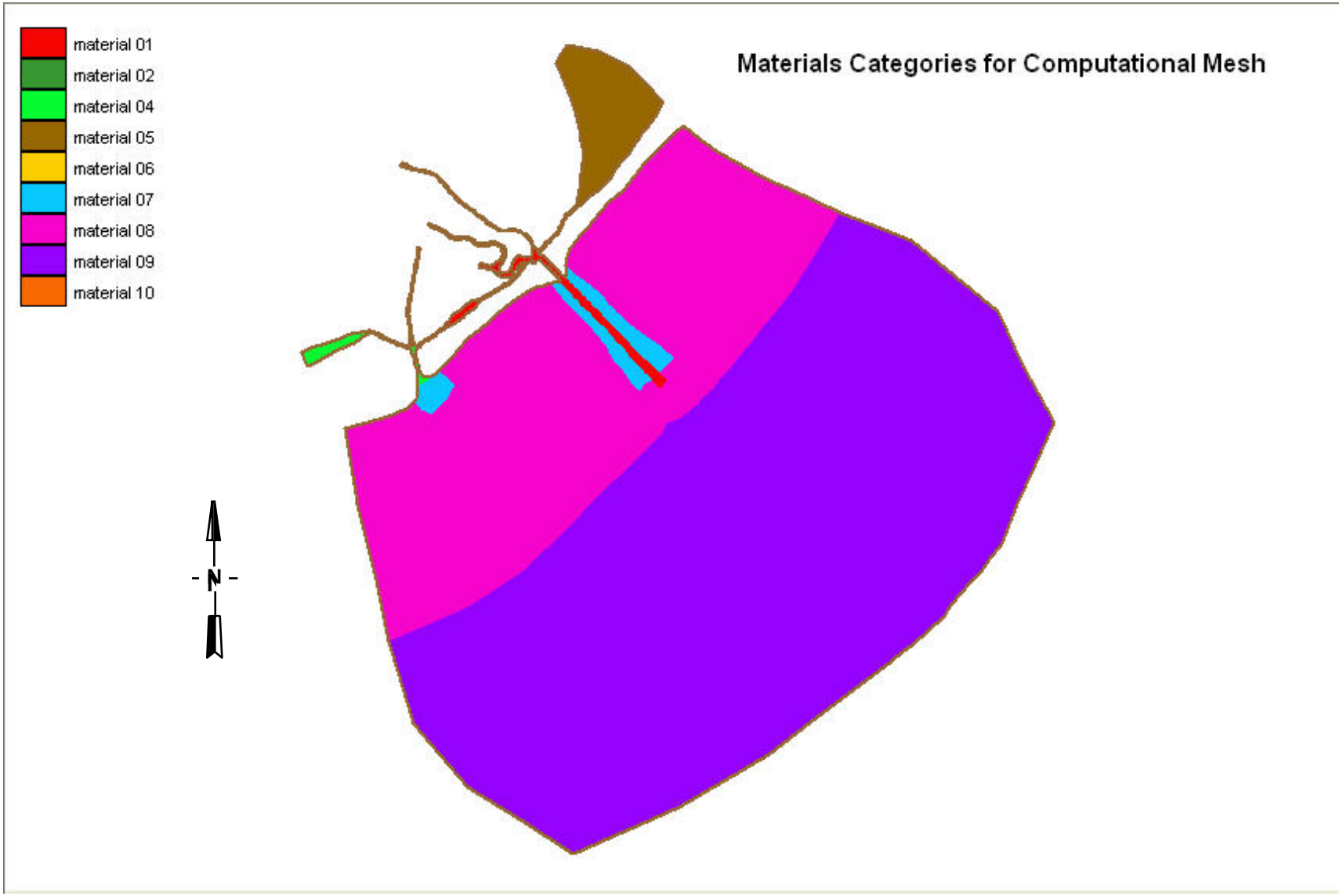

Figure 2-3. Materials Categories in the Computational Mesh

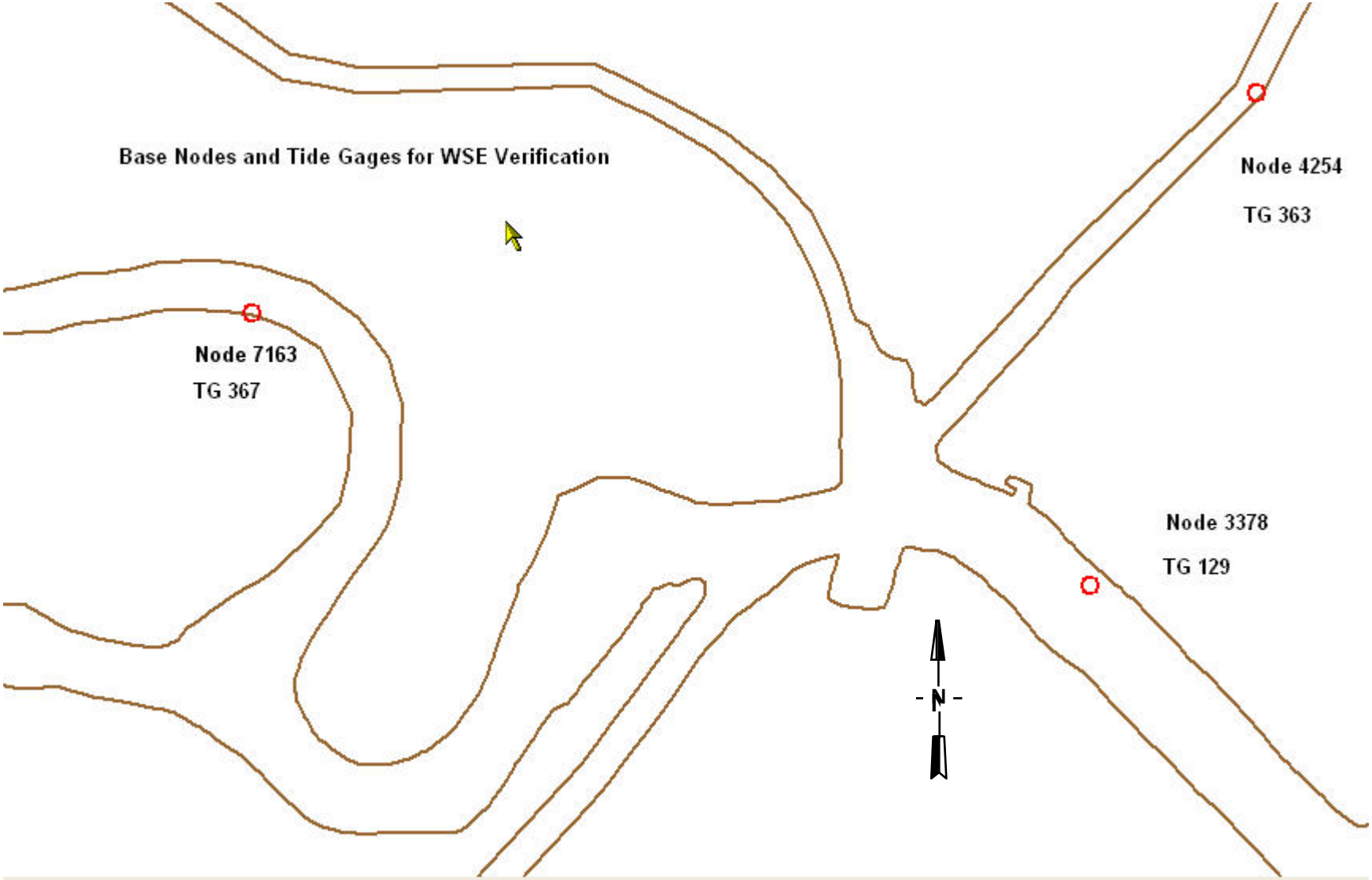

Figure 2-4. Base Nodes at Tide Gage Locations for Water Surface Elevation Verification

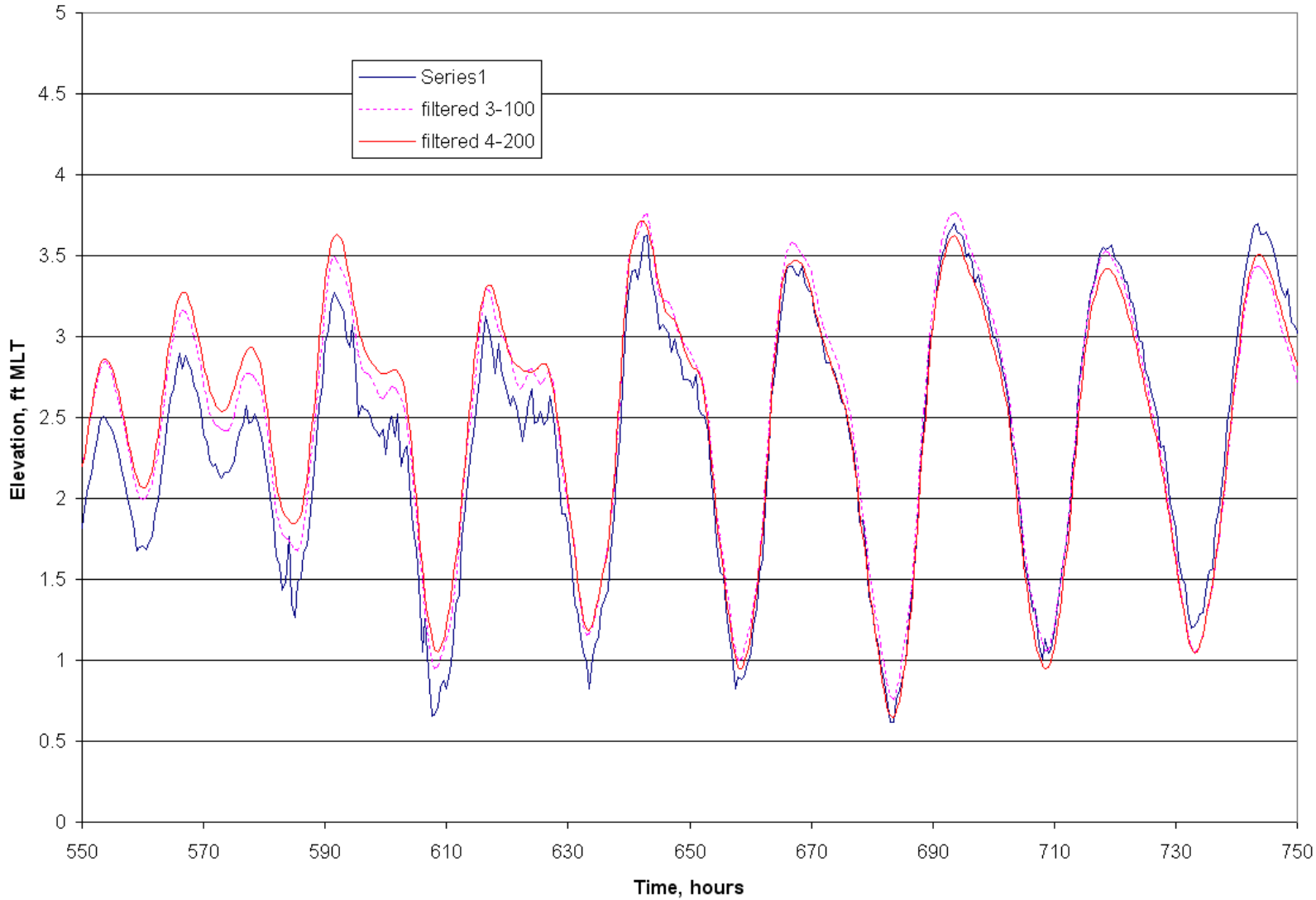

Figure 2-5. Filtering of the boundary condition tide from Freeport gage.

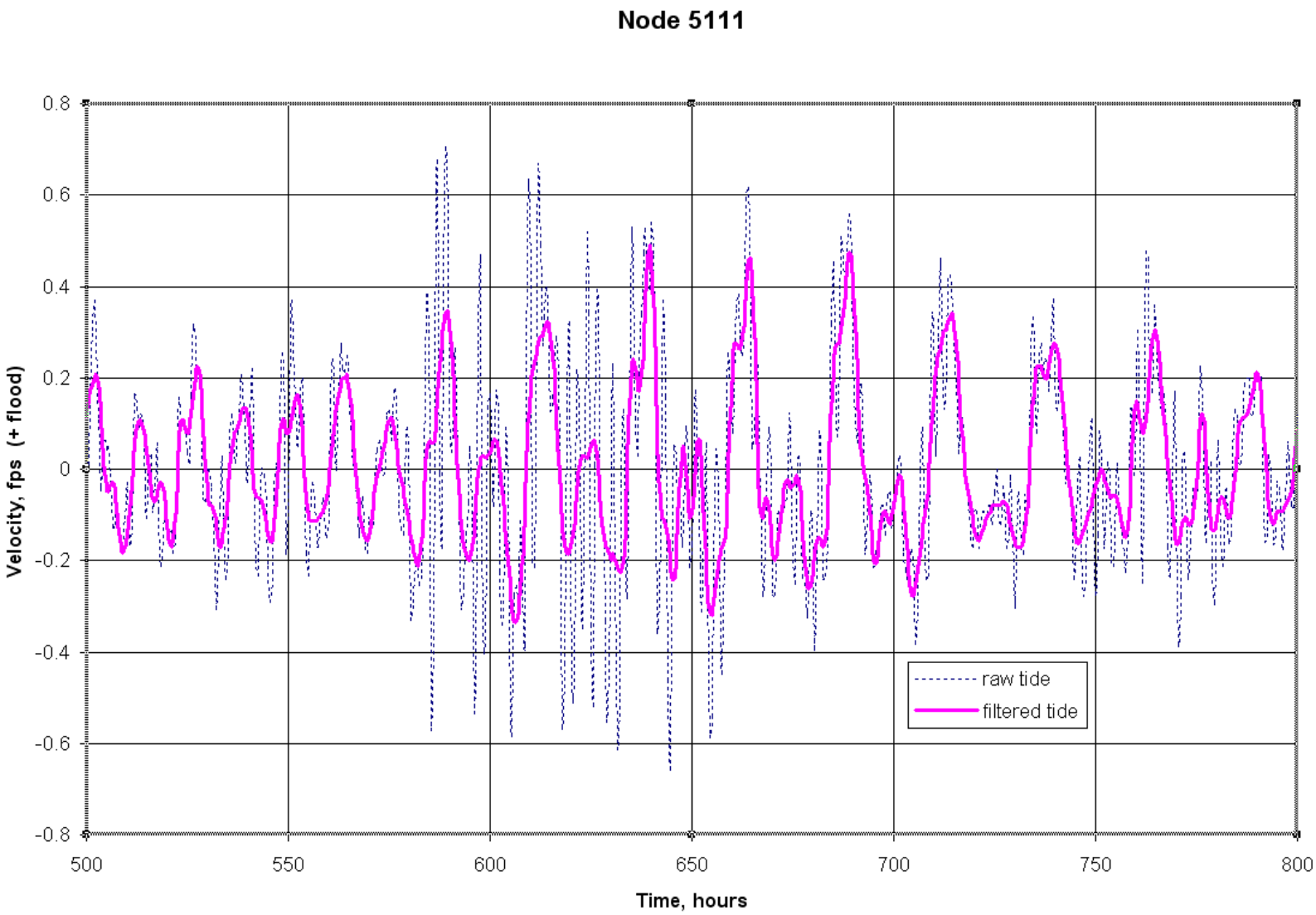

Figure 2-6. Effect of filtering boundary condition tide on current velocities in GIWW west of Freeport

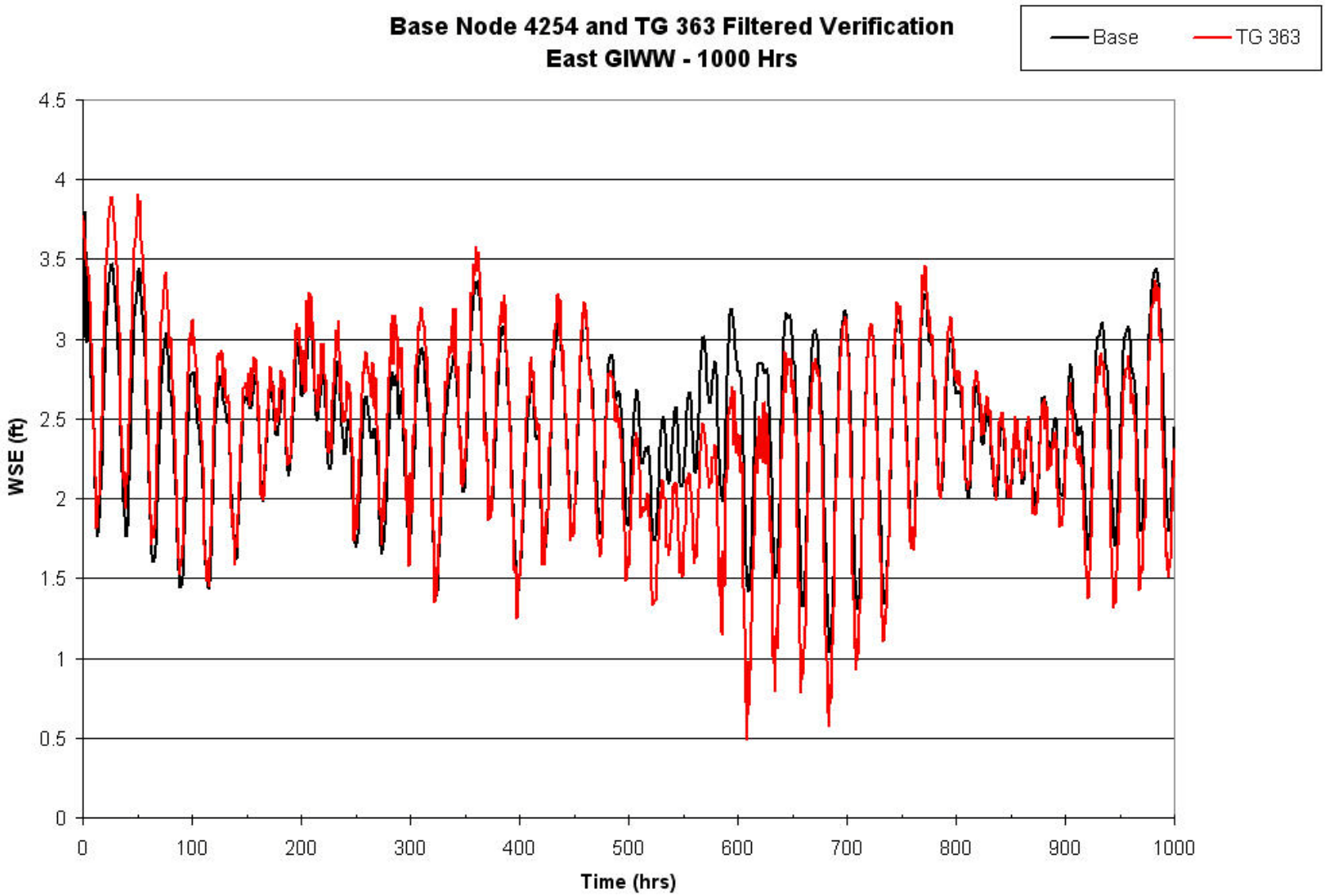

Figure 2-7. Base Node 4254 and TG 363 East GIWW Water Surface Elevation – 1000 hrs

-

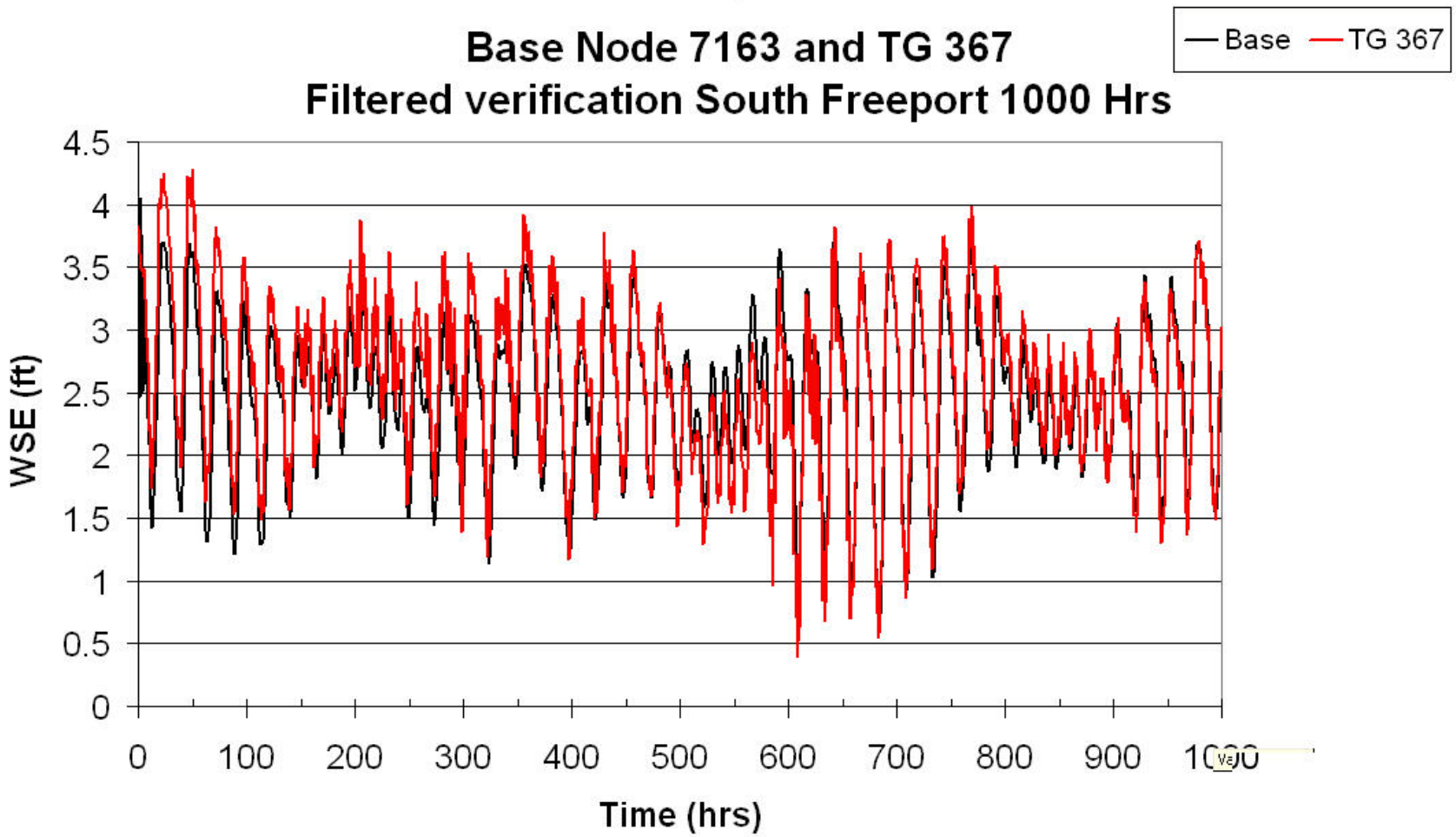

Figure 2-8. Base Node 7163 and TG 367 South Freeport Water Surface Elevation – 1000 hr

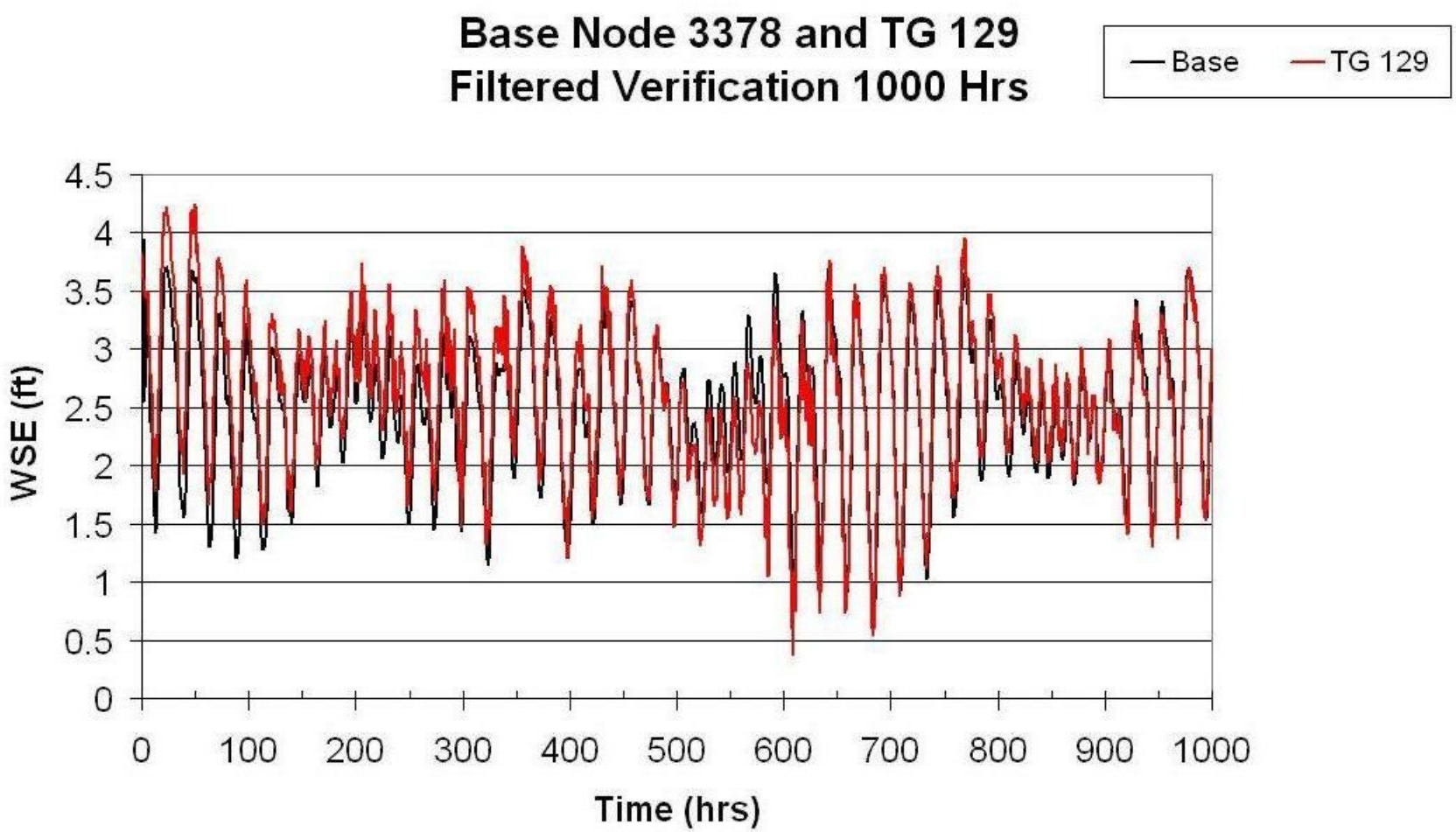

Figure 2-9. Base Node 3378 and TG 129 Entrance Channel Water Surface Elevation – 1000 hrs

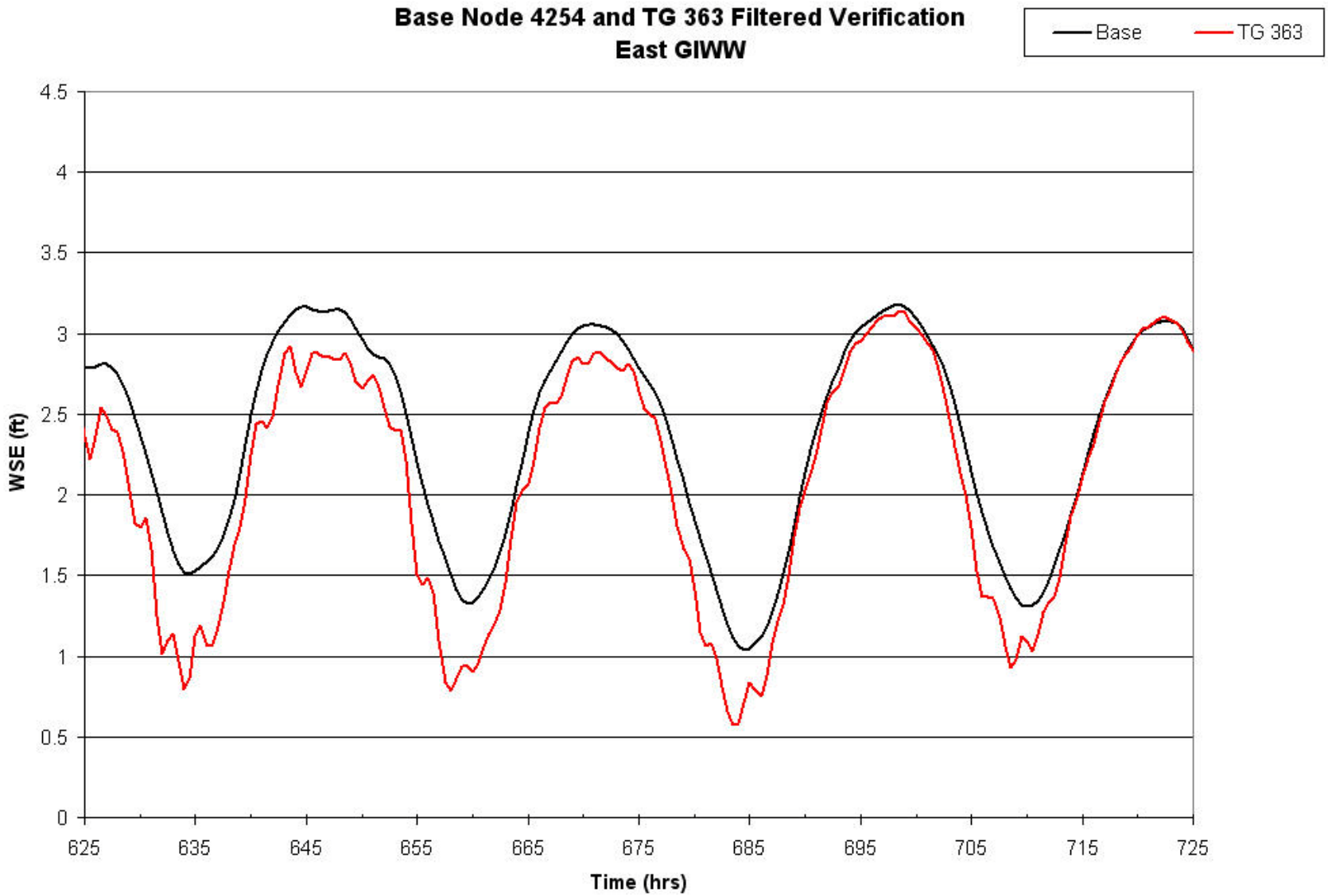

Figure 2-10. Base Node 4254 and TG 363 South East GIWW Water Surface Elevation

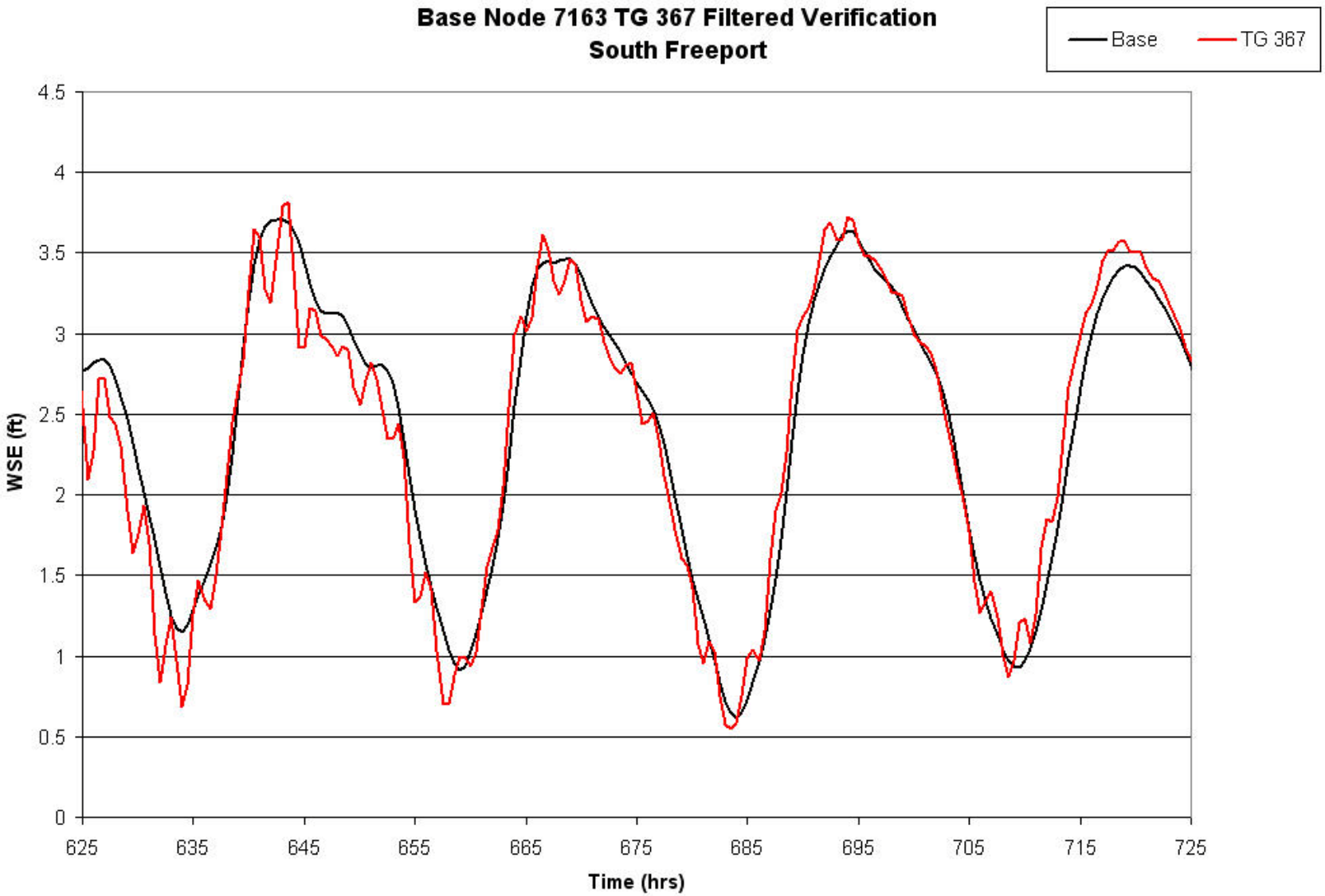

Figure 2-11. Base Node 7163 and TG 367 South Freeport Water Surface Elevation

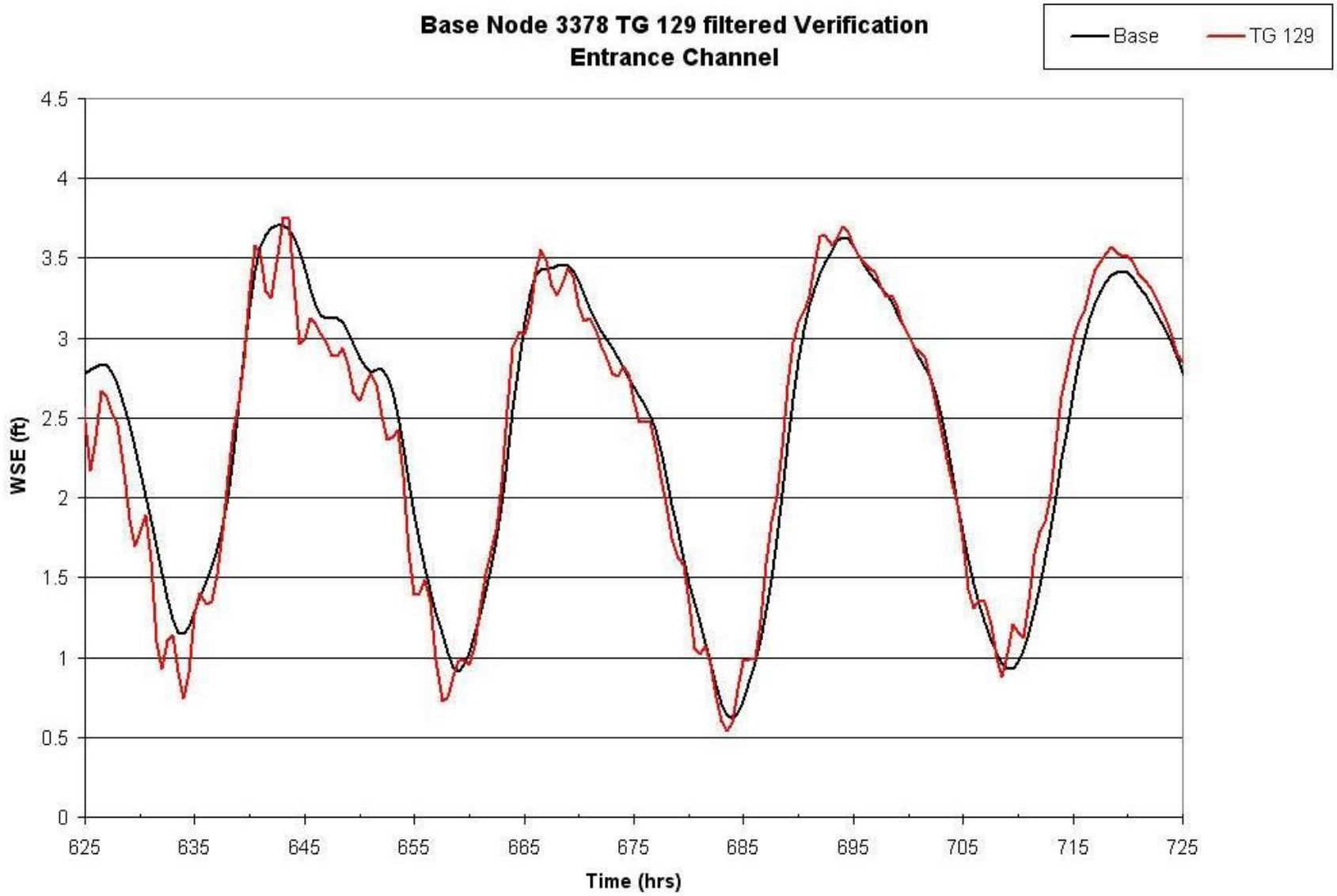

Figure 2-12. Base Node 3378 and TG 129 Entrance Channel Water Surface Elevation

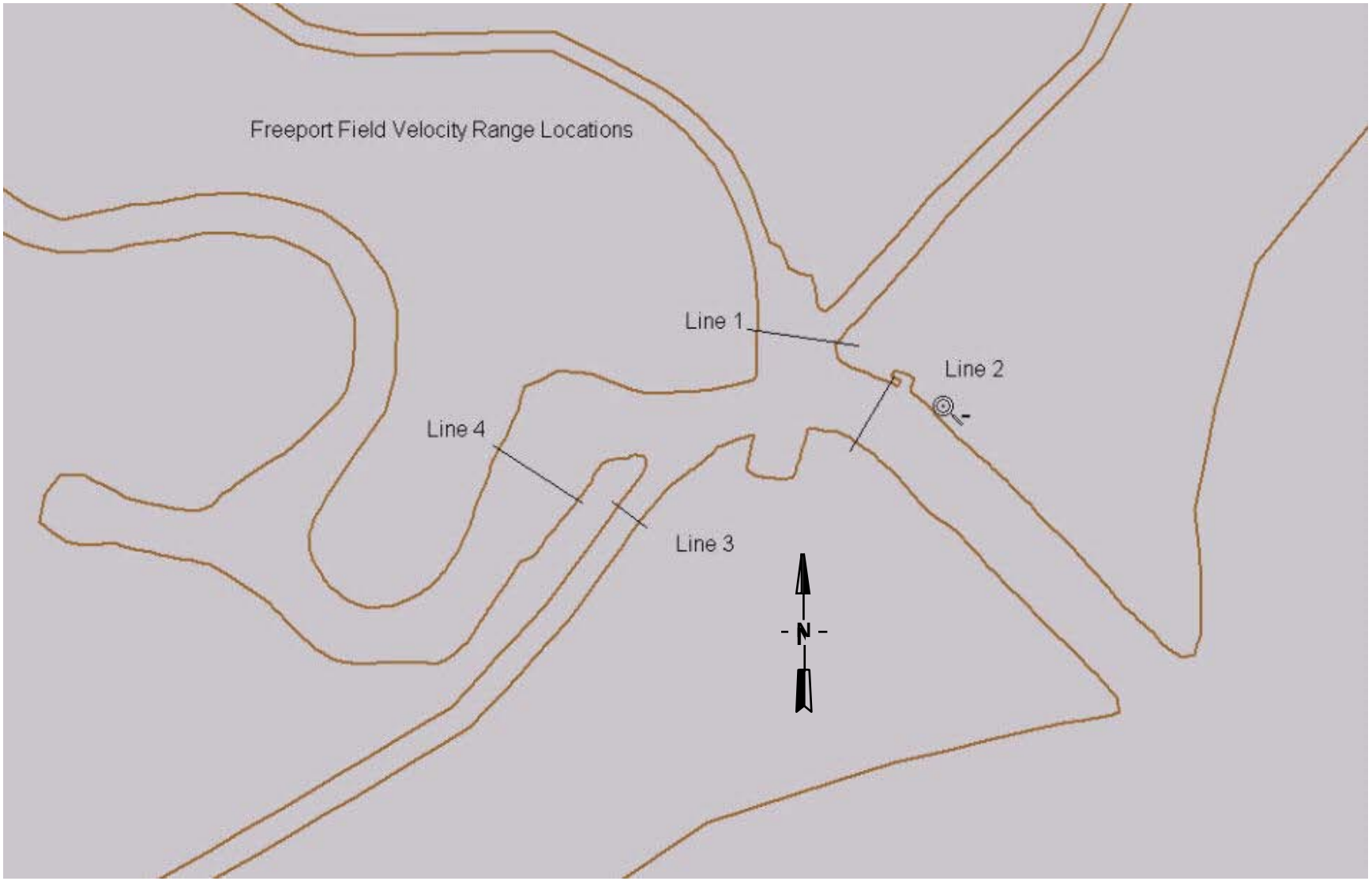

Figure 2-13. Location Map for the Field Velocity Ranges

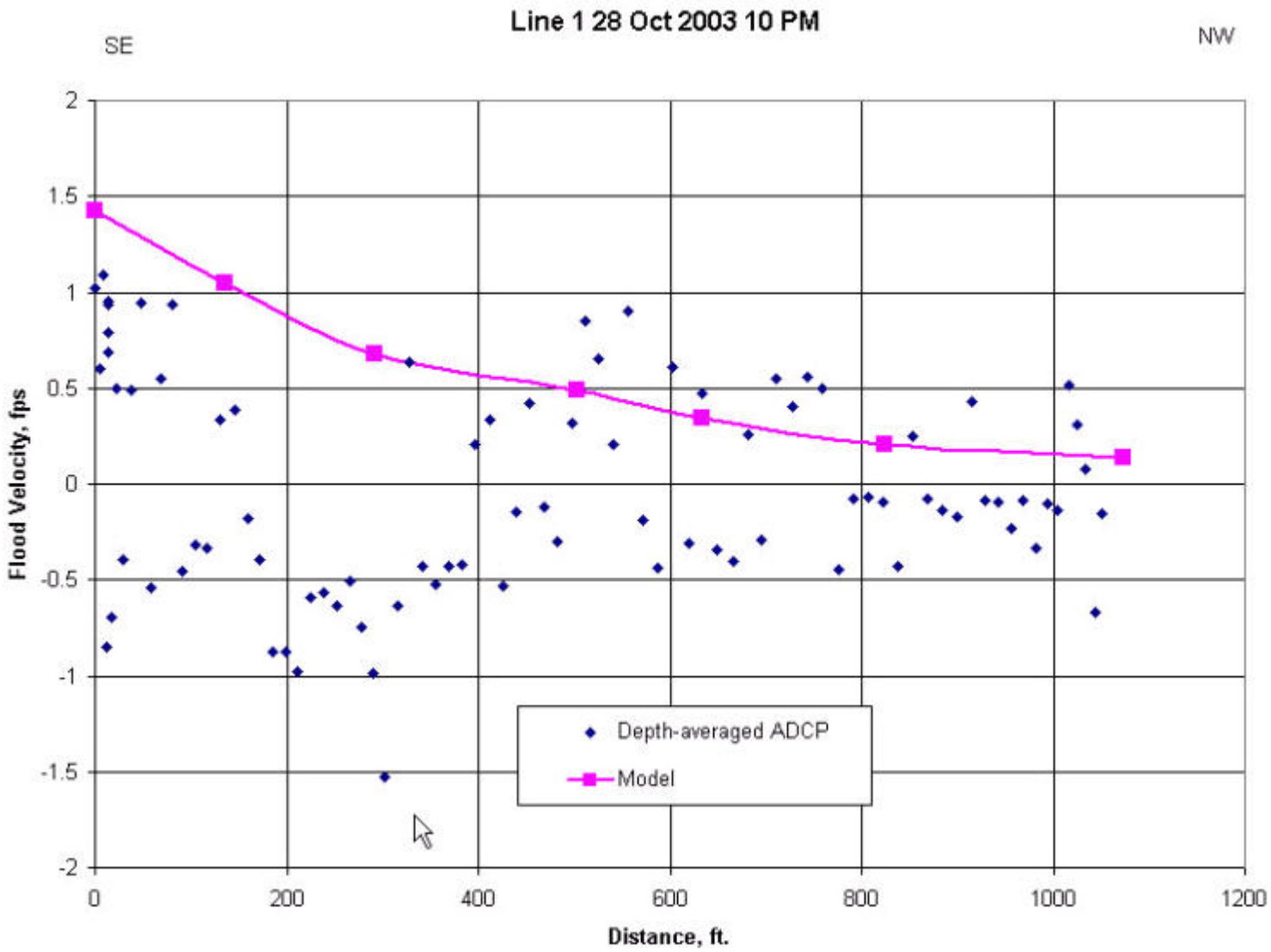

Figure 2-14. Maximum Flood Velocity Line 1

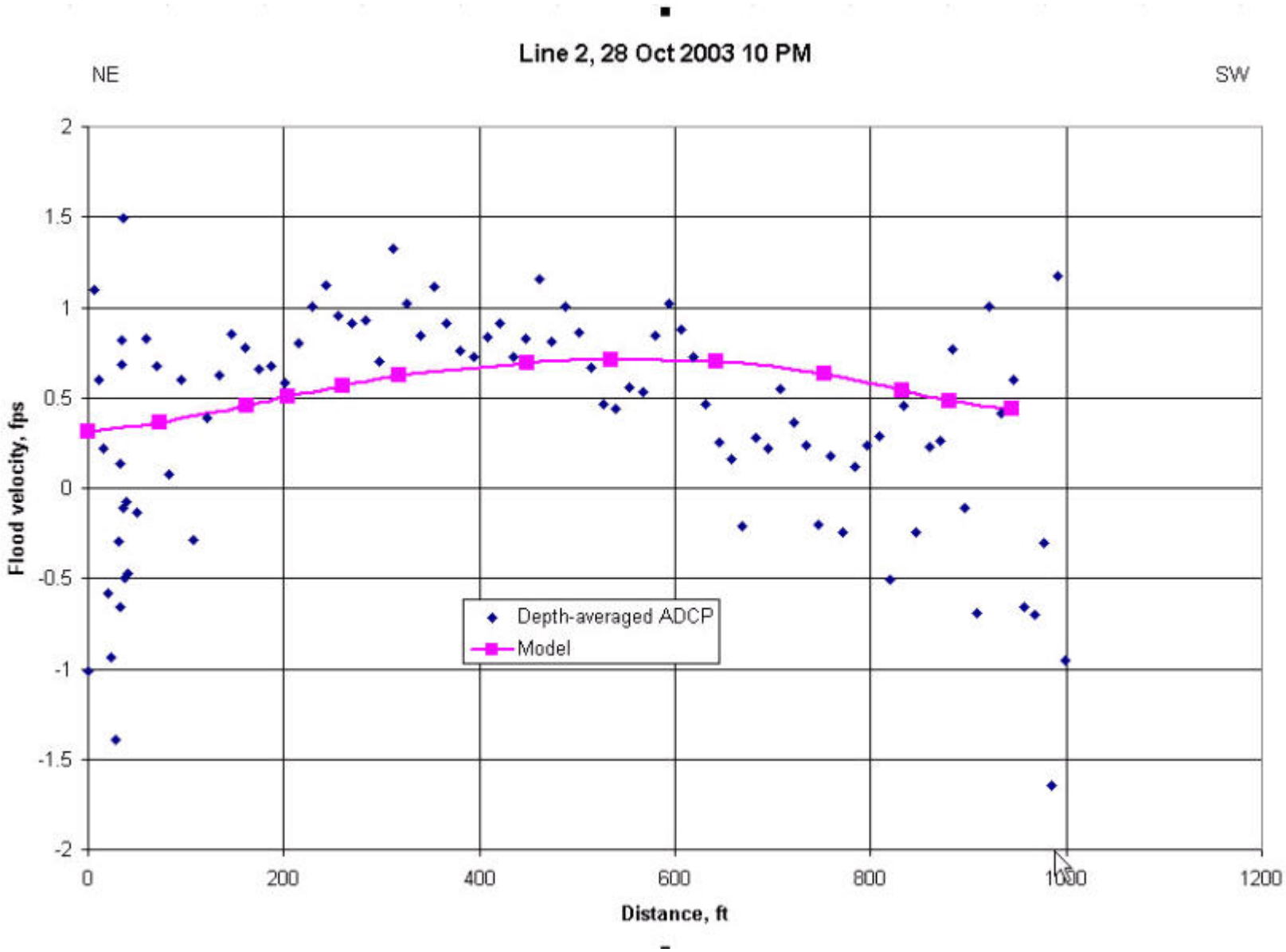

Figure 2-15. Maximum Flood Velocity Line 2

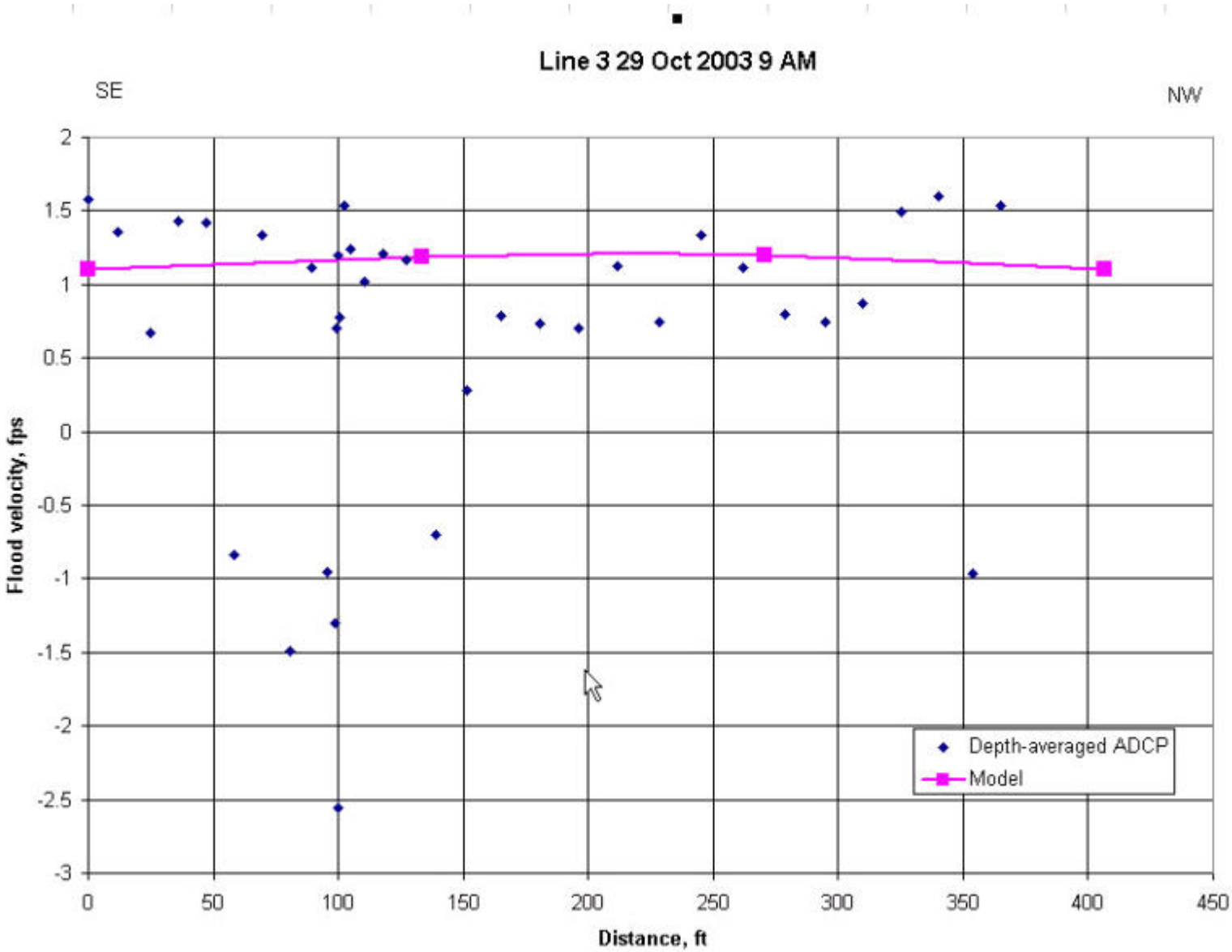

Figure 2-16. Maximum Flood Velocity Line 3

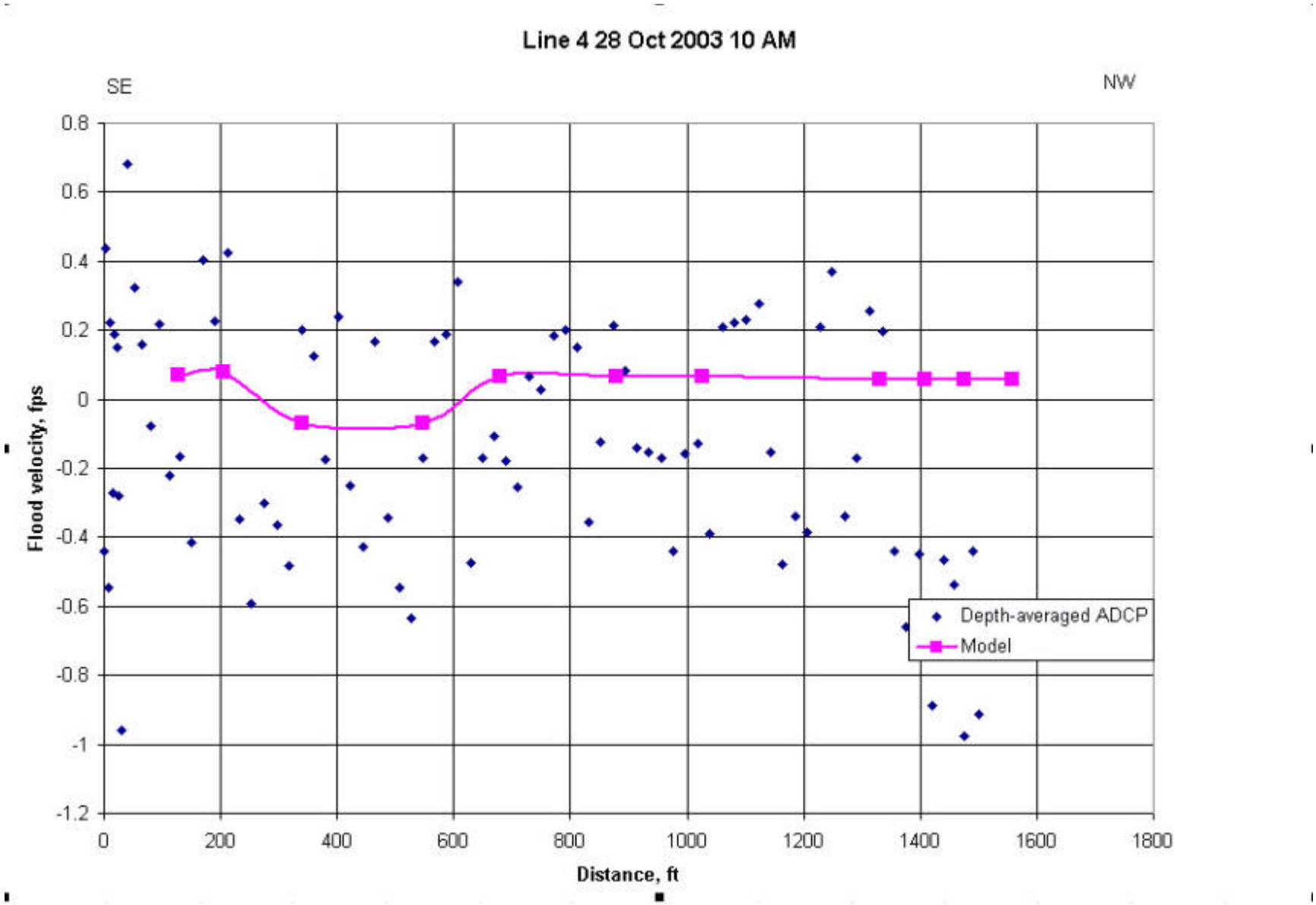

Figure 2-17. Maximum Flood Velocity Line 4

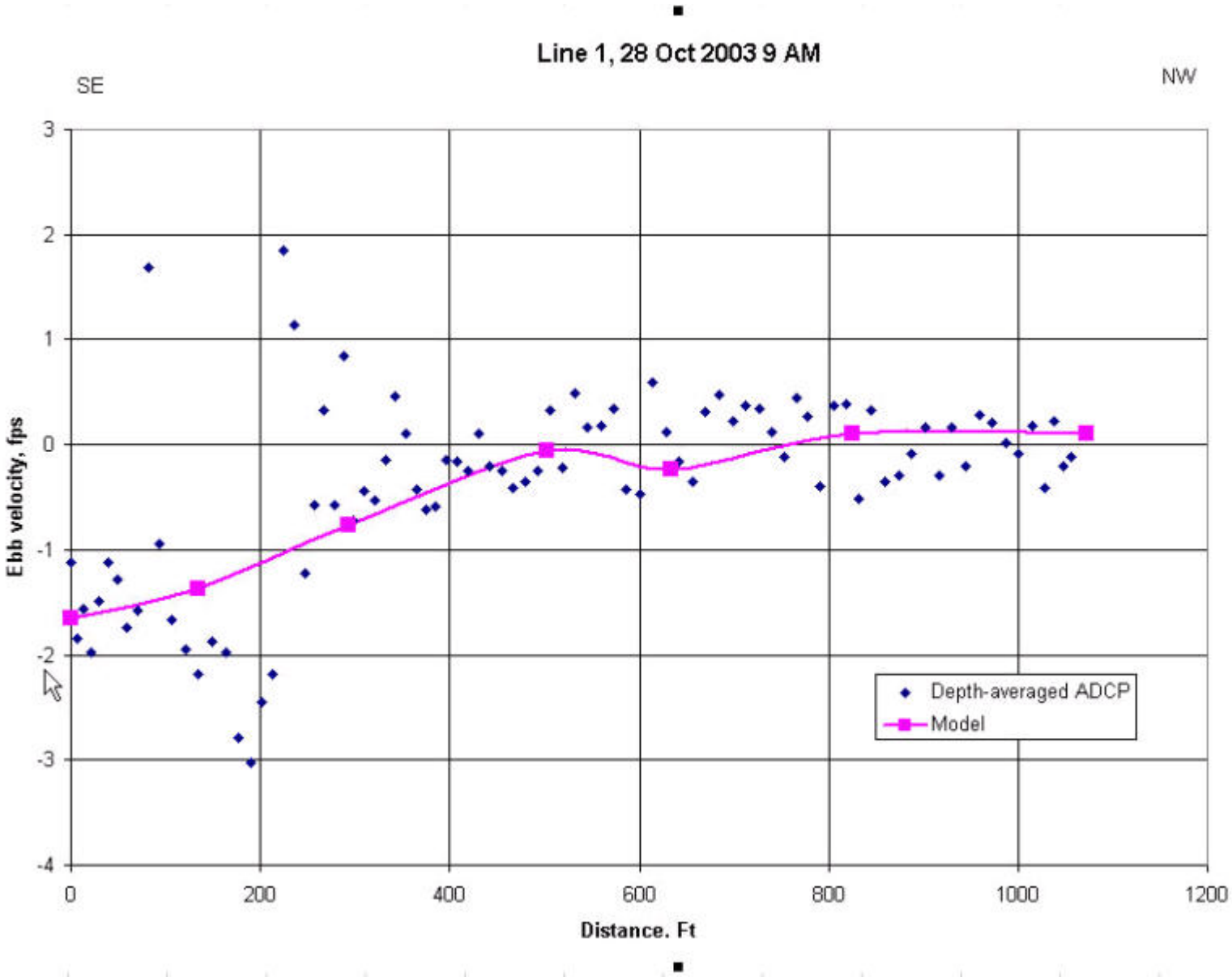

Figure 2-18. Maximum Ebb Velocity Line 1

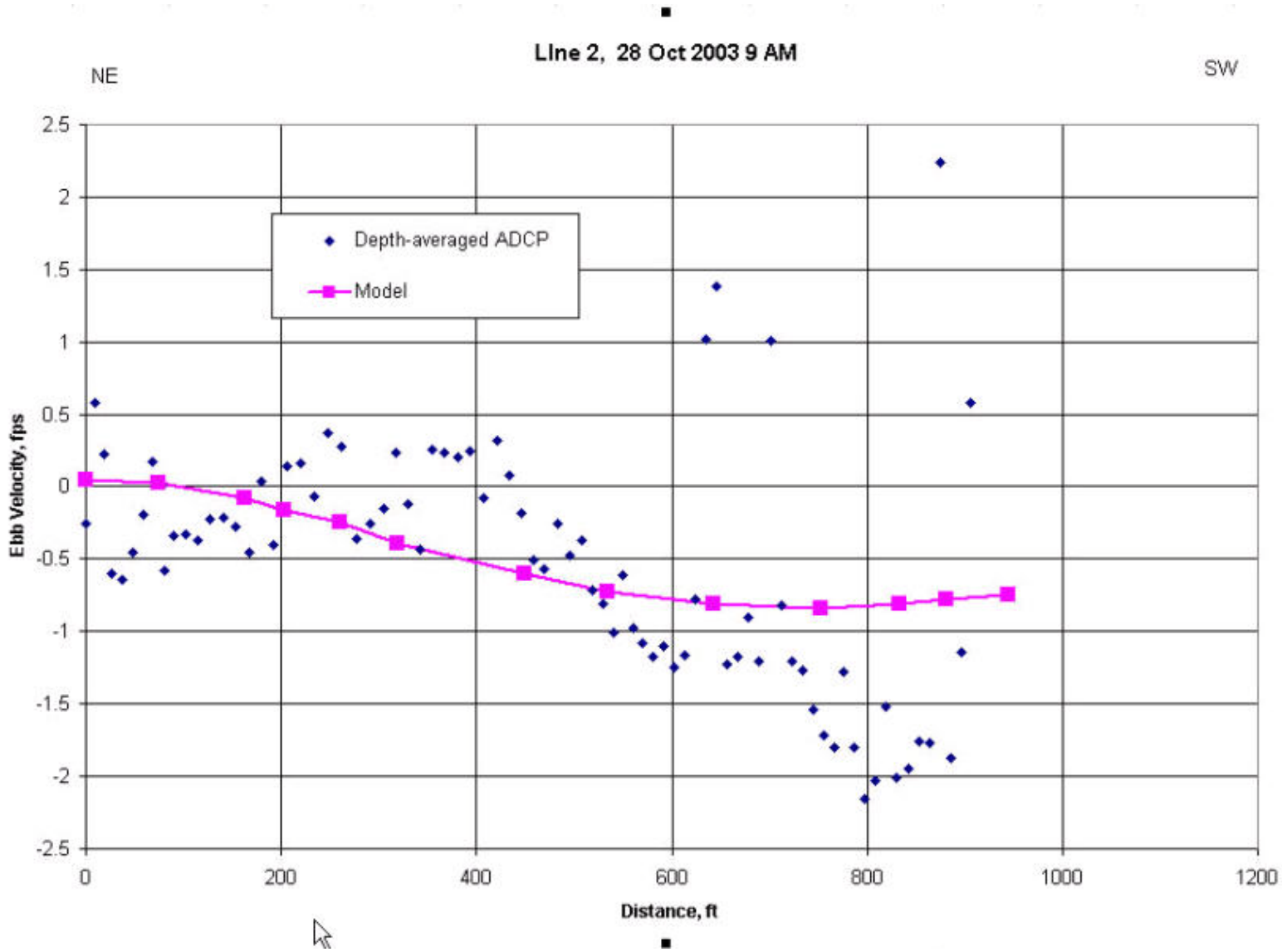

Figure 2-19. Maximum Ebb Velocity Line 2

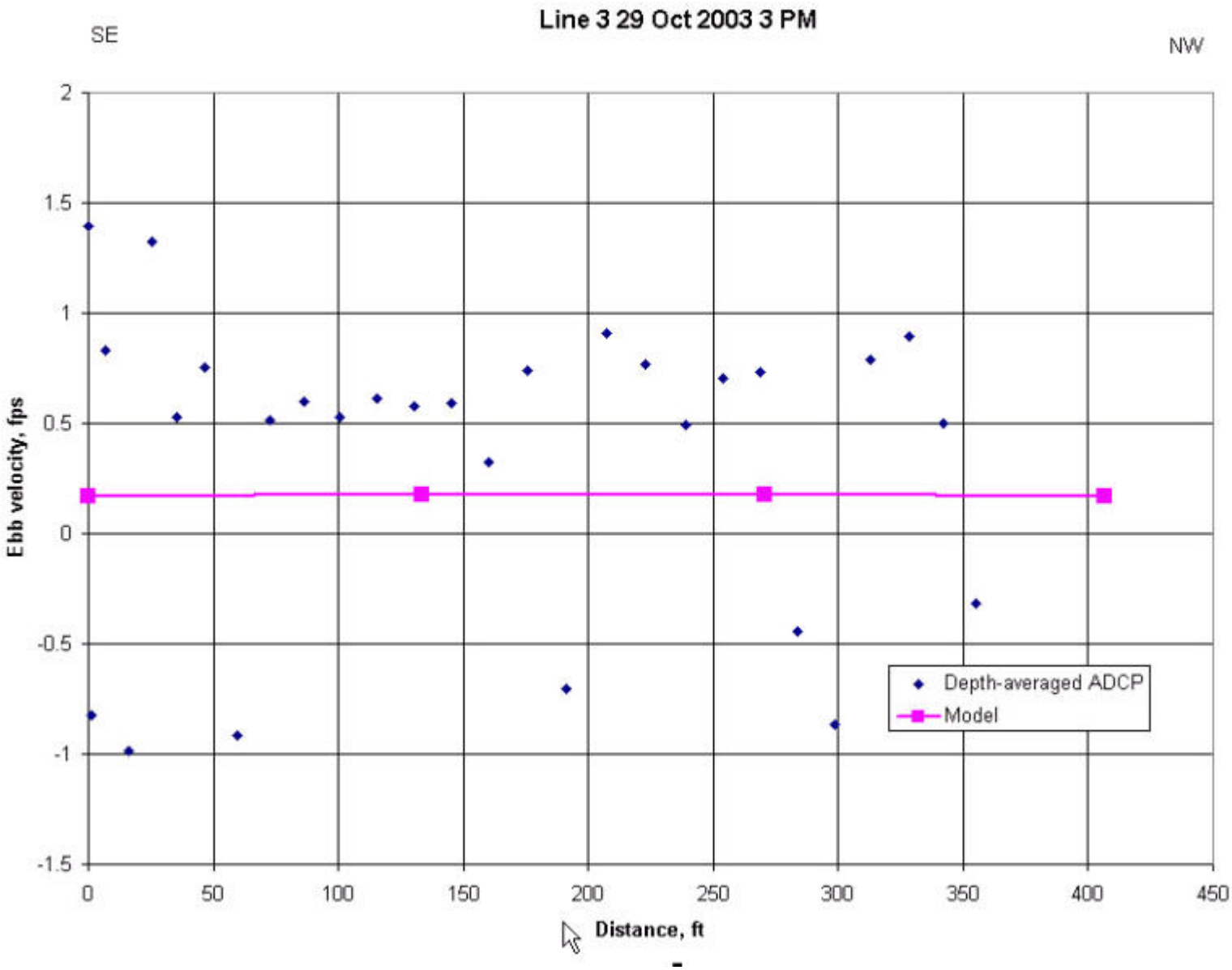

Figure 2-20. Maximum Ebb Velocity Line 3

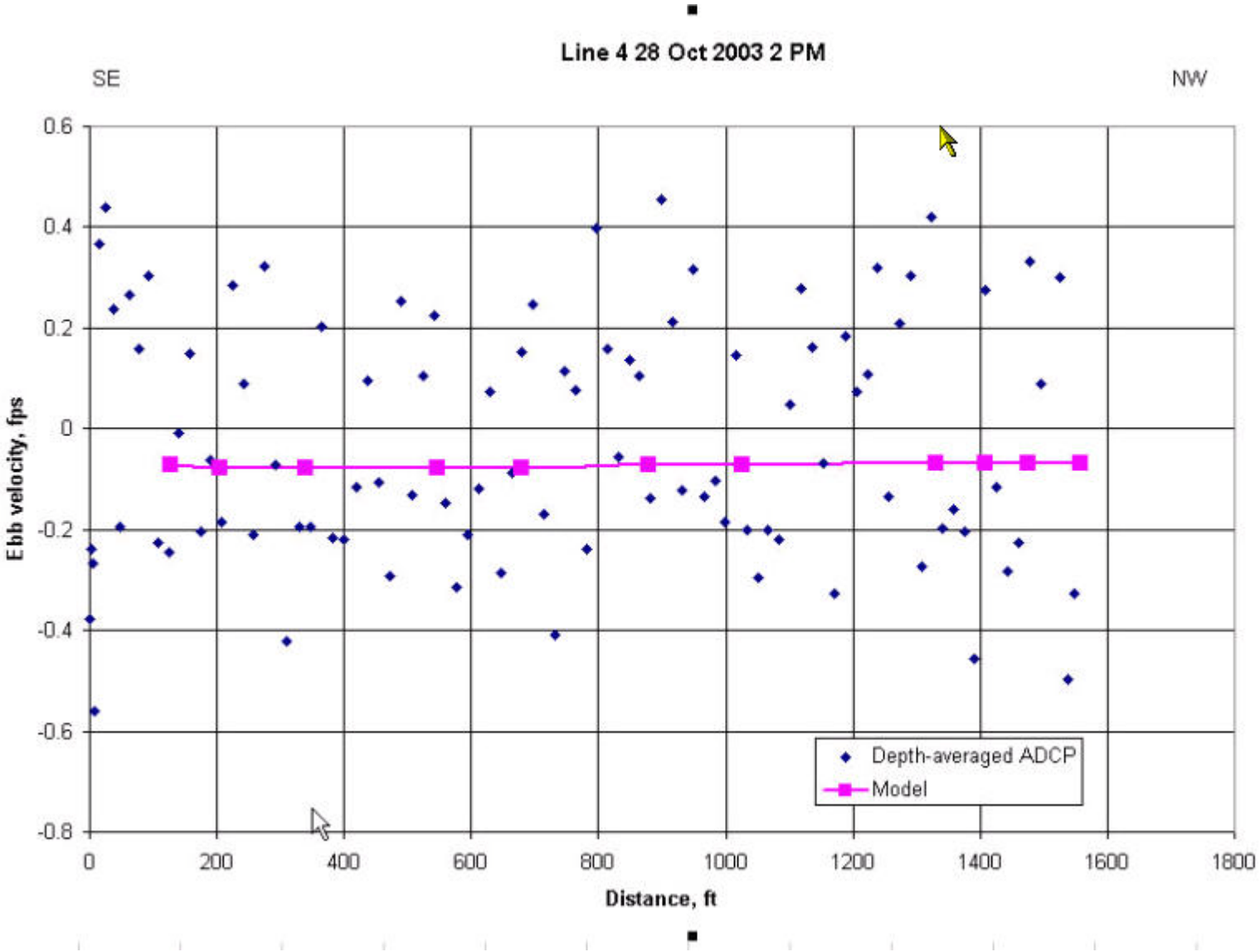

Figure 2-21. Maximum Ebb Velocity Line 4

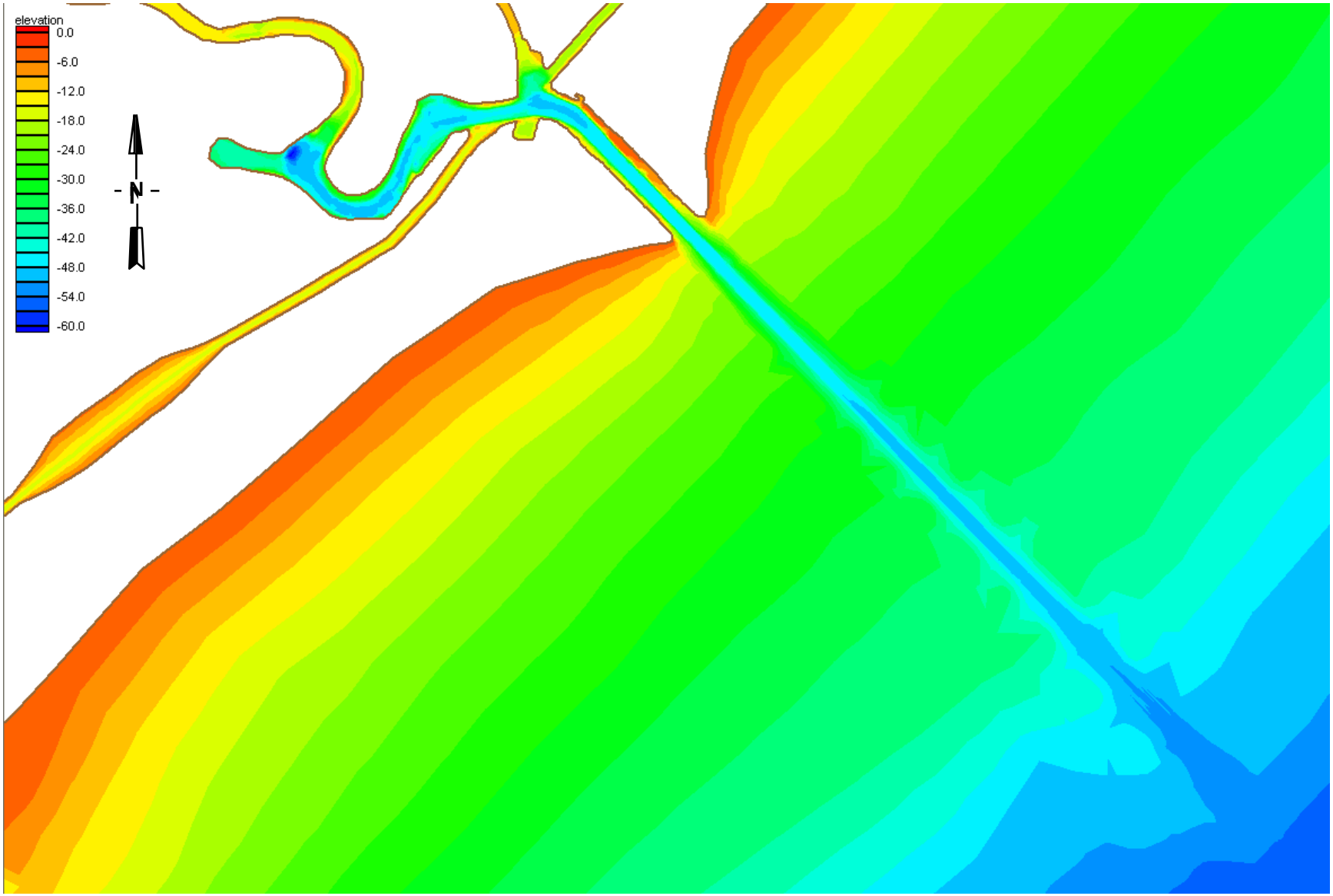

Figure 3-1. Base channel condition

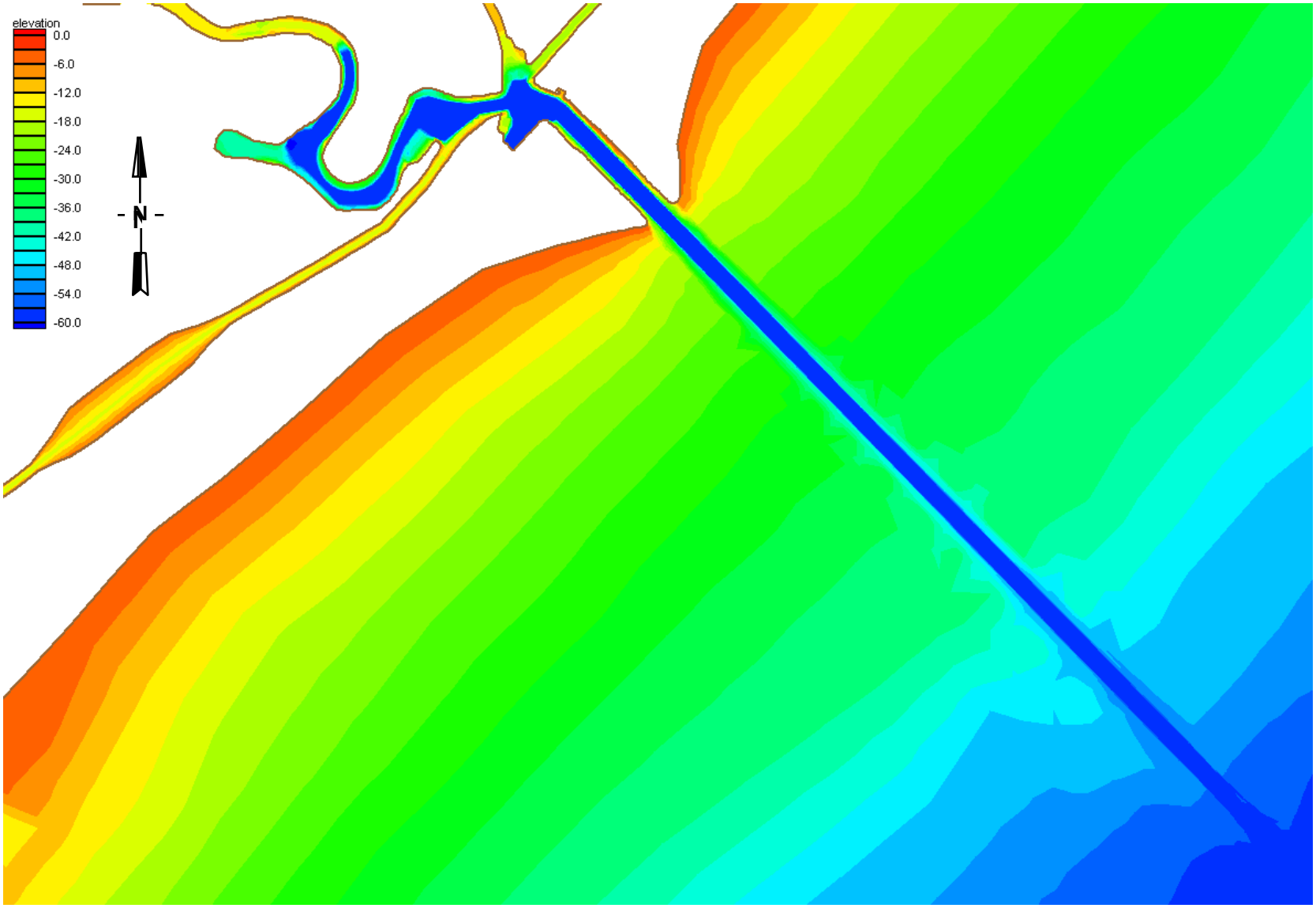

Figure 3-2. Plan 4 channel condition

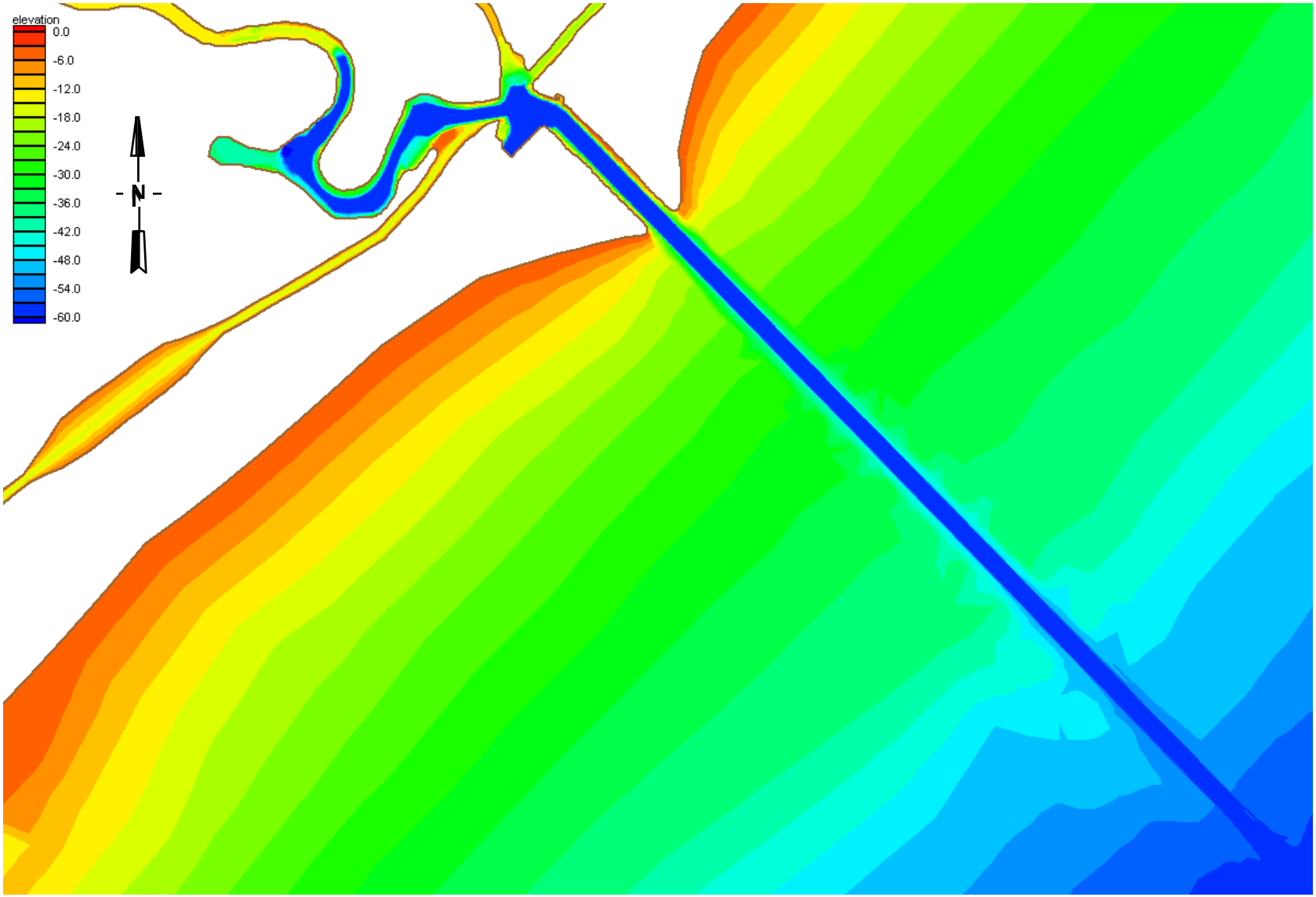

Figure 3-3. Plan 5 channel condition

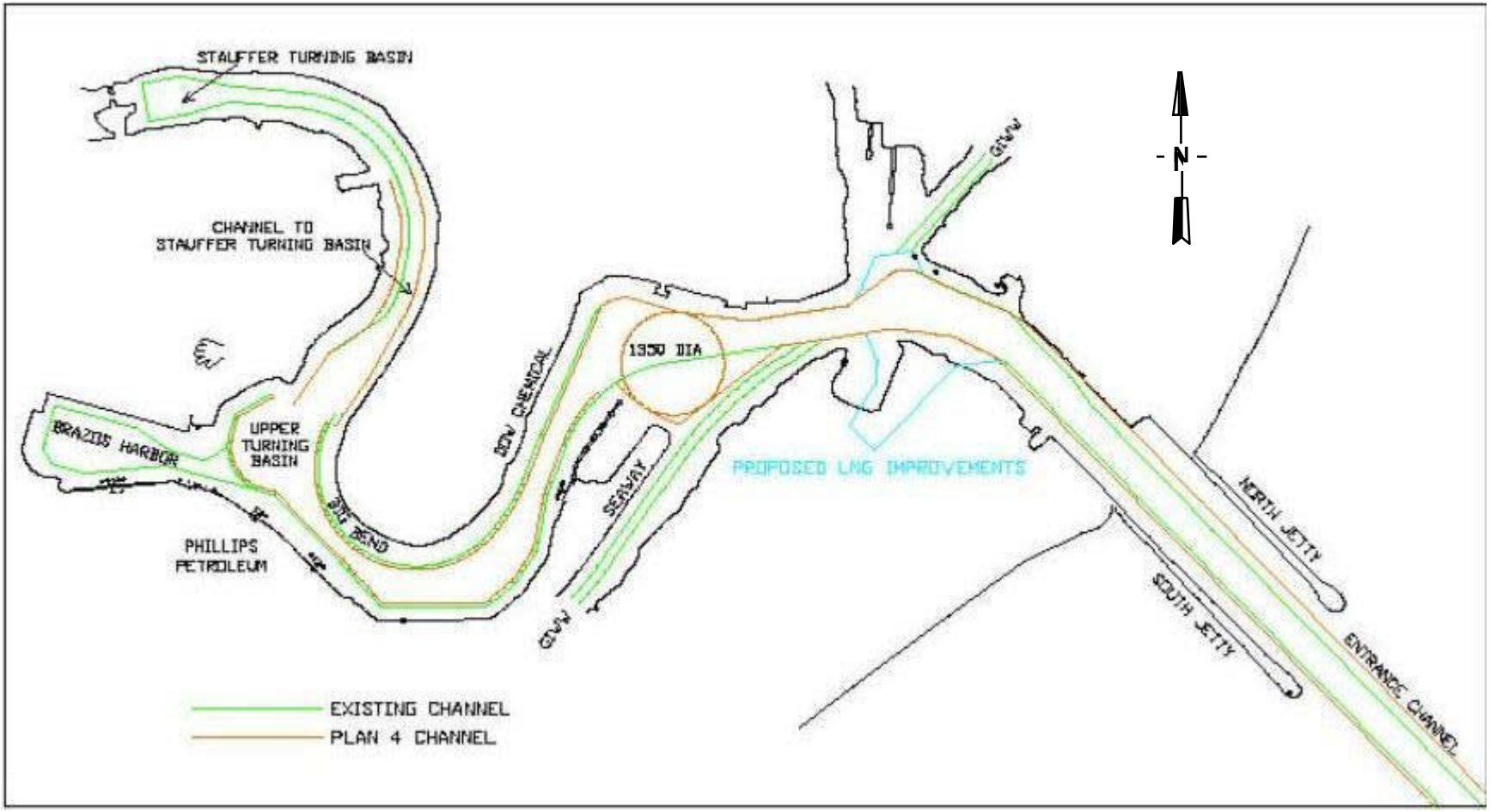

Figure 3-4. Freeport Harbor Plan 4

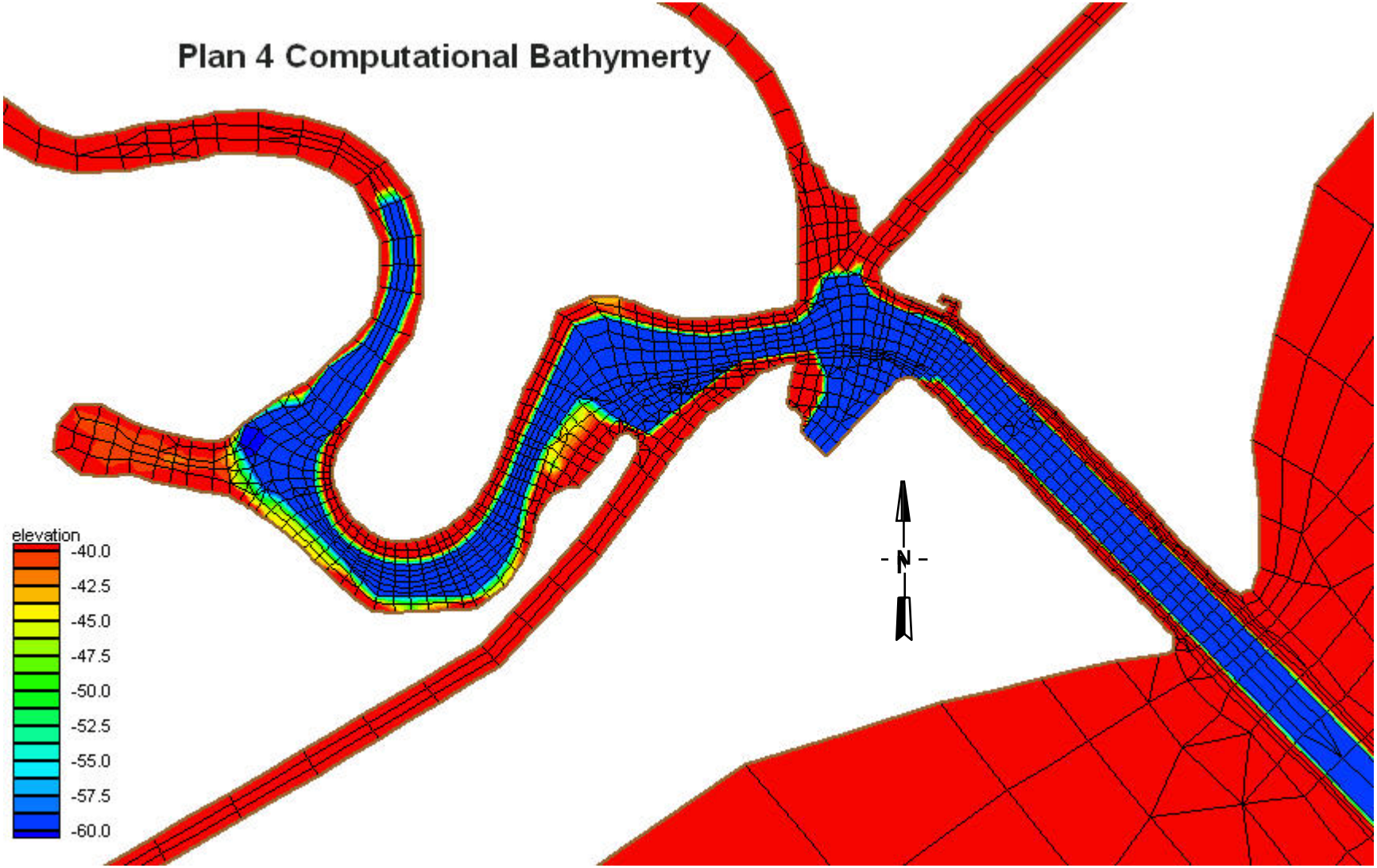

Figure 3-5. Plan 4 computational mesh and bathymetry

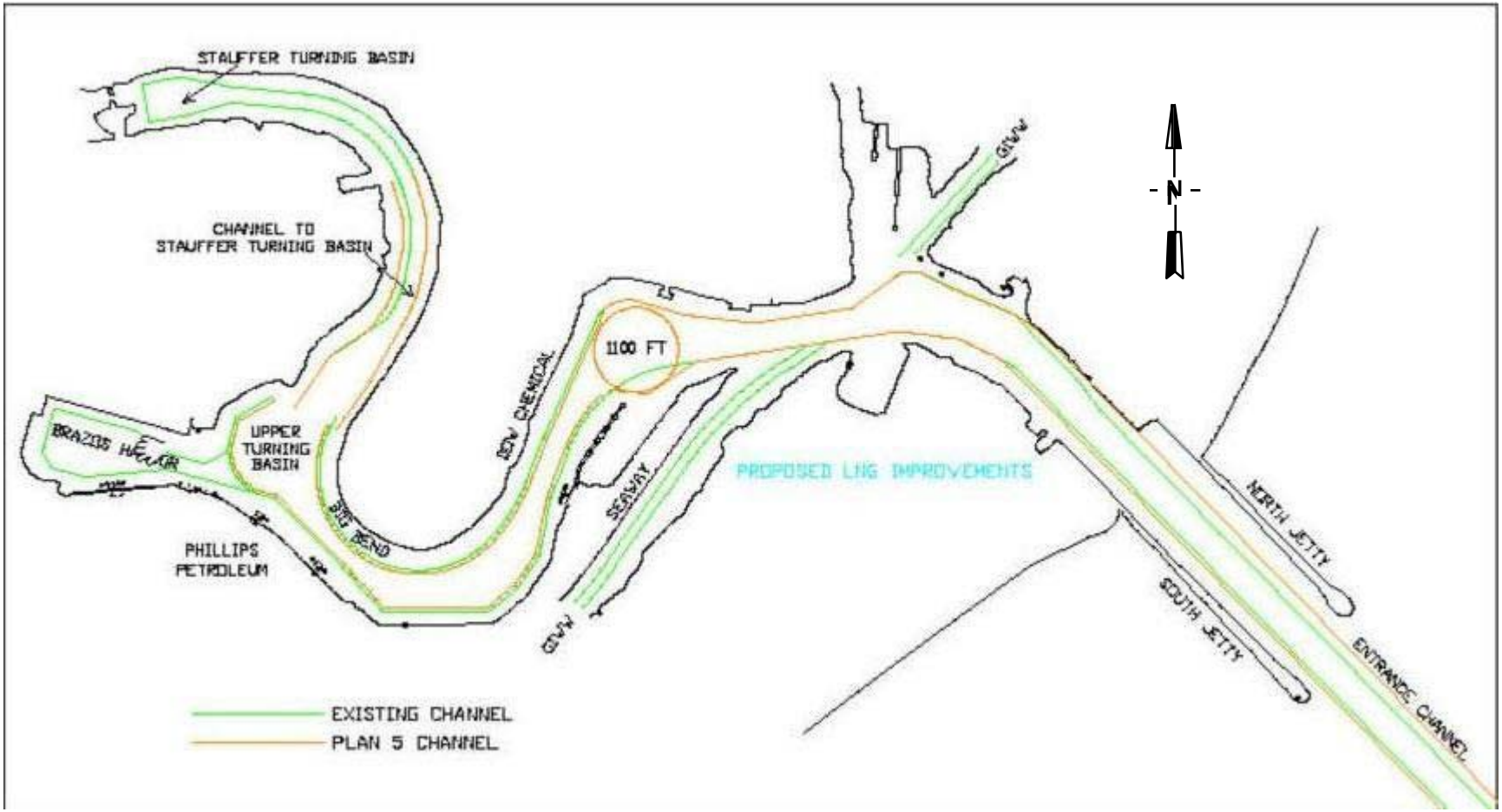

Figure 3-6. Freeport Harbor Plan 5

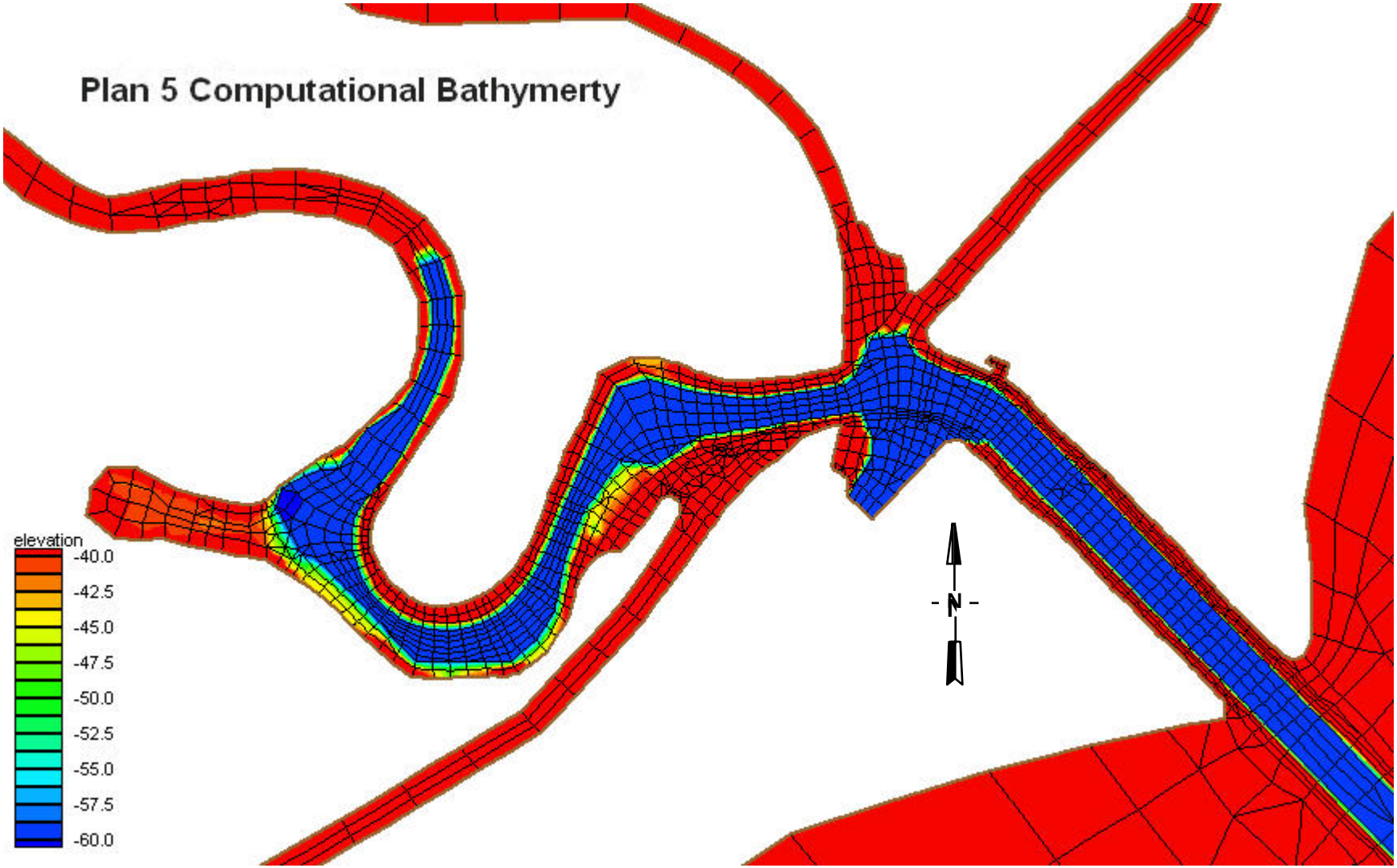

Figure 3-7. Plan 5 computational mesh and bathymetry

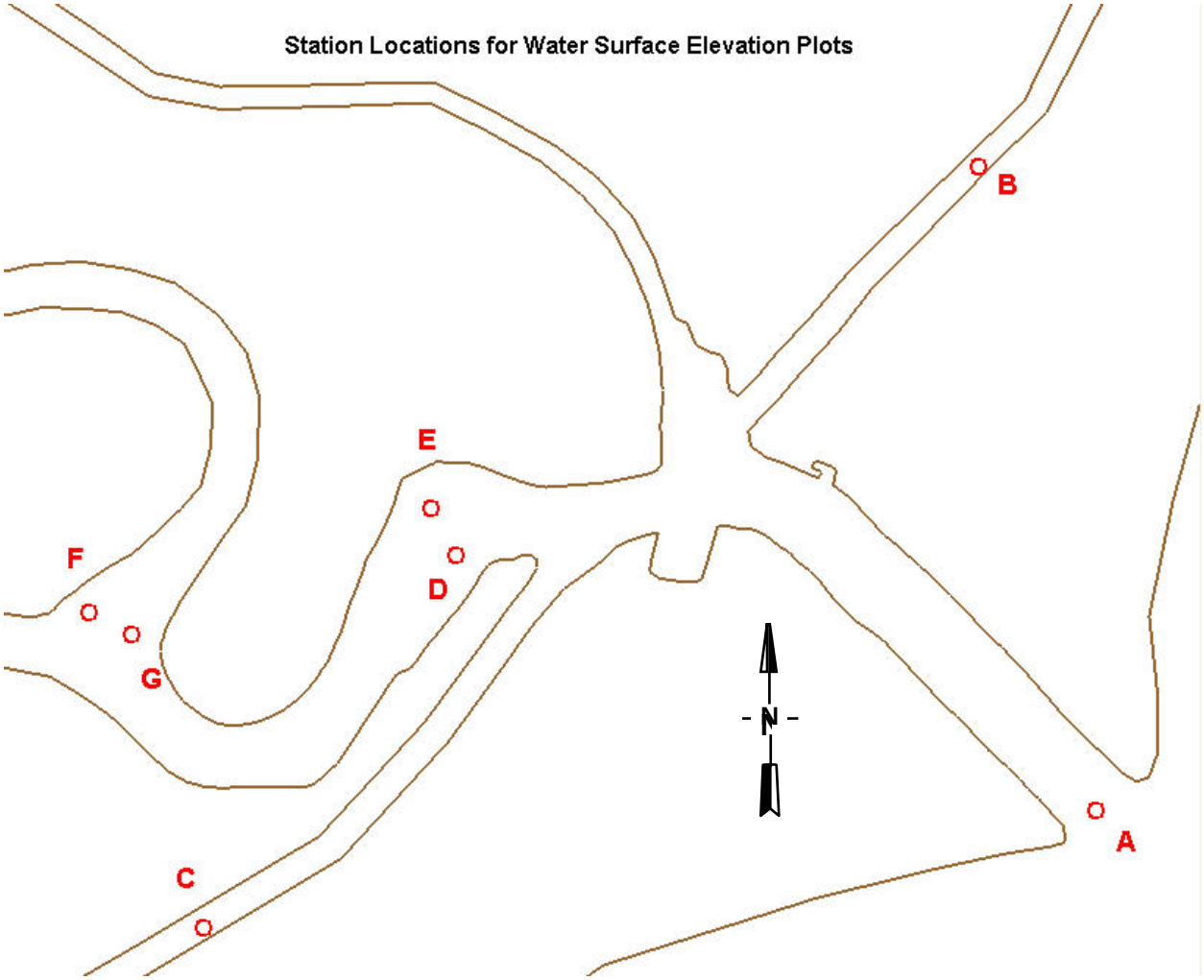

Figure 3-8. Station Locations for Water Surface Elevation Plots

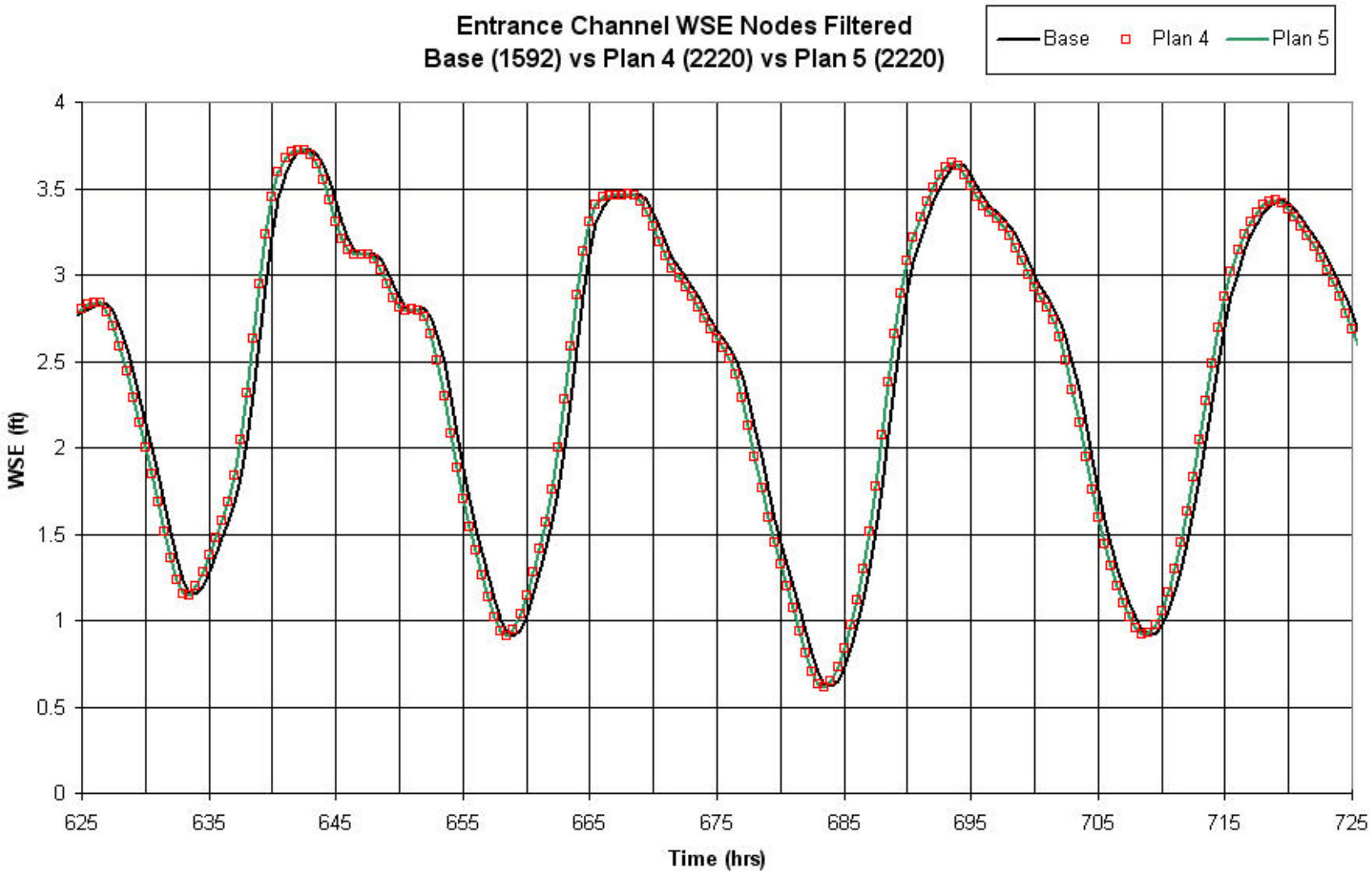

Figure 3-9. Entrance Channel Water Surface Elevation Comparisons at Station A

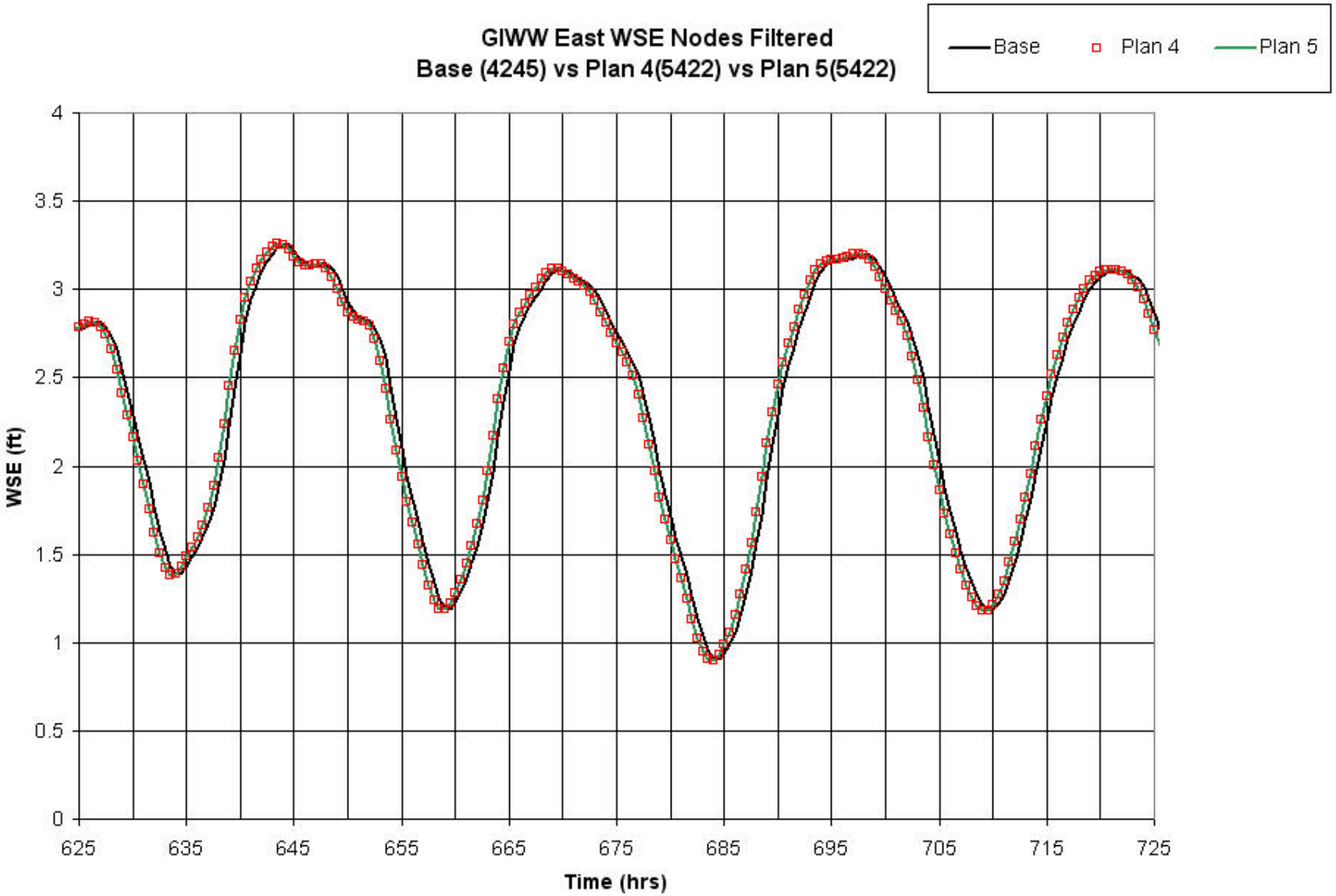

Figure 3-10. GIWW East Water Surface Elevation Comparisons at Station B

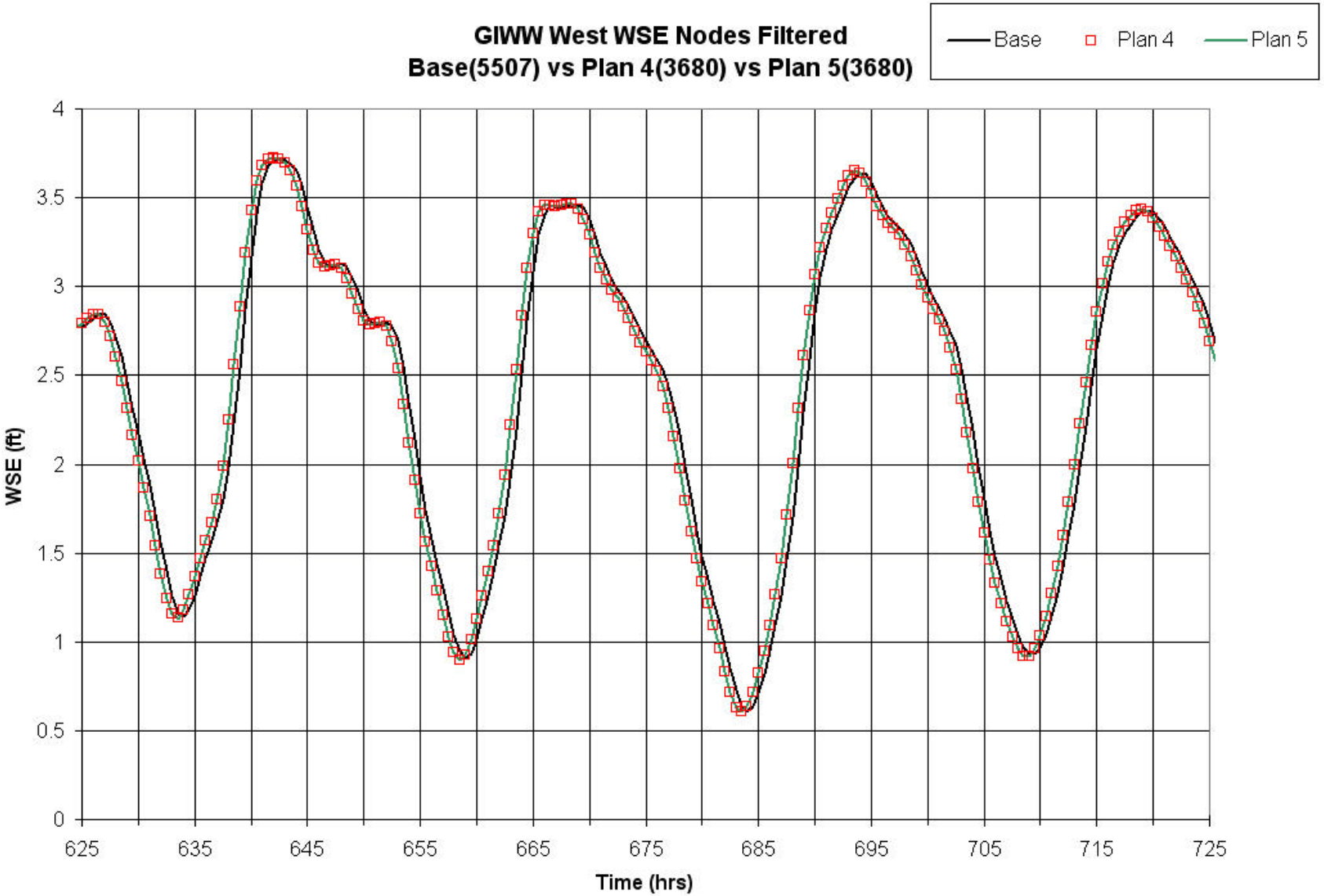

Figure 3-11. GIWW West Water Surface Elevation Comparisons at Station C

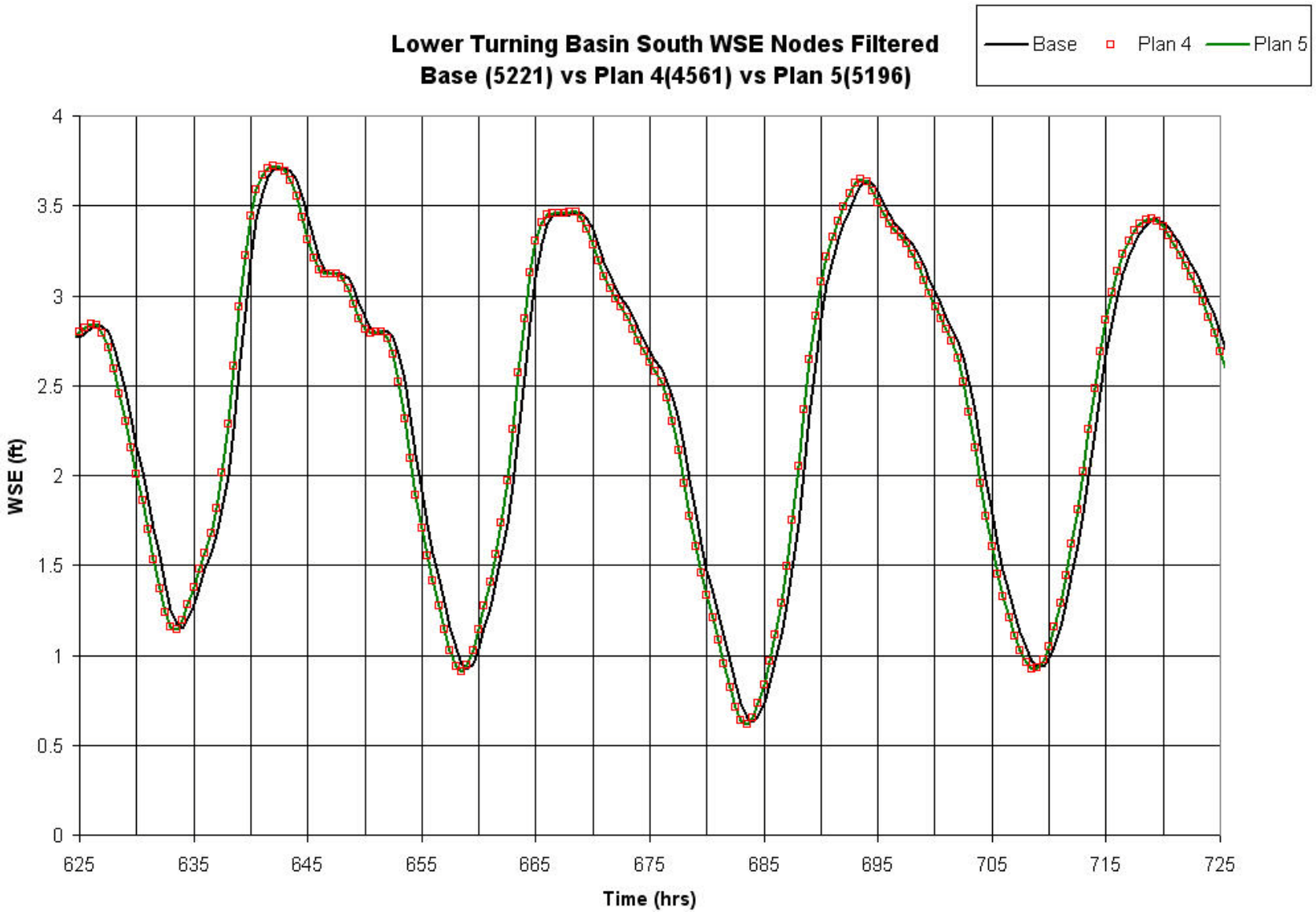

Figure 3-12. Lower Turning Basin South Water Surface Elevation Comparisons at Station D

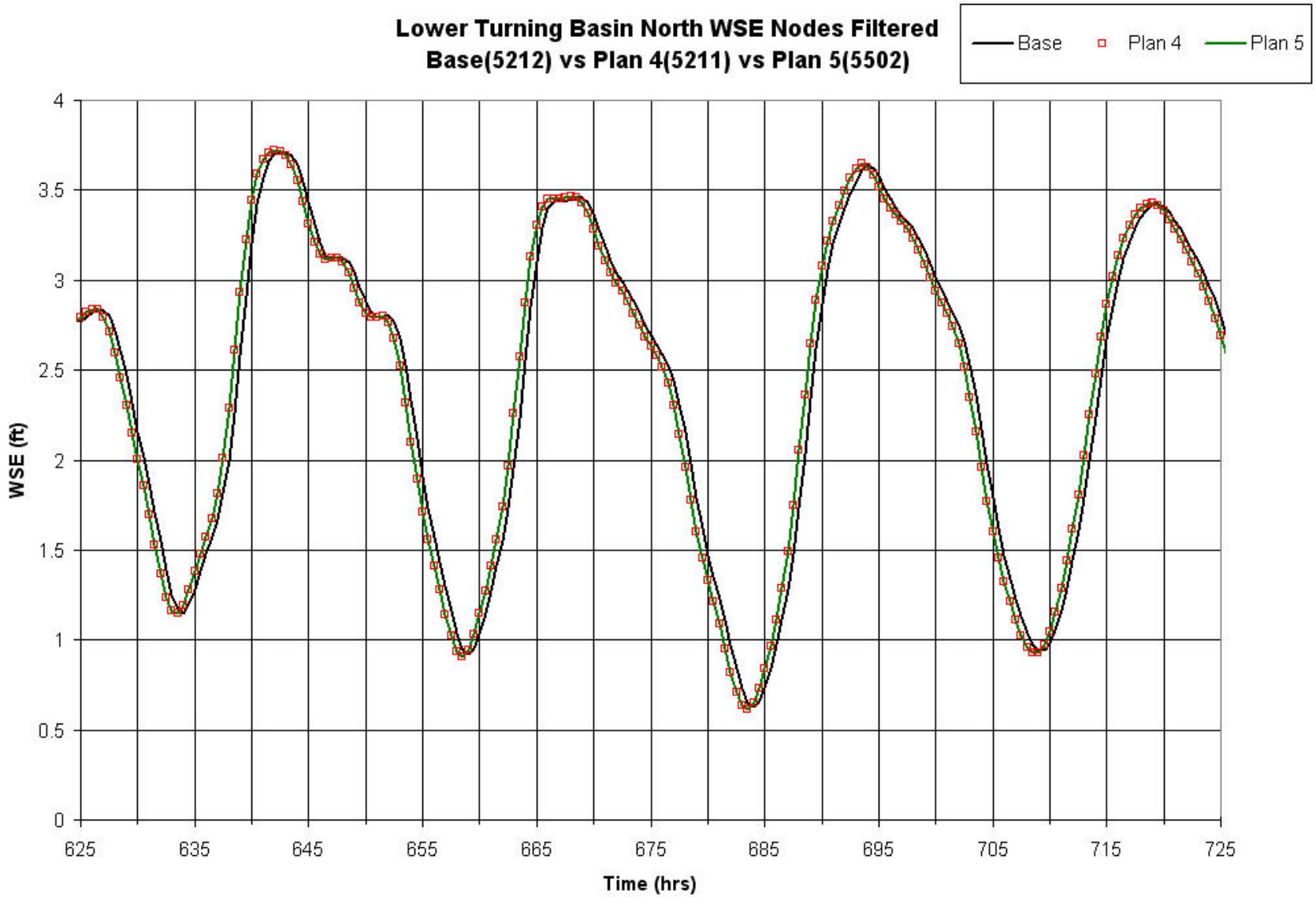

Figure 3-13. Lower Turning Basin North Water Surface Elevation Comparisons at Station E

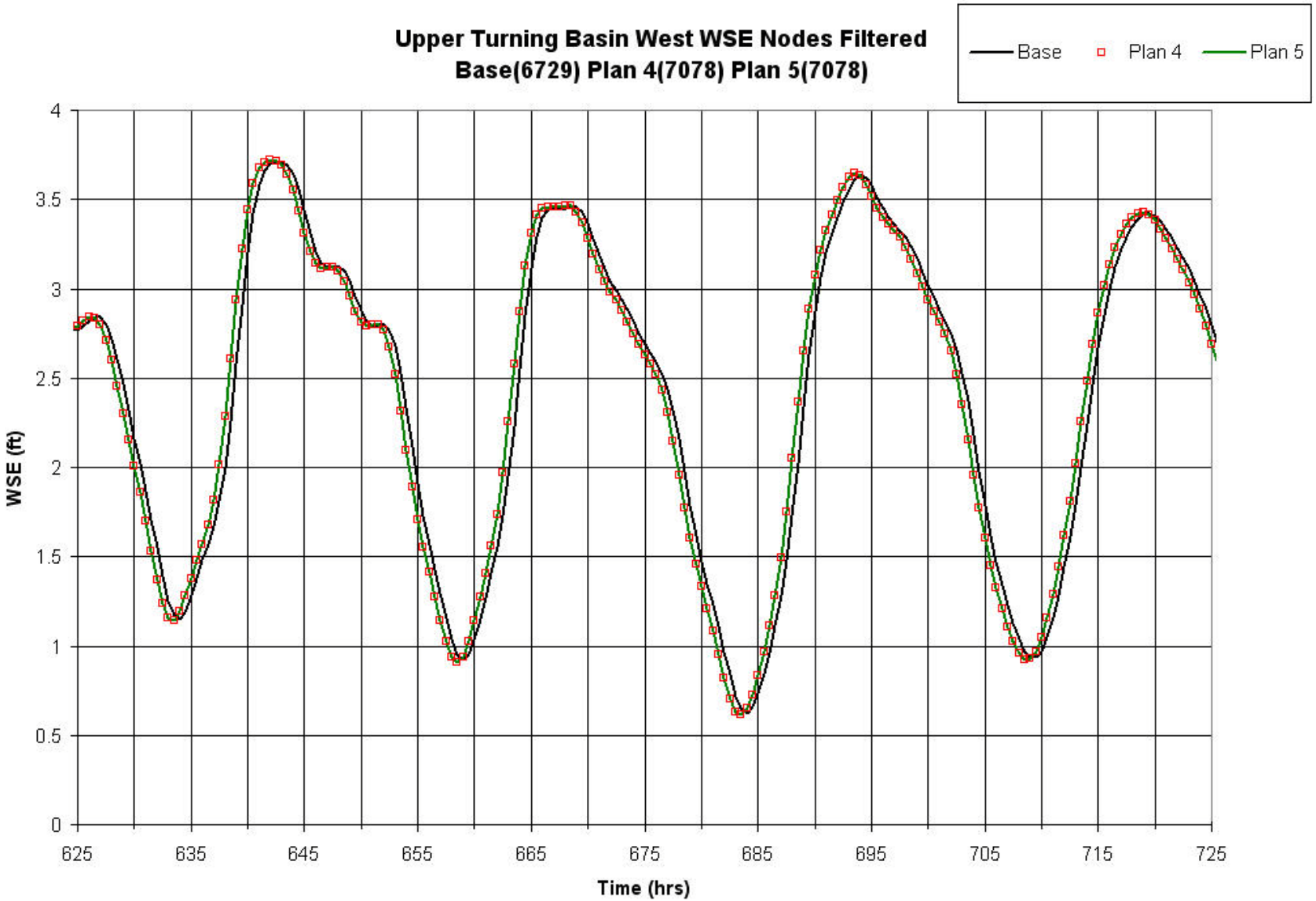

Figure 3-14. Upper Turning Basin West Water Surface Elevation Comparisons at Station F

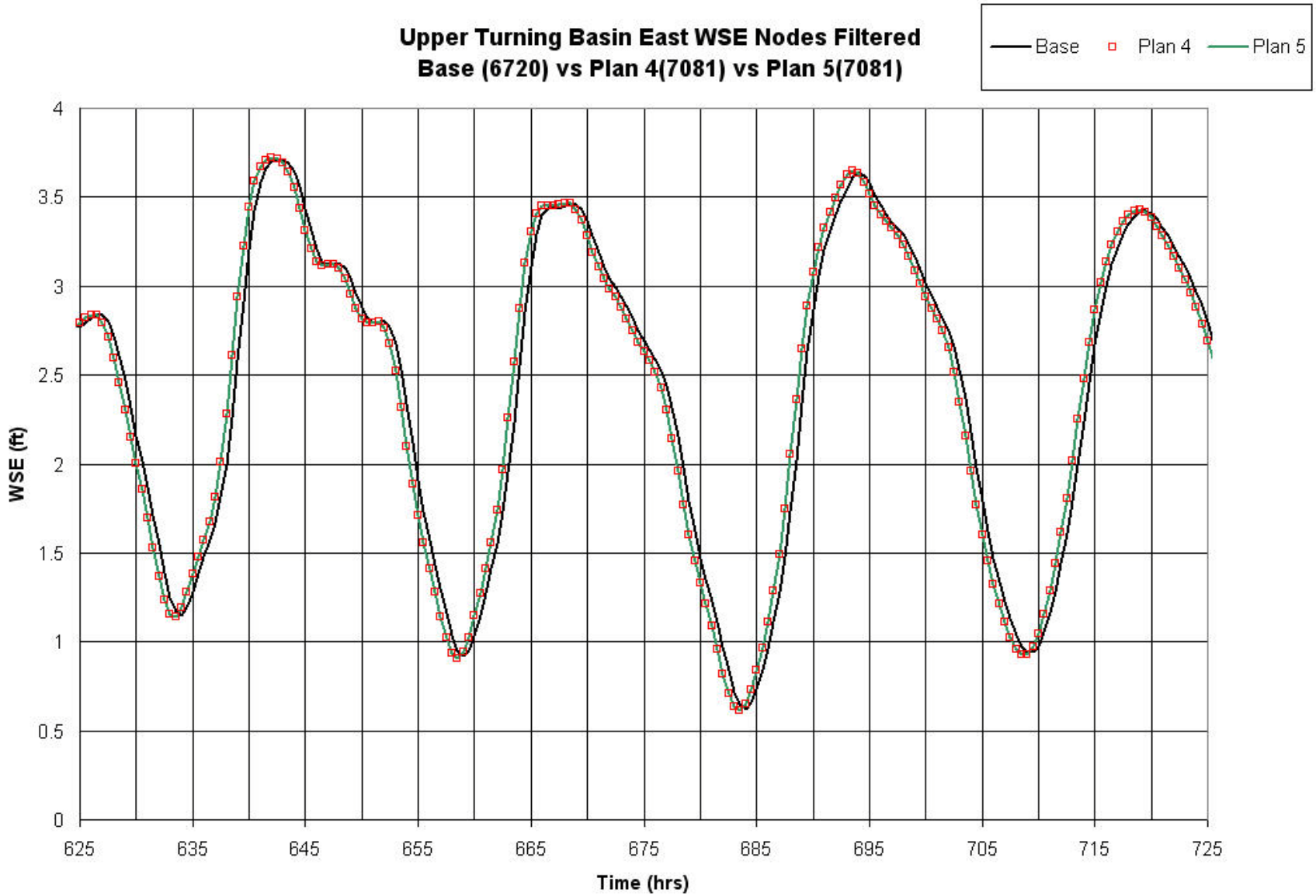

Figure 3-15. Upper Turning Basin East Water Surface Elevation Comparisons at Station G

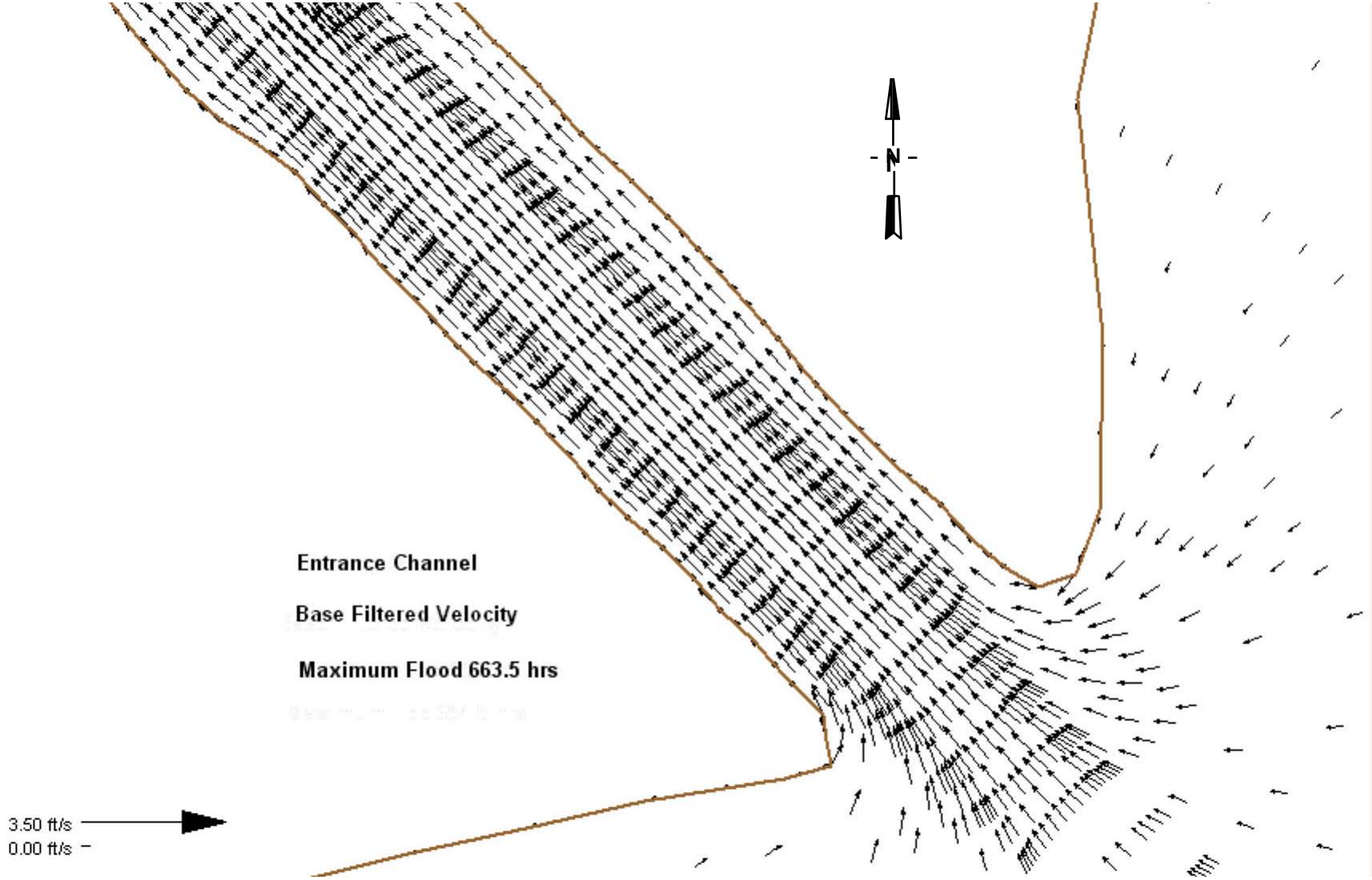

Figure 3-16. Base maximum flood velocity in the entrance channel

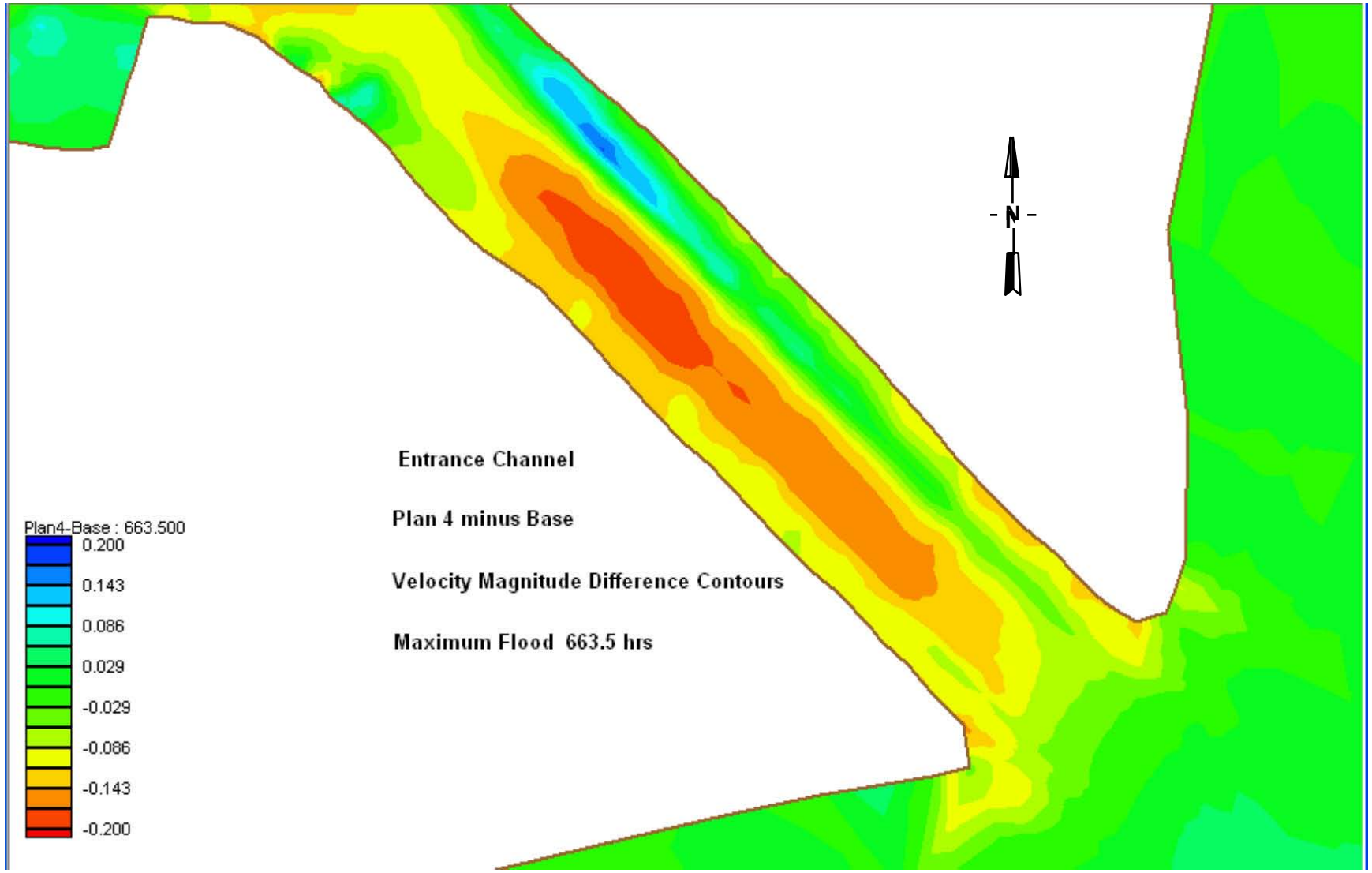

Figure 3-17. Plan 4 Minus Base Velocity Differences Maximum Flood in the Entrance Channel

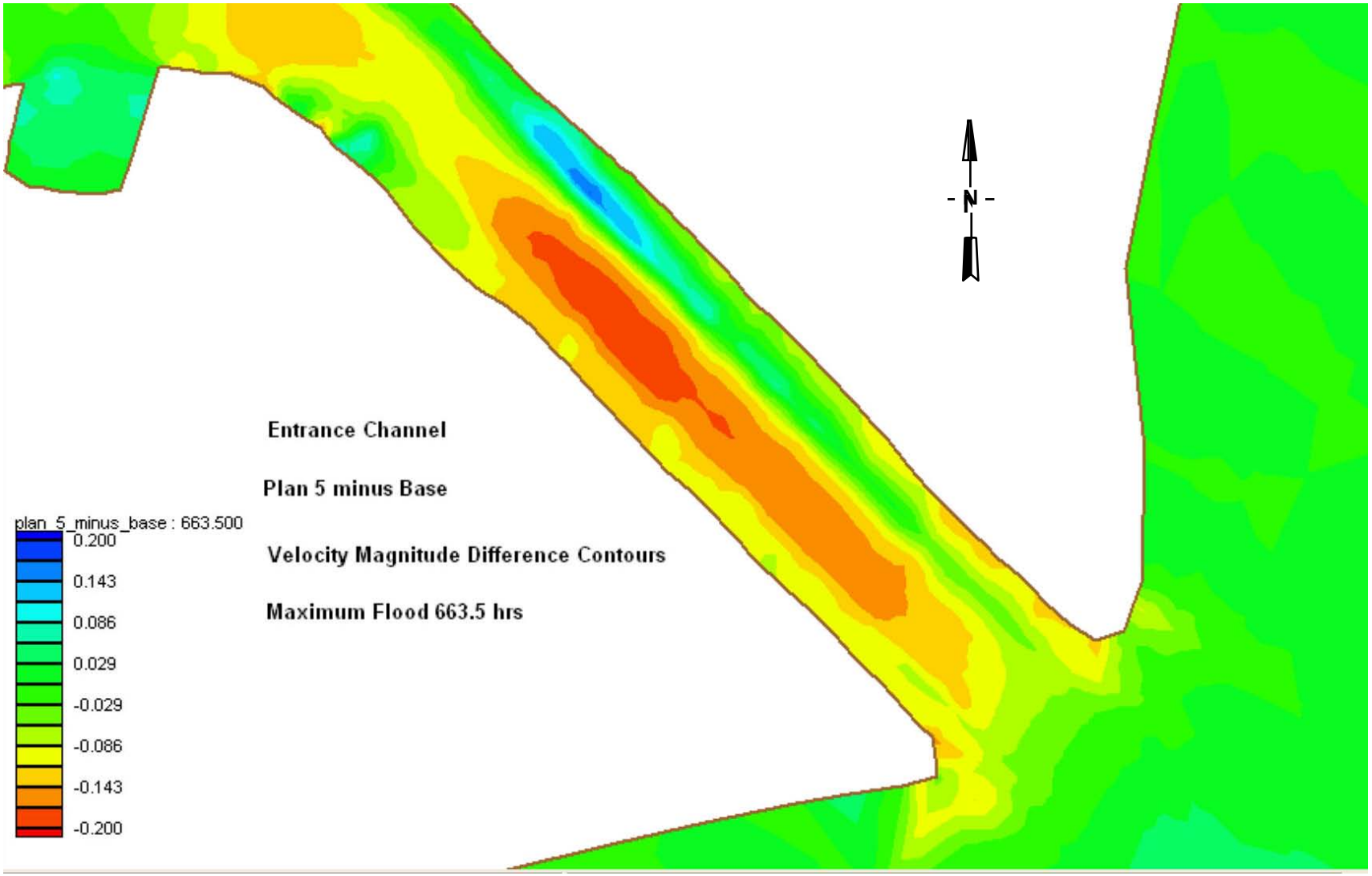

Figure 3-18. Plan 5 Minus Base Velocity Differences Maximum Flood in the Entrance Channel

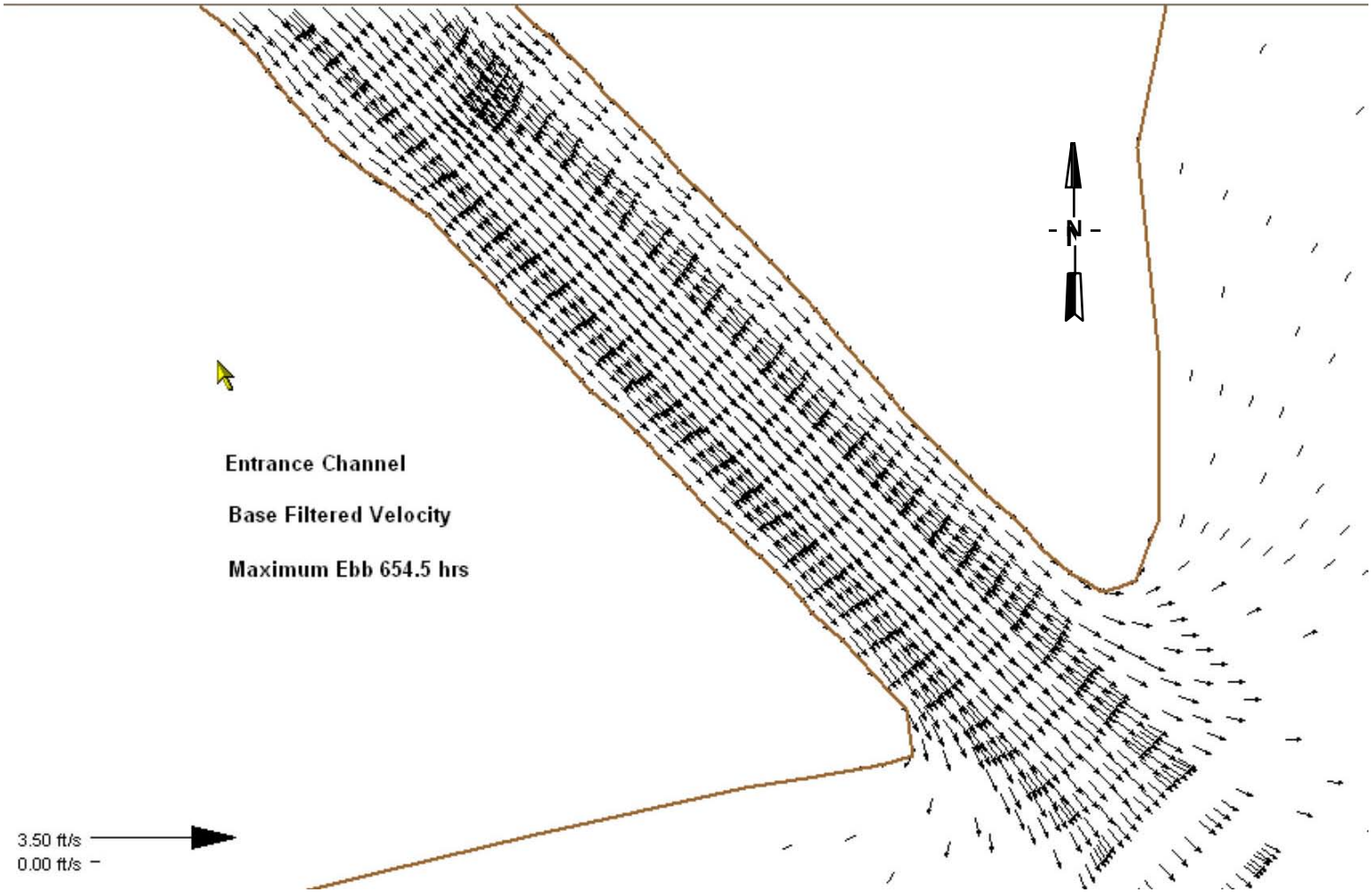

Figure 3-19. Base Maximum Ebb Velocity in the Entrance Channel

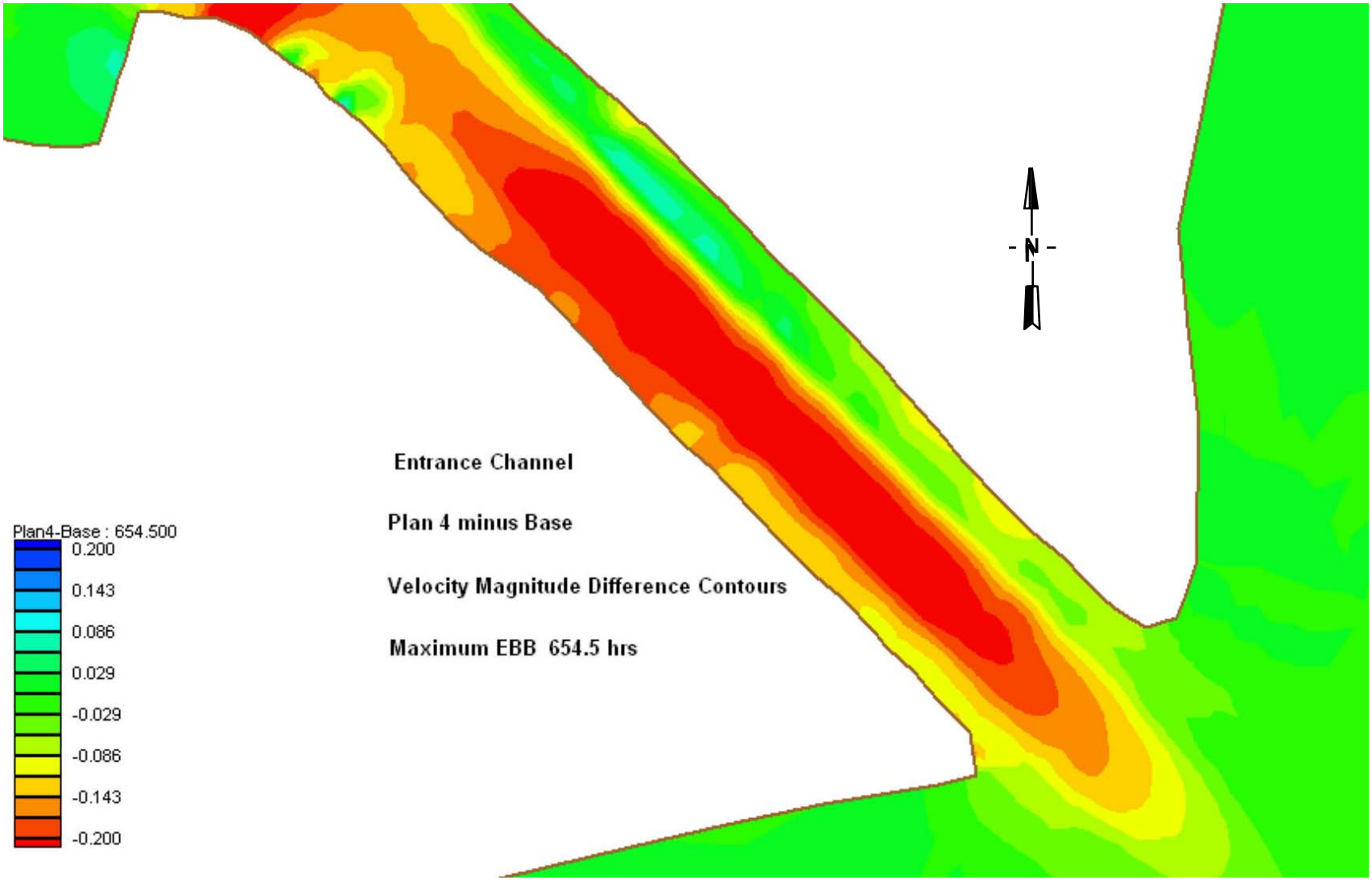

Figure 3-20. Plan 4 Minus Base Velocity Differences Maximum Ebb in the Entrance Channel

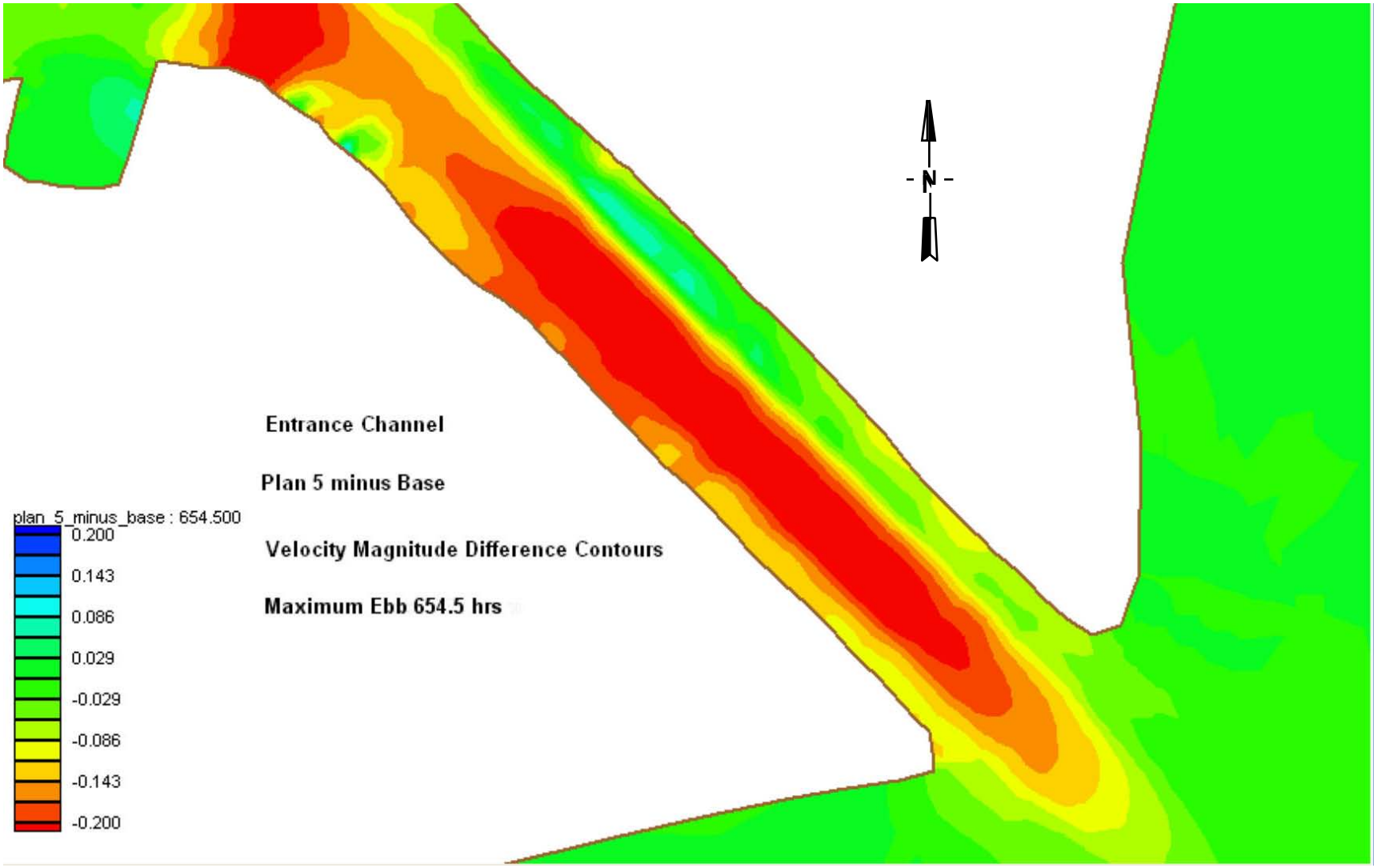

Figure 3-21. Plan 5 Minus Base Velocity Differences Maximum Ebb in the Entrance Channel

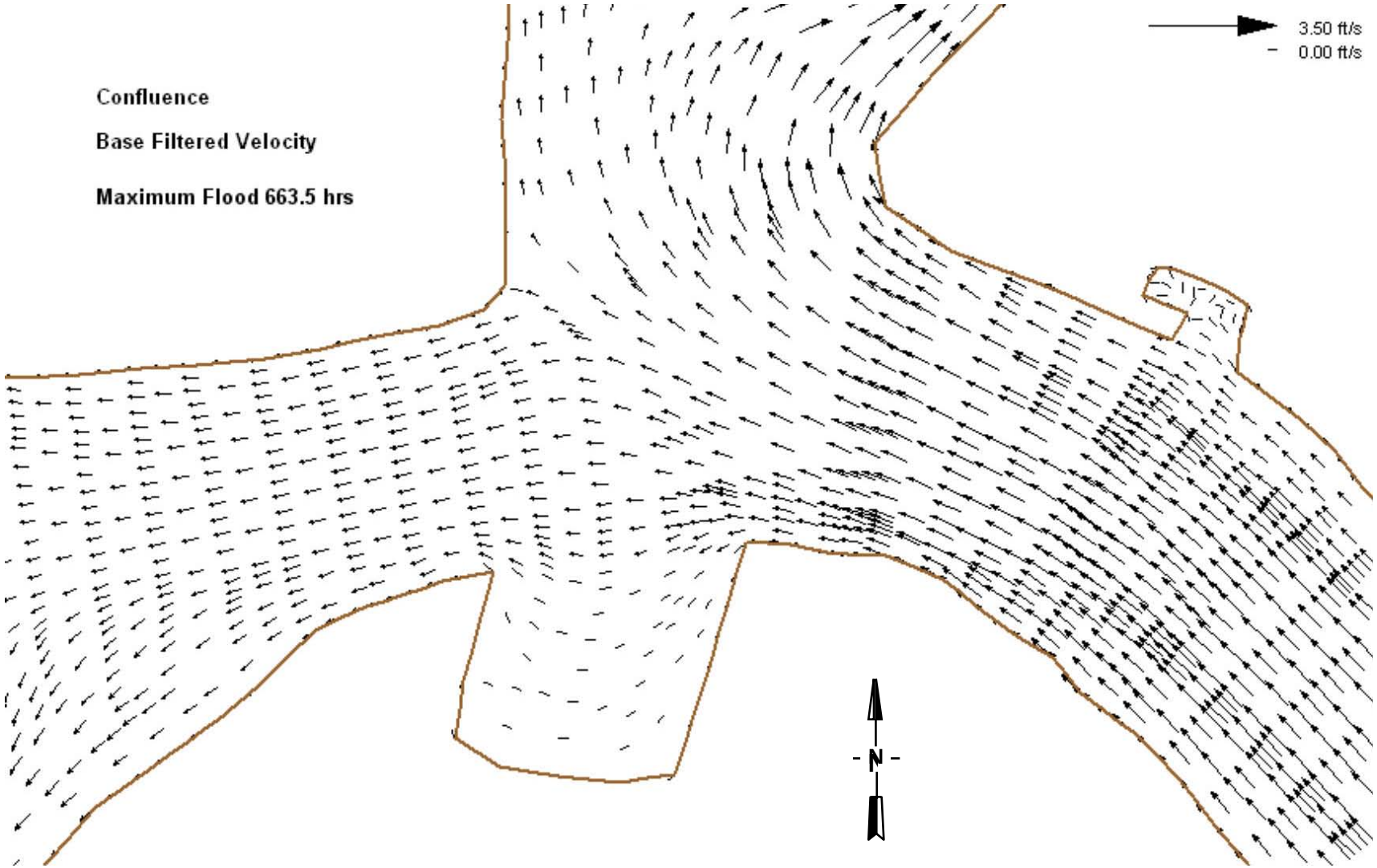

Figure 3-22. Base Maximum Flood Velocities in the Confluence

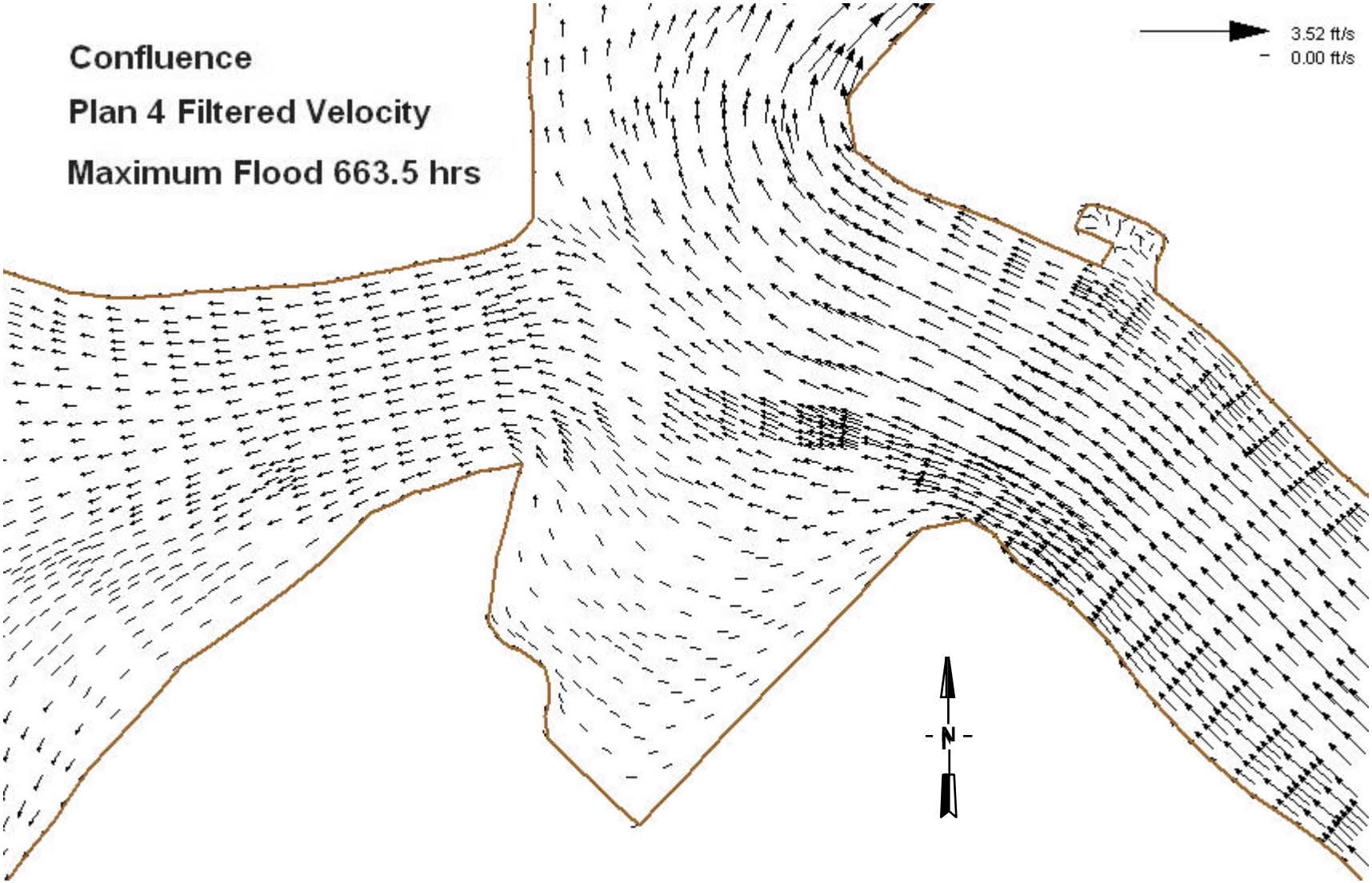

Figure 3-23. Plan 4 Maximum Flood Velocities in the Confluence

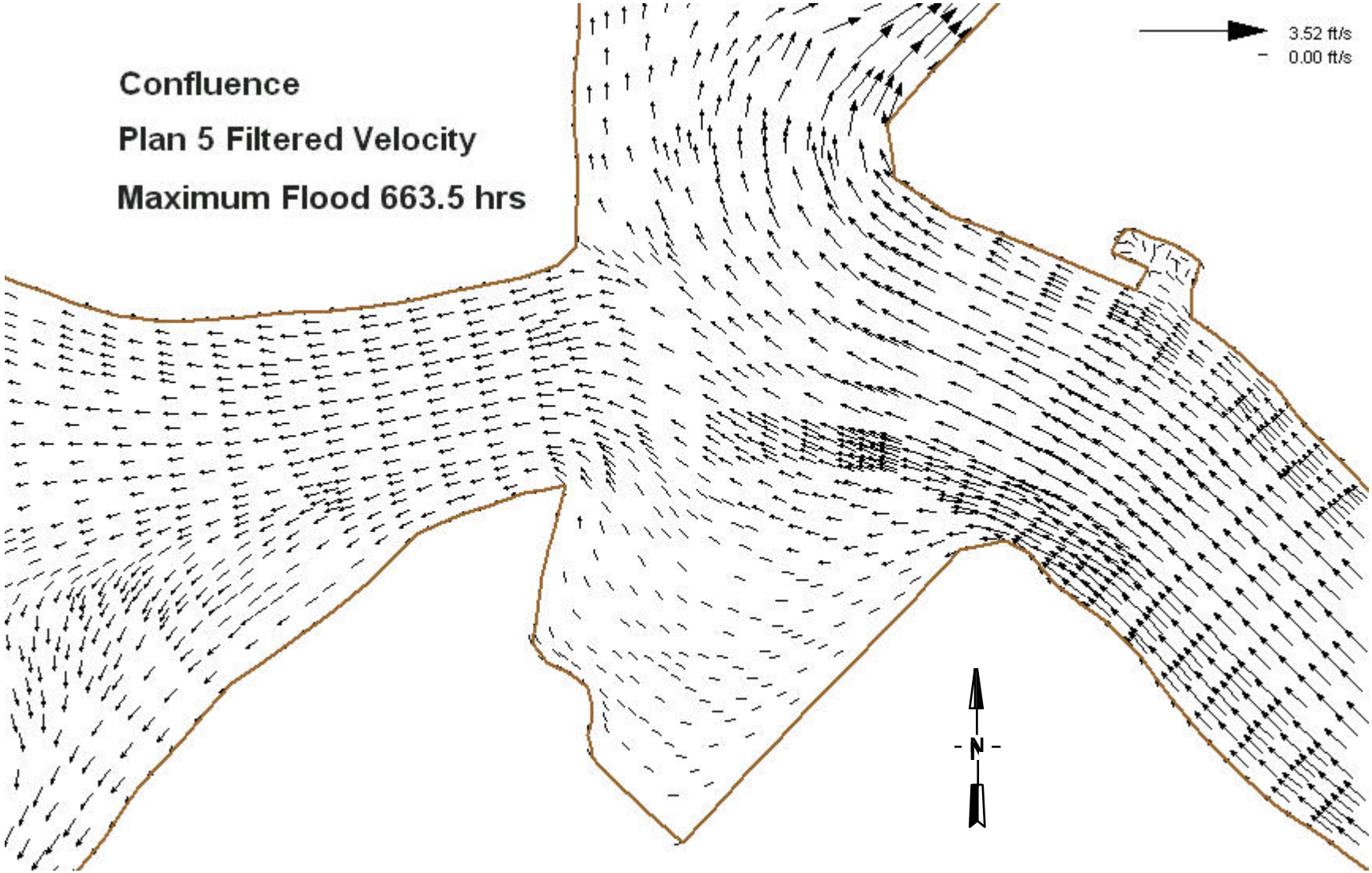

Figure 3-24. Plan 5 Maximum Flood Velocities in the Confluence

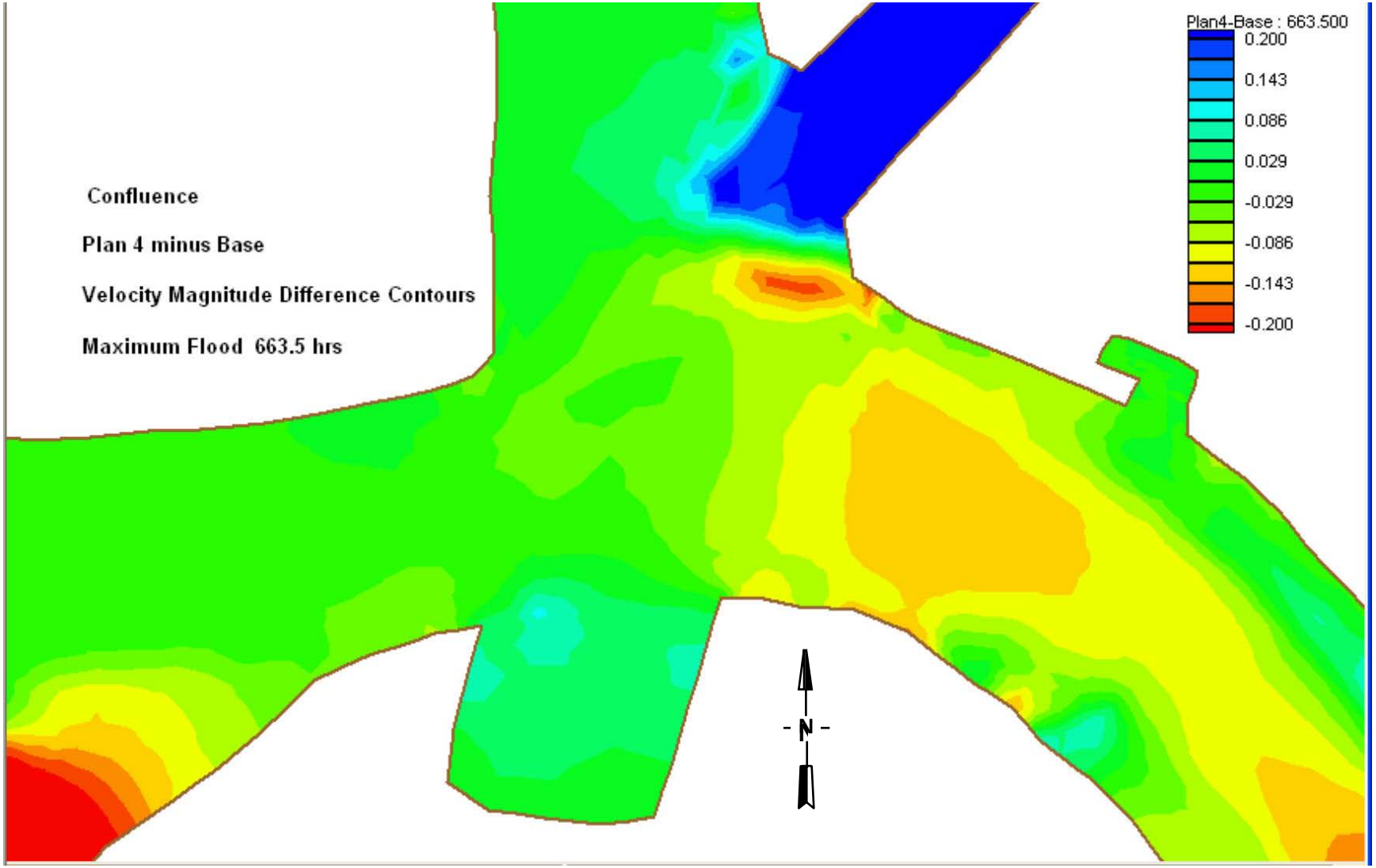

Figure 3-25. Plan 4 Minus Base Maximum Flood Velocity Differences in the Confluence

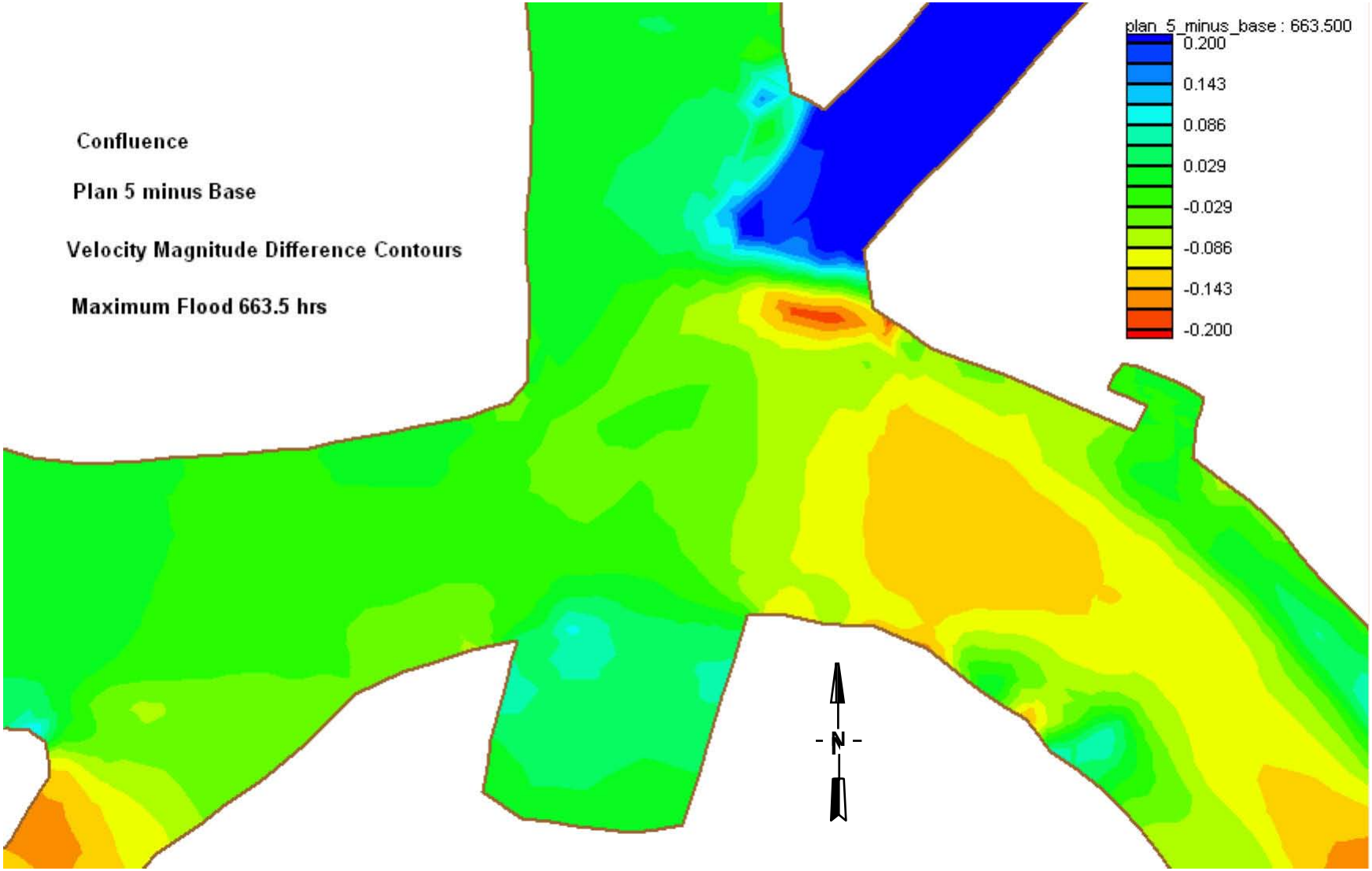

Figure 3-26. Plan 5 Minus Base Maximum Flood Velocity Differences in the Confluence

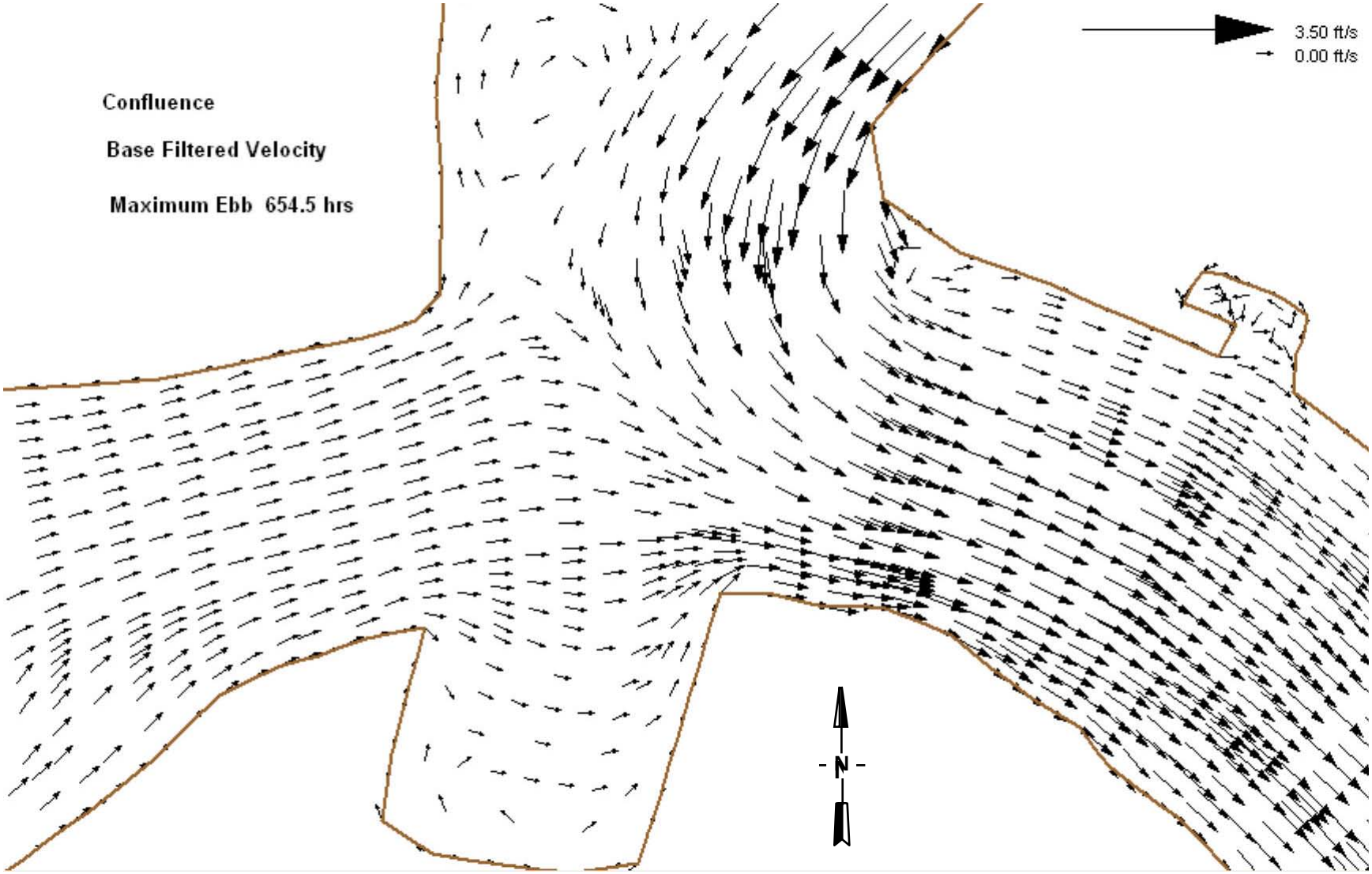

Figure 3-27. Base Maximum Ebb Velocities in the Confluence

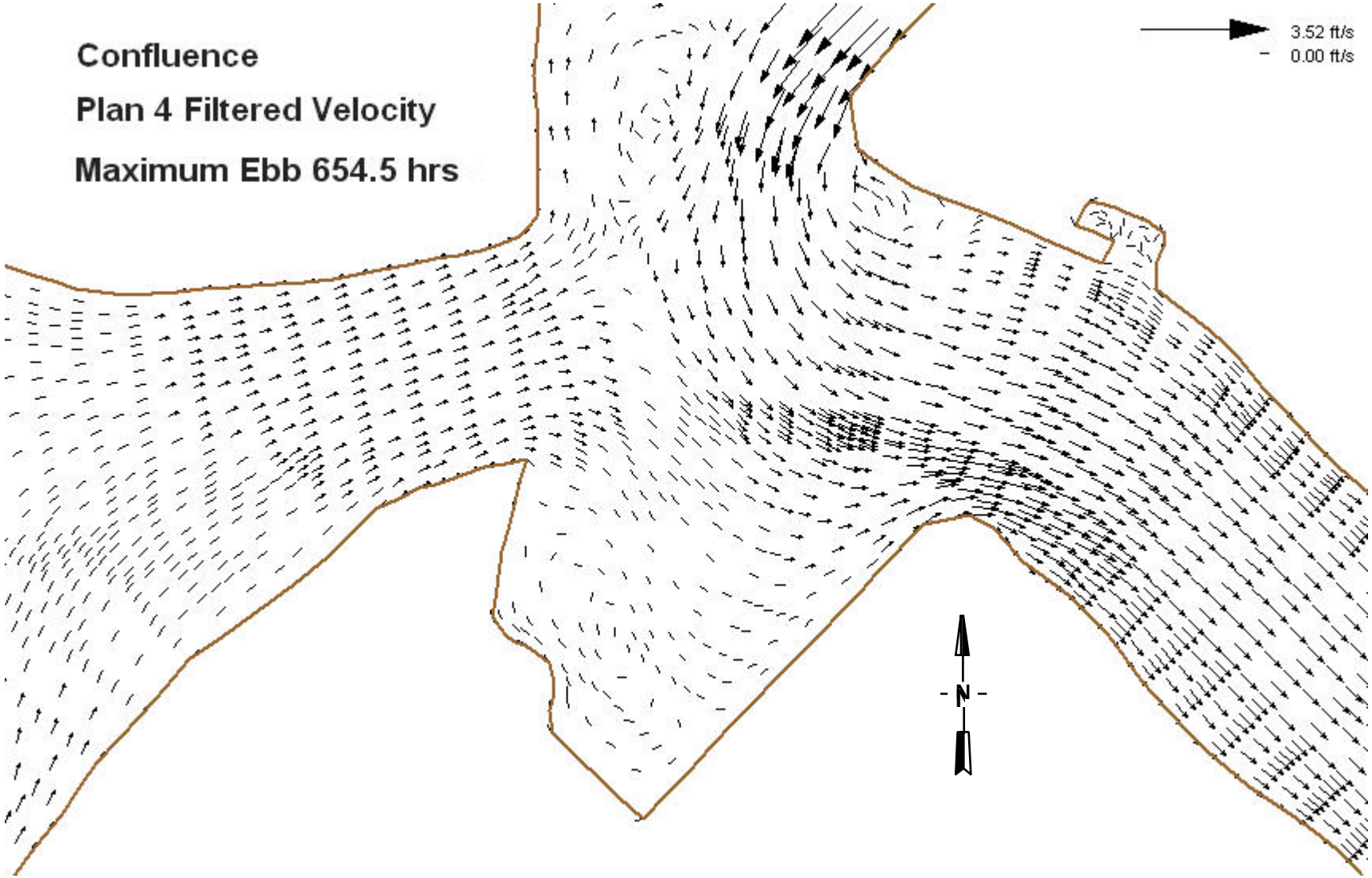

Figure 3-28. Plan 4 Maximum Ebb Velocities in the Confluence

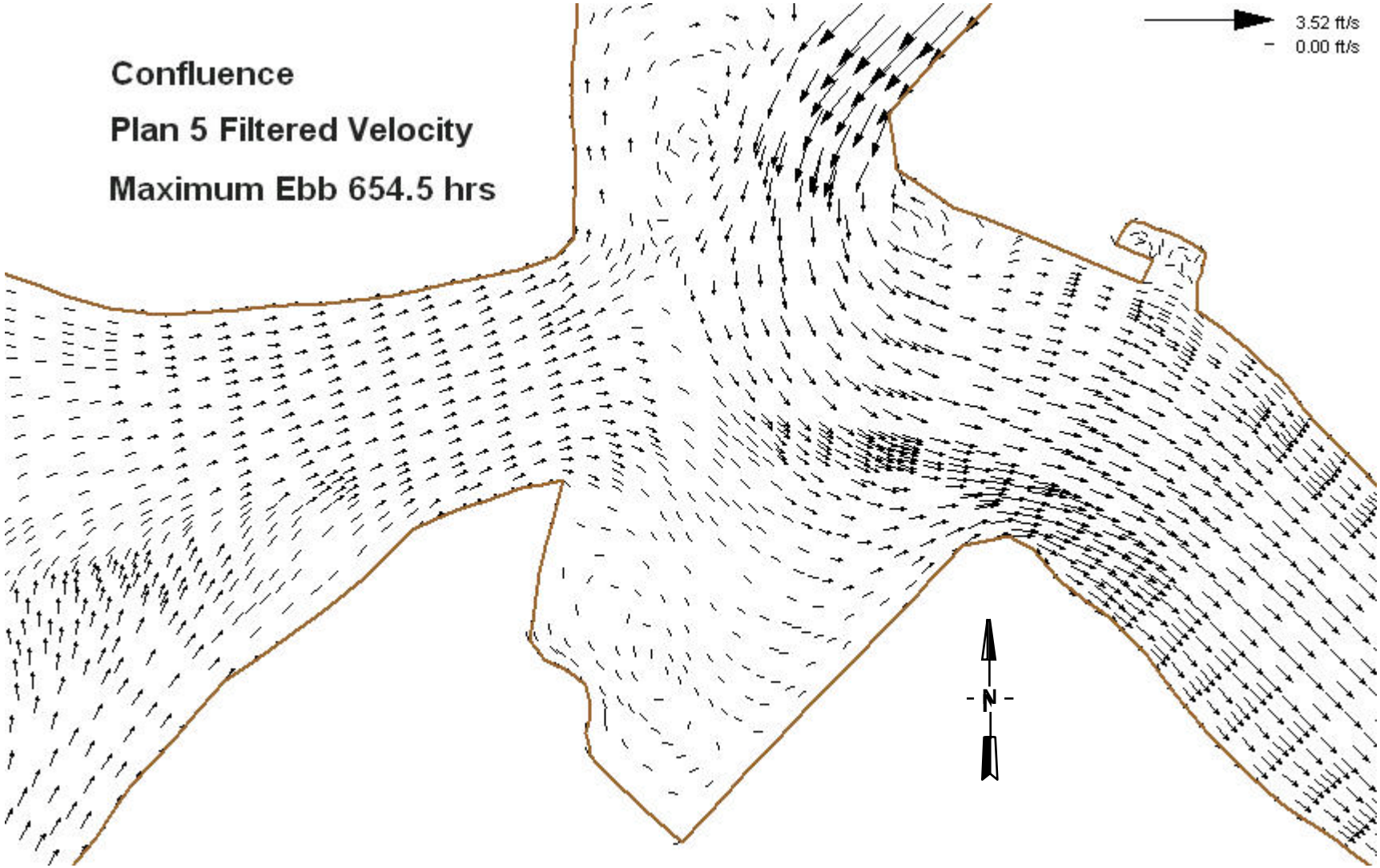

Figure 3-29. Plan 5 Maximum Ebb Velocities in the Confluence

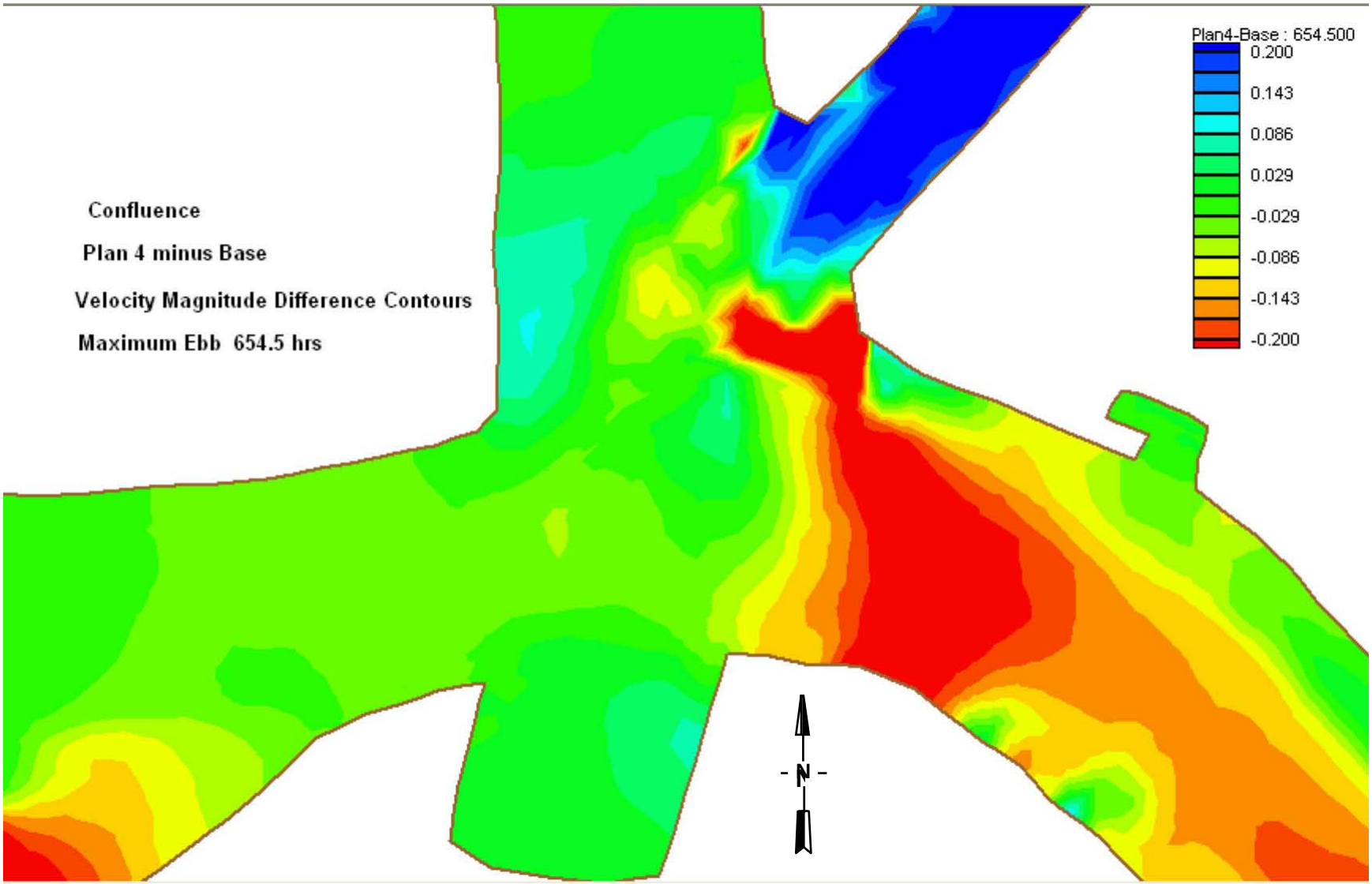

Figure 3-30. Plan 4 Minus Base Maximum Ebb Velocity Differences in the Confluence

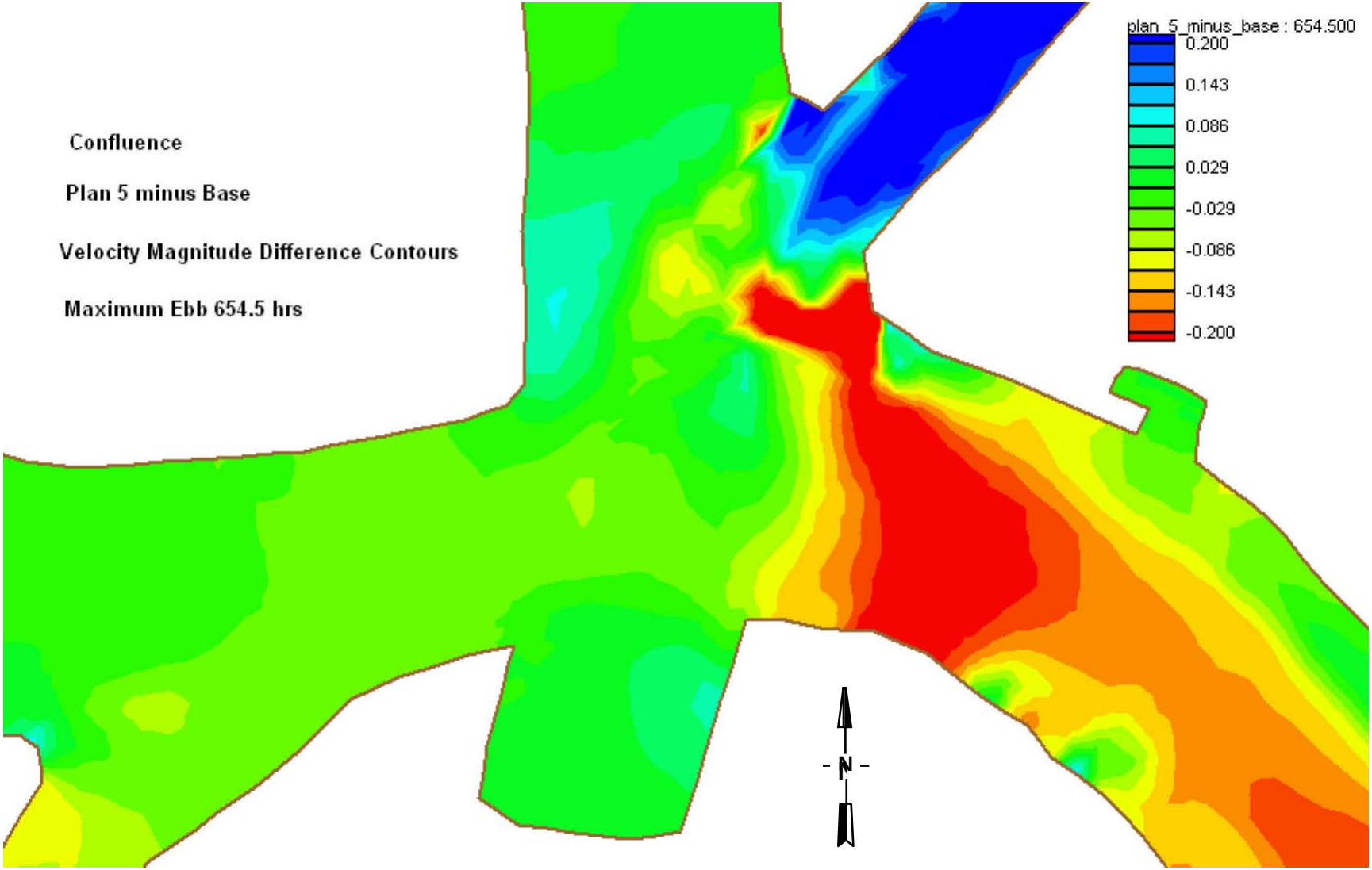

Figure 3-31. Plan 5 Minus Base Maximum Ebb Velocity Differences in the Confluence

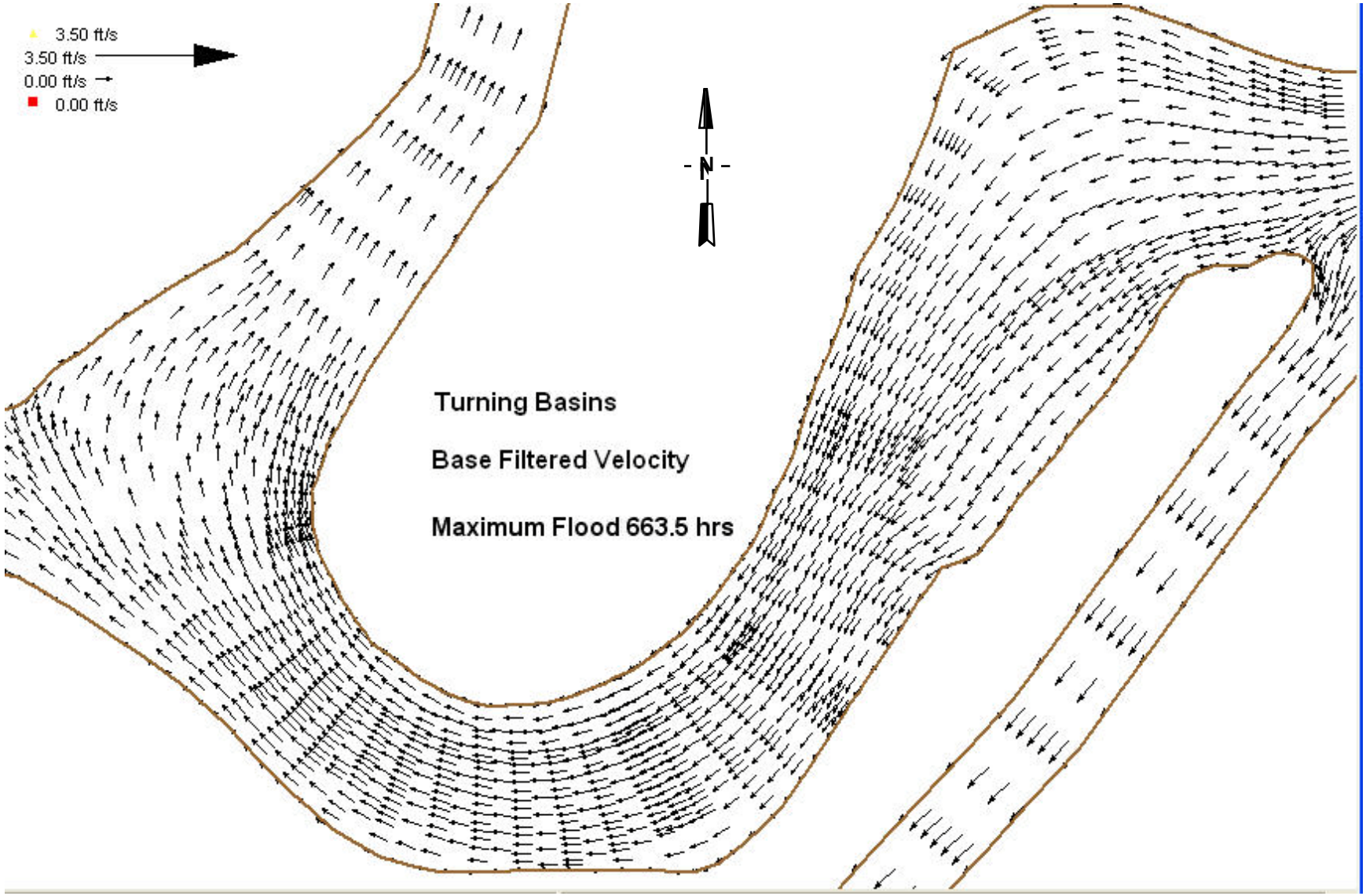

Figure 3-32. Base Maximum Flood Velocities in the Turning Basins

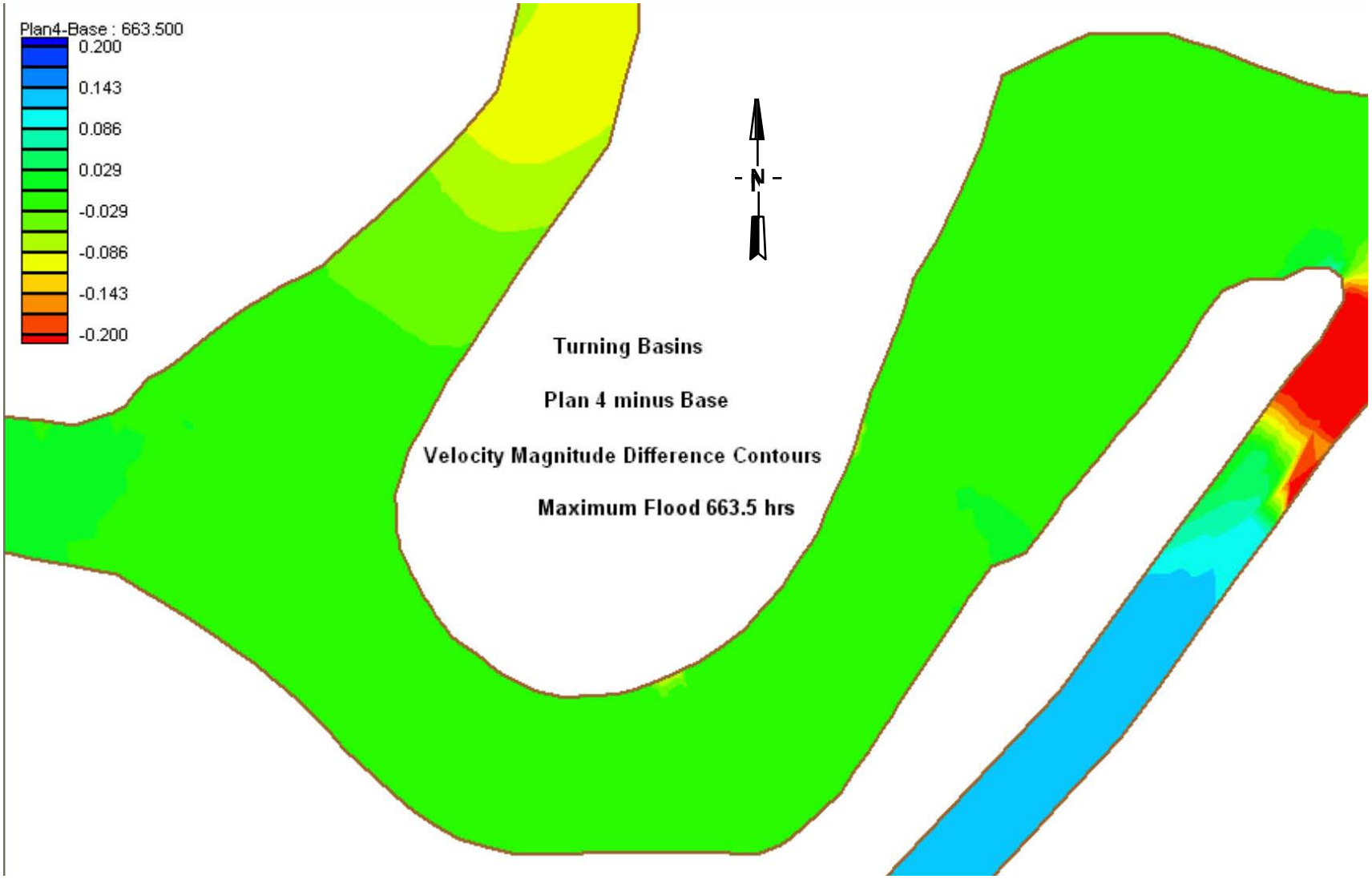

Figure 3-33. Plan 4 Minus Base Velocity Differences Maximum Flood in the Turning Basins

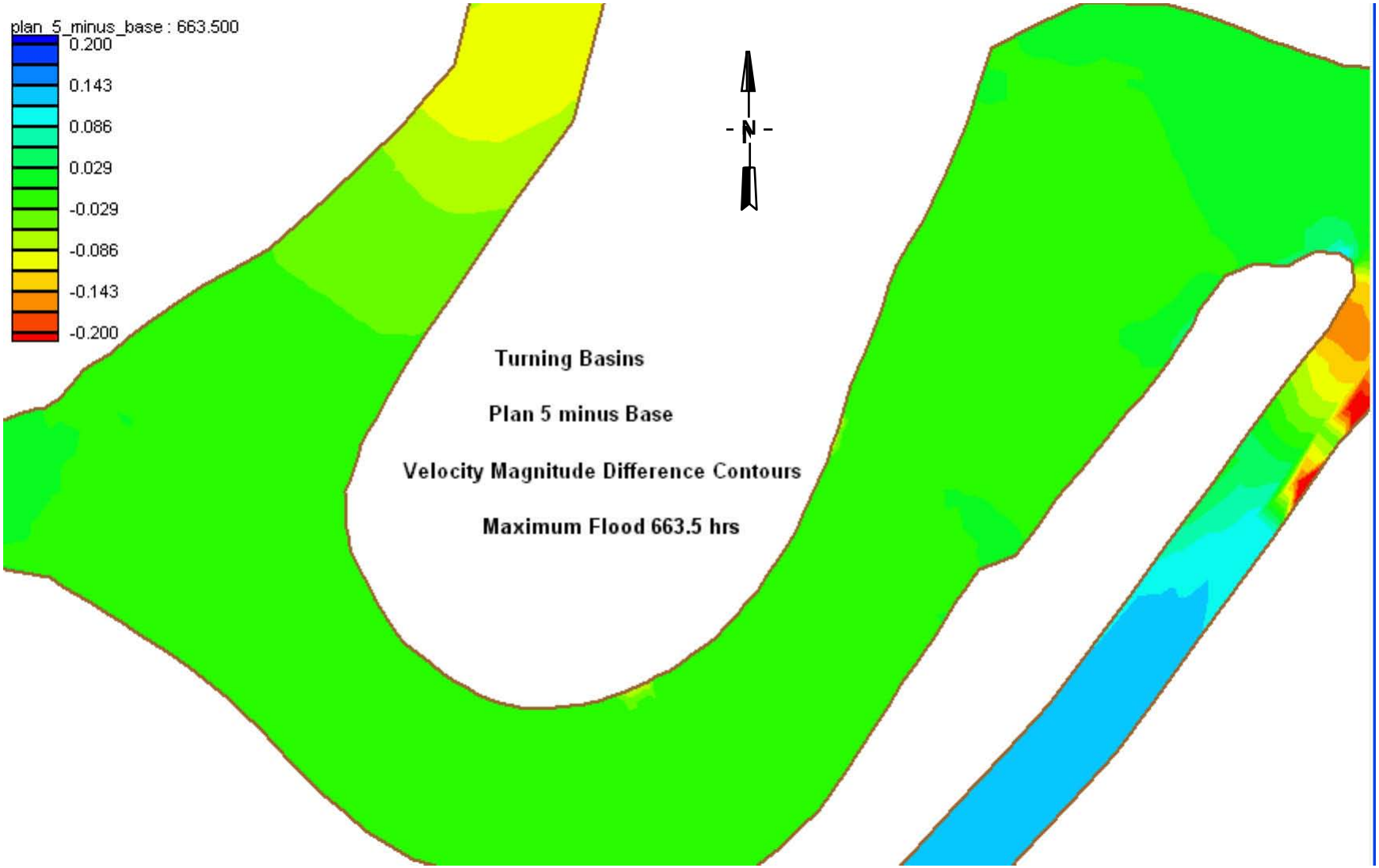

Figure 3-34. Plan 5 Minus Base Velocity Differences Maximum Flood in the Turning Basins

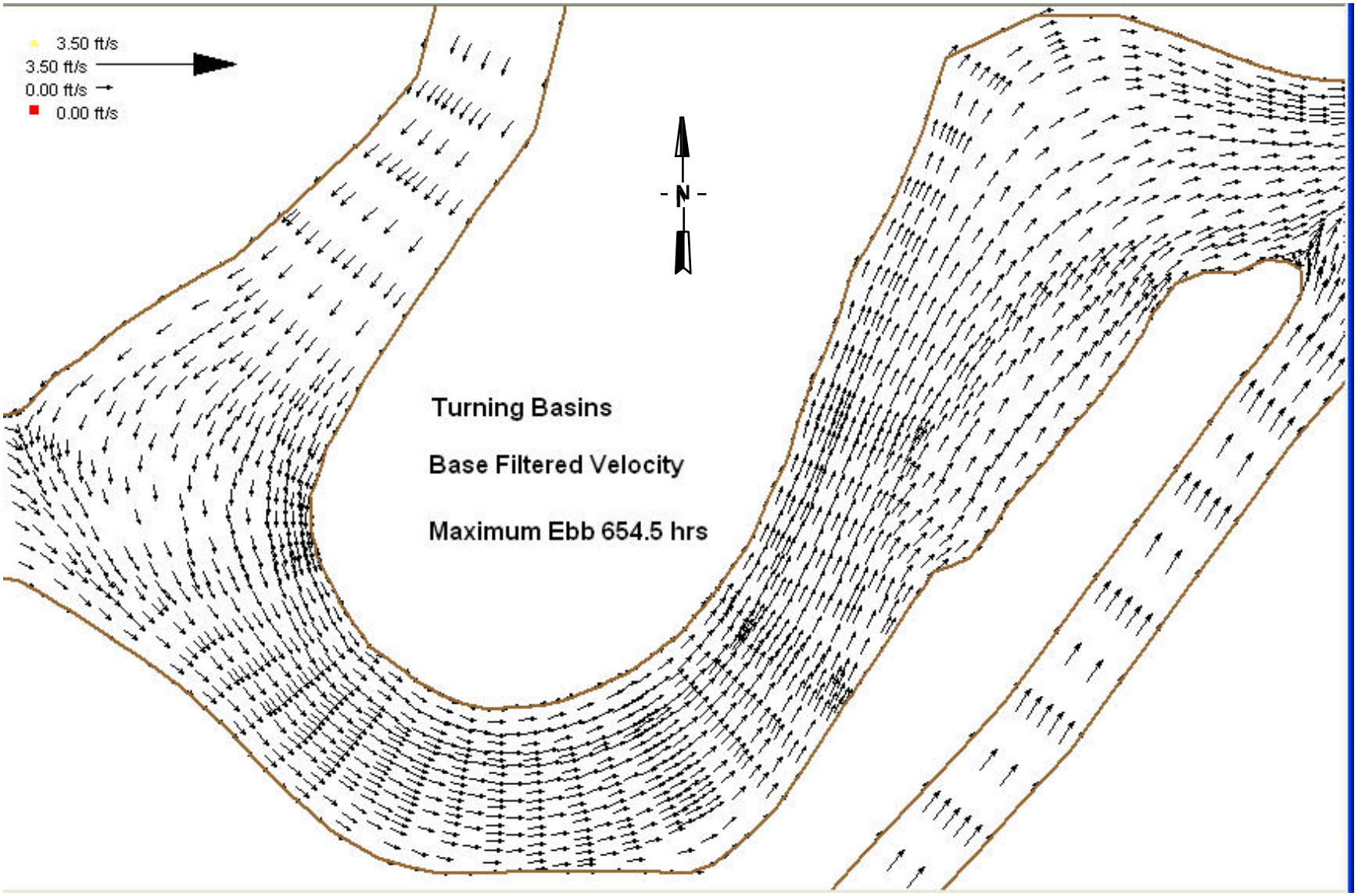

Figure 3-35. Base Maximum Ebb Velocities in the Turning Basins

Figure 3-36. Plan 4 Minus Base Velocity Differences Maximum Ebb in the Turning Basins

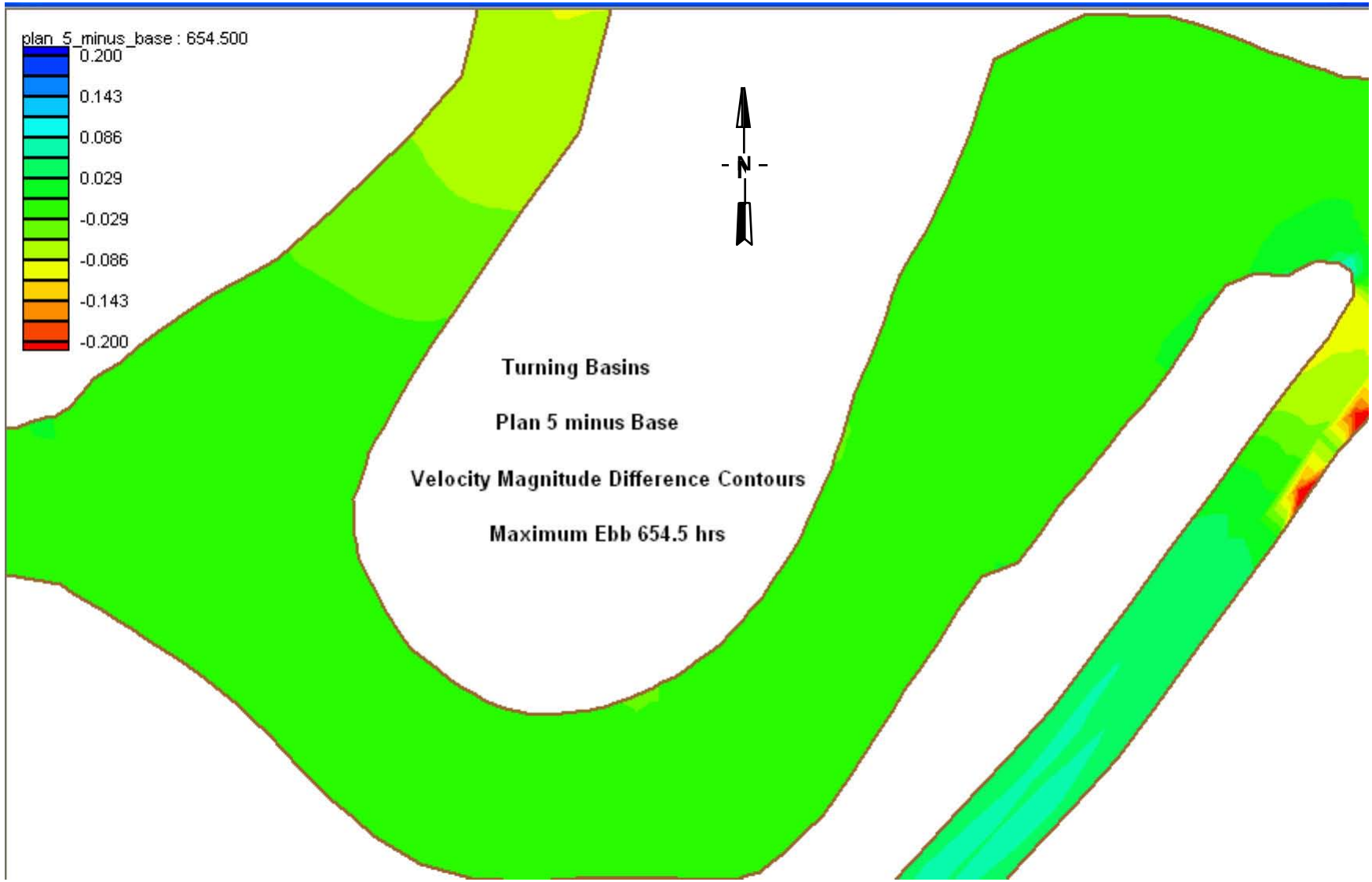

Figure 3-37. Plan 5 Minus Base Velocity Differences Maximum Ebb in the Turning Basins